D I P L O M A R B E I T

M A S T E R ' S   T H E S I S

Multiscale Modelling of Transport Processes in Softwood under the Fiber Saturation Point

ausgeführt zum Zwecke der Erlangung des akademischen
Grades eines Diplom-Ingenieurs

unter der Anleitung von

Univ.-Ass. Dipl.-Ing. Dr. techn. **Karin Hofstetter**
Institut für Mechanik der Werkstoffe und Strukturen
Fakultät für Bauingenieurwesen
Technische Universität Wien

und

Univ. Prof. Dipl.-Ing. Dr. techn. **Josef Eberhardsteiner**
Institut für Mechanik der Werkstoffe und Strukturen
Fakultät für Bauingenieurwesen
Technische Universität Wien

eingereicht an der Technischen Universität Wien
Fakultät für Bauingenieurwesen

von

Johannes Eitelberger

Matr.Nr.: 03 26 390
Wallererstraße 103
A - 4600 Wels

Wien, im Juni 2008

Holzhacken ist deshalb so beliebt, weil man bei dieser Tätigkeit den Erfolg sofort sieht.
Albert Einstein

People love chopping wood. In this activity one immediately sees results.
Albert Einstein

Danksagung

Diese Diplomarbeit stellt den Abschluss meines Diplomstudiums an der Technischen Universität Wien dar. An dieser Stelle möchte ich mich bei allen bedanken, die zu meinem Studium und dieser Arbeit beigetragen haben, und ohne die ich dieses abschließende Ziel nicht erreicht hätte.

Mein größter Dank gilt meiner ganzen Familie, ohne deren Unterstützung ich dieses Studium nicht hätte derart problemlos absolvieren können. Ganz besonders danke ich meinen Eltern Dr. Franz und Dr. Gertraud Eitelberger. Sie haben mir ein sorgenfreies Studium ermöglicht und waren auch in für mich schwierigen Zeiten immer für mich da. Meiner ganzen (Groß-)familie, Geschwistern, Großeltern, Tanten, Onkeln, Cousins und Cousine möchte ich für den Rückhalt danken, den sie mir jederzeit gegeben haben und geben. Auch meine verstorbene Mutter Mag. Sandra Eitelberger möchte ich nicht unerwähnt lassen, sie hat mir sicher einiges an mathematischem Verständnis und Freude an der Technik vererbt.

Wenn man eines lernt im Studium, dann die Tatsache, dass nichts ohne Freunde und Wegbegleiter geht. Ich hatte das Glück, zu einer Gruppe zu gehören, die sich gegenseitig zu Höchstleistungen motivierte, was dazu führte, dass ich mit meinen zehn Semestern Studienzeit bereits der "Langsamste" bin. Markus Fegerl, Stefan Gloimüller, Christoph Grömer und Martina Kainz, danke für euren vielfältigen Beitrag zu einem gelungenen Studium sowohl auf der Universität als auch in der Freizeit.

In den letzten zwei Studienjahren wurde mein Leben zusätzlich von meiner Freundin Sabine bereichert. Danke, dass du immer für mich da bist!

Frau Univ.-Ass. Dipl.-Ing. Dr. techn. Karin Hofstetter danke ich ebenso herzlich für die ausgezeichnete Betreuung und genaue Korrektur meiner Diplomarbeit. Sowohl sie als auch Mitglieder der von ihr geleiteten Holzgruppe am Institut für Mechanik der Werkstoffe und Strukturen standen jederzeit bei Fragen zur Verfügung und gaben mir wertvolle Hinweise, die zum Gelingen dieser Arbeit wesentlich beitrugen.

Abschließend sei es Univ.-Prof. Dipl.-Ing. Dr. techn. Josef Eberhardsteiner gedankt, dass er mir diese Diplomarbeit ermöglicht hat, die gleichzeitig ein Einstieg in die Forschungstätigkeit innerhalb der Holzgruppe ist, die ich nach Absolvierung der Diplomprüfung antreten kann.

Abstract

Wood is currently facing a boom in the construction sector and is increasingly used, both for common building and for special civil engineering purposes. To meet the resulting high demands on wood in design and dimensioning, accurate knowledge of the material and its properties is necessary.

Thereby the moisture content is one of the determining factors in matters of technological and mechanical properties of the material wood. For instance strength and elasticity vary with changing moisture content. Furthermore, wood swells and shrinks when the moisture content is changed in ranges typical of structural applications. Moreover, the moisture content has a great influence on the degradation of the material by means of fungi and insects.

In order to investigate these phenomenons, and, further, also to model them, it is indispensable to have a model for the conduction of moisture through wood on one's disposal. Since the moisture transport process strongly depends on temperature, also a model for heat transport in wood is needed. In this thesis models for both processes are developed and validated by comparing model predictions for transport properties to corresponding measured values.

After an introduction to the structure and microstructure of wood, an abstract model for transport processes in wood is defined that predicts the macroscopic behavior of wood from its microstructure. By consideration of the cellular structure, some phenomenons can be explained on a physical basis, that can be simulated on the macroscale only in phenomenological ways. In order to proof the suitability of the model, it is compared to a model based on the unit cell method which provides a more accurate representation of the microstructure. The transport behavior of the unit cell is analyzed by means of the finite element method (FEM), using the FEM-program Abaqus.

After formulation of the required homogenization steps, the model is applied to moisture transport in wood. After defining some fundamental terms, the input parameters are determined, in particular the diffusion coefficients of both cell walls and lumens. Since the energy relationships of the water molecules in the cell wall have a great influence on the overall moisture transport behavior of wood, they are analyzed in detail. Afterwards the developed moisture transport model is compared to measured values from the literature.

The partial differential equations describing the moisture transport in wood are identical to the corresponding equations for thermal conduction. Thus, with few adjustment, the developed model for moisture transport can also be applied to this second process. As before, the behavior of the model is checked by comparing model predictions to experimental results from the literature, after defining the thermal conductivities of the single components of the cell assembly.

With the completion of this diploma thesis insight is gained into the topic "moisture in wood". On the one hand it is pointed out where further research is needed, on the other hand the developed models for water transport and thermal conduction provide a basis for further research into the influence of moisture on wood. Moreover, this diploma thesis is the first step of my future research work at the Institute for Mechanics of Materials and Structures, Vienna University.

Kurzfassung

Der Werkstoff Holz erfährt zur Zeit einen starken Aufschwung im Bausektor und eine immer weitere Verbreitung sowohl im allgemeinen Bauwesen als auch im Ingenieurbau. Um den daraus resultierenden Anforderungen in der ingenieurmäßigen Bemessung gerecht werden zu können, sind genaue Kenntnisse des Werkstoffes und dessen Eigenschaften vonnöten.

Die Holzfeuchtigkeit ist dabei eine ausschlaggebende Zustandsgröße des Werkstoffes Holz in Bezug auf seine technologischen und mechanischen Eigenschaften. So verändern sich die Festigkeit und Elastizität mit dem Feuchtigkeitsgehalt. Außerdem schwindet Holz bei Änderungen der Holzfeuchtigkeit im für konstruktive Anwendungen relevanten Bereich. Weiters hat die Holzfeuchte einen großen Einfluss auf die Gefährdung durch Holzschädlinge wie Pilze und Insekten. Um diese Phänomene näher untersuchen und in weiterer Folge auch numerisch modellieren zu können, ist es unabdingbar, ein Modell für den Feuchtigkeitstransport in Holz zur Verfügung zu haben. Da das Transportverhalten in Holz auch stark temperaturabhängig ist, wird parallel dazu auch ein Modell für den Wärmetransport erforderlich. In dieser Arbeit werden Modelle für beide Prozesse entwickelt und zur Validierung Modellaussagen mit entsprechenden gemessenen Werten verglichen.

Nachdem die Struktur von Holz – vor allem auf der Mikroskala – geklärt ist, wird ein allgemeines Modell für Transportprozesse in Holz formuliert, das vom Verhalten auf der Zellebene auf jenes auf der Makroebene schließt. Durch die Berücksichtigung der Zellstruktur können dabei einige der Phänomene, die auf der Makroskala nur phänomenologisch nachgebildet werden können, physikalisch basiert erklärt werden. Um die Funktionsweise des Modells zu überprüfen, wird anschließend ein Vergleich mit einem Modell nach der Unit-Cell-Methode durchgeführt, welches eine genauere Beschreibung der Mikrostruktur bietet. Die Analyse des Transportverhaltens der Unit-Cell erfolgt mit Hilfe der Methode der finiten Elemente (FEM) unter Anwendung des FEM-Programms Abaqus.

Nachdem die Homogenisierungsschritte geklärt sind, folgt die Anwendung des entwickelten Modells auf die Simulation des Wassertransports in Holz. Nach der Definition von Grundbegriffen folgt die Ermittlung der benötigten Eingangsparameter, im speziellen Fall der Diffusionskoeffizienten von Zellwänden und Lumen. Hierbei wird sehr genau auf die Energieverhältnisse der Wassermoleküle in der Zellwand eingegangen, die einen großen Einfluss auf das gesamte Feuchtigkeitstransportverhalten von Holz haben. Anschließend erfolgt zur Modellvalidierung ein Vergleich der errechneten Werte mit gemessenen Werten aus der Literatur.

Die partiellen Differentialgleichungen, die dem Modell für Wasserdiffusion in Holz zugrunde liegen, sind dieselben wie jene für Wärmeleitung in Holz. Deshalb kann das entwickelte Modell mit leichten Adaptionen auf diesen Prozess übertragen werden. Auch hier wird nach Ermittlung der Wärmeleitfähigkeiten der einzelnen Komponenten der Zellstruktur das Verhalten des Modells anhand von Literaturdaten überprüft.

Mit Abschluss dieser Arbeit ist der Einstieg in das Thema "Feuchtigkeit in Holz" geschafft. Einerseits wird aufgezeigt, wo noch weiterer Forschungsbedarf nötig ist, andererseits ist mit den beiden entwickelten Modellen für Wasser- und Wärmetransport eine Basis für weitere Forschung in diese Richtung gelegt. Zusätzlich stellt diese Diplomarbeit auch den ersten Schritt meiner Forschungstätigkeit am Institut für Mechanik der Werkstoffe und Strukturen an der Technischen Universität Wien dar.

Contents

1 Introduction **1**

1.1 Motivation . . . 1

1.2 Previous work . . . 2

1.3 Scope . . . 3

1.4 Nomenclature . . . 3

2 The structure of wood **5**

2.1 Structure on the macroscopic level . . . 6

2.2 Structure on the microscopic level - softwood . . . 7

2.2.1 Earlywood cells and latewood cells . . . 8

2.2.2 Pit aspiration . . . 9

2.3 Structure on the microscopic level - hardwood . . . 10

2.4 Ultra- and molecular structure . . . 12

3 Microscale transport model for wood **13**

3.1 Fundamentals of continuum modeling on the microscale . . . 13

3.2 Eshelby's problem in linear diffusion . . . 15

3.2.1 Introduction . . . 15

3.2.2 The inclusion problem . . . 16

3.2.3 The second order $\mathbb{P}$-tensor . . . 19

3.3 Application of the homogenization scheme to wood . . . 24

3.3.1 Calculation of the geometric parameters . . . 24

3.3.2 Homogenization step 1: Diffusion coefficients of the cell assembly . . . 26

3.3.3 Homogenization Step 2: Diffusion coefficients of a whole sample . . . 26

4 The unit cell method **28**

4.1 Introduction . . . 28

4.2 Basics of the comparison . . . 29

4.3 Comparison 1: The unit cell for earlywood . . . 30

4.3.1 Dimensions of the unit cell . . . 30

4.3.2 Results and comparison . . . 30

4.4 Comparison 2: The unit cell for latewood . . . 32

4.4.1 Dimensions of the unit cell . . . 32

4.4.2 Results and comparison . . . 33

4.5 Further results of the unit cell method . . . 33

5 Evaluation of the model for moisture diffusion 36
5.1 Basics 36
5.1.1 Moisture content 36
5.1.2 The equilibrium moisture content 37
5.1.3 The fiber saturation point 37
5.1.4 The sorption isotherm 38
5.2 Constants 39
5.2.1 The universal gas constant 39
5.2.2 The Avogadro constant 39
5.2.3 The density of the cell wall 39
5.2.4 The molar mass of water 40
5.3 Properties of steam and water 40
5.3.1 The saturation vapor pressure 40
5.3.2 The density of water 42
5.3.3 The heat of evaporation 43
5.3.4 The viscosity of water 44
5.3.5 The specific heat at constant pressure of steam 45
5.4 The diffusion tensor of the lumen 46
5.4.1 The diffusion coefficient of air 46
5.4.2 The diffusion coefficient of the lumen 46
5.4.3 Assembly of the diffusion tensor 49
5.5 The diffusion tensor of the cell wall 49
5.5.1 The Arrhenius equation 49
5.5.2 Energy relationships, activation energy 50
5.5.3 The activation energy, lower limit 52
5.5.4 The activation energy, upper limit 54
5.5.5 Assembly of the diffusion tensor 55
5.6 The multiscale moisture diffusion model 55
5.6.1 Homogenization step 1: Diffusion coefficients of the cell assembly . 56
5.6.2 Homogenization step 2: Diffusion coefficients of a whole sample . . 56
5.7 Validation of the multiscale diffusion model 57
5.7.1 Radial diffusion coefficient at different moisture contents 57
5.7.2 Comparison of the activation energies 58
5.7.3 Discussion 59

6 Evaluation of the model for thermal conduction 60
6.1 Basics 60
6.1.1 Fourier's law 60
6.1.2 Comparison of thermal conductivities 60
6.1.3 The thermal conductivity of water 61
6.1.4 The thermal conductivity of air 61
6.2 The thermal conductivities of lumen and cell wall 63
6.2.1 The thermal conductivity of the lumen 63
6.2.2 The thermal conductivity of the cell wall 63
6.3 The multiscale thermal conduction model 64

6.3.1 Homogenization step 1: Thermal conductivities of the cell assembly 64
6.3.2 Homogenization step 2: Thermal conductivities of a whole sample . 64
6.4 Validation of the multiscale thermal conduction model 64
6.4.1 Thermal conductivity at different densities 64
6.4.2 Thermal conductivity at different moisture contents 65
6.4.3 Thermal conductivities for single specimens 66

7 Summary, conclusions and future work 67

A Steam table in SI-Units 73

B Program code 76
B.1 Fitting of tabulated values 76
B.1.1 The density of water 76
B.1.2 The heat of evaporation 77
B.1.3 The viscosity of water 77
B.1.4 The specific heat of steam 77
B.1.5 The thermal conductivity of water 78
B.1.6 The thermal conductivity of air 78
B.2 The multiscale moisture diffusion model 79
B.2.1 Program structure 79
B.2.2 Source code 80
B.3 The multiscale thermal conduction model 92
B.3.1 Program structure 92
B.3.2 Source code 92

Chapter 1

Introduction

1.1 Motivation

To almost all intents and purposes, water and wood are two inseparable substances. In the living tree the flow and content of water-borne nutrients are important indicators of the health status. After felling, the green wood must be dried before it can be used as structural timber. This drying process is associated with significant costs, because green wood may contain up to 800 kg/m^3 water that has to be removed. Furthermore, the quality of the end product depends to a large extent on the drying process, since wood may deform (see Figure 1.1) when the water is removed in a non-uniform way. At last, when being used for example as structural timber, the water in wood induces a number of unwanted effects, including further moisture induced mechanical deformations (swelling and shrinking) as well as rot, fungal growth and other types of biological degradation, all of which are highly sensitive to the moisture content [18]. Furthermore, also the mechanical properties of wood (like stiffness and elasticity) vary with the moisture content. The transport process is in addition influenced by temperature, where the heat transport in turn depends on the actual moisture content.

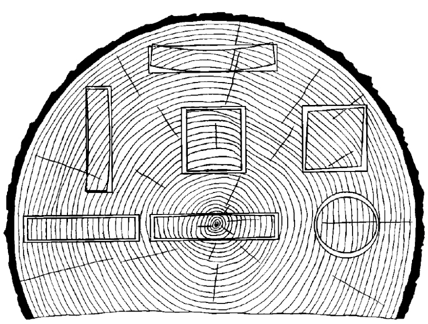

Figure 1.1: Shrinking of wood because of variations in moisture content

Thus, the moisture transport and heat transfer play a key role in a large number of scenarios. Therefore it is essential for wood research to have an adequate model for these transport processes at one's hand. Such a model should provide accurate estimates of the transport behavior, that agree with corresponding experimental observations. Moreover, it should also be extendable to new scenarios. The basics for such a model are summarized and advanced in this diploma thesis.

1.2 Previous work

The importance of heat and moisture transport in wood motivated a large number of research activities by both experimental and numerical means, which are exemplarily reviewed in the following.

One of the most quoted books is that by Siau [32], which contains a summary of the basic wood-moisture relationships, the structure of wood, and models for thermal and electrical conductivity and for the different ways of moisture movement in wood. Also a simple homogenization model is published in this book based on the rules of mixture. This book turns out to be a good introduction to the topic "transport processes", but with some inaccuracies in detail.

Perré and Turner [28, 29] developed a comprehensive heat and mass transfer computational model for the simulation of drying of porous media called TransPore. They also devised a geometric model that describes the shape of the tracheids in softwood as a function of the actual density. Since TransPore is partly based on the work of Siau [32], the same detail inaccuracies can be found.

Krabbenhoft [18] developed models for the description of the transport behavior of wood with particular emphasis on water transport. After a brief review of the basic features of wood as related to the transport of moisture, a general theoretical approach to transport of water in wood is described. Thereon a transport model is introduced and validated by comparing model predictions with a number of experimental results.

Since the behavior of the cell wall of the wood cells is the determinant factor in moisture transport processes in wood, several authors are engaged in this topic. Nelson [23, 24, 25, 26] describes in detail the energy relationships in the cell wall, while Skaar [33] specifies the mathematical background for moisture movement in the cell wall.

Gu [13] and Thunman [35] analyzed the thermal conduction in wood. Their developed models agree quite well with their reported test results.

Dormieux [3, 4, 5], Gross [12], and Zaoui [38] provide the mathematical background of the homogenization model used in this thesis. Its first reported application to wood was done by Hofstetter et. al. [15] for mechanical properties.

The book of Kollmann [17] is one of the best sources of values and test results for various wood properties, although it was already published in 1951. It includes a detailed chapter about the structure of wood including possible wood defects. Further chapters deal with the chemistry, physics, elasticity, and strength of wood and refer of course also to water diffusion and thermal conduction. Heuristic and phenomenological models are described for various aspects of the material behavior that, however, can't describe all phenomenons.

1.3 Scope

The thesis is organized in seven chapters. After this introductory chapter, the structure and basic features of wood as related to transport processes are briefly discussed in Chapter 2. Furthermore, the microstructure of both softwood and hardwood from the cross section down to the molecular scale is described. Special attention is paid to the geometric properties since they are required for the following homogenization model.

Chapter 3 describes the homogenization model for moisture diffusion in wood based on the Mori-Tanaka scheme. After the definition of the characteristic length scales and the introduction of the homogenization scheme (Section 3.1), the $\mathbb{P}$-Tensor needed for this scheme is derived step-by-step in Section 3.2 for diffusion and ellipsoidal inclusions. In Section 3.3.1 equations for the geometric properties of the microstructure of wood are reported, and Sections 3.3.2 and 3.3.3 finally deal with the application of the homogenization schemes to wood. It includes the influence of the microstructure of the cell assembly and the density variation within the annual rings on the transport behavior.

In Chapter 4 the unit cell method is used to verify the model obtained in Chapter 3. The transport behavior of the unit cell was calculated by means of the finite element method using the program Abaqus. Thereon some further results gained with the unit cell method will be reported.

In Chapter 5 the problem of moisture transport below the fiber saturation point is treated. First the developed homogenization model is specialized to this application. As in previous research on the modeling of water transfer below the fiber saturation point, the transport of bound water and water vapor are described separately. At first several fundamental terms are explained in Section 5.1. Sections 5.2 and 5.3 provide constants and properties of steam and water, that are needed in the thereon following sections. In Section 5.4 the diffusion coefficient for water in the lumen is derived, while Section 5.5 treats with the diffusion properties of the cell wall. Since the energy relationships of water molecules in the cell wall turn out to be very important in water diffusion, they are discussed in detail within this section. Section 5.6 explains the assembly of the model for water diffusion, while in Section 5.7 this model is validated by comparing its predictions with corresponding measured values.

Chapter 6 treats the homogenization model for thermal conduction. After an introduction, the input parameters for the cell walls and lumens are derived in Section 6.1 and 6.2. The model thereon is assembled in Section 6.3. A comparison of model estimates to several measured values follows in Section 6.4.

Finally, Chapter 7 contains the conclusions of this work.

1.4 Nomenclature

The quantities, units, and indices used throughout this thesis are summarized in the Tables 1.1 and 1.2.

Symbol	Name of quantity	Symbol	Name of SI unit
a	Cell dimension	m	meter
c_p	Specific heat capacity	J/kg K	joule per kilogram kelvin
d	characteristic inhomogeneity length	m	meter
D	Diffusion coefficient	m^2/s	square meter per seconds
$\mathbb{D}$	Diffusion tensor	m^2/s	square meter per seconds
E_a	Activation energy	J/mol	joule per mole
f	Volume fraction	%	percent
h	Specific enthalpy	J/kg	joule per kilogram
j	Mass flux	$mol/m^2\,s$	mole per square meter second
$\mathbb{K}$	Thermal conductivity tensor	W/m K	watt per meter kelvin
ℓ	characteristic length of RVE	m	meter
$\mathscr{L}$	characteristic length of structure	m	meter
m	Mass	kg	kilogram
mc	Moisture content	%	percent
M	Molar mass	g/mol	gram per mole
n	Amount of a substance	1	one
N_A	Avogadro constant	1/mol	reciprocal mole
p	Pressure	Pa	pascal
p_0	Saturation vapor pressure	Pa	pascal
$\mathbb{P}$	P-tensor for diffusion	s/m^2	seconds per square meter
$\mathbb{P}$	P-tensor for heat conduction	m K/W	meter kelvin per watt
Q	Heat (energy)	J/kg	joule per kilogram
r	Effective molecular radius	m	meter
R	Universal gas constant	J/mol K	joule per mole kelvin
t	Celsius temperature	°C	degree Celsius
T	Temperature	K	kelvin
V	Volume	m^3	cubic meter
α	Effective area	1	one
η	Viscosity	Pa s	pascal second
λ	Thermal conductivity	W/m K	watt per meter kelvin
ρ	Concentration	mol/m^3	mole per cubic meter
ϱ	Density	kg/m^3	kilogram per cubic meter
τ	Tortuosity	1	one
ϕ_q	Heat flux	W/m^2	watt per square meter
φ	Relative humidity	%	percent

Table 1.1: Quantities and units used in this thesis

Symbol	Name	Symbol	Name
$earlywood$	Earlywood	γ	Substance γ
$latewood$	Latewood	est	Estimated
rad	Radial	hom	Homogenized
$tang$	Tangential	ell	ellipsoidal
$long$	Longitudinal	$ovendry$	Oven-dry
$trans$	Transversal	$green$	Green
$lumen$	Lumen	w	Water
$cellwall$	Cell wall	v	Vapor
s	Solid phase	a	Air
p	Pore phase	r	Self-diffusion
I	Inclusion		

Table 1.2: Indices used in this thesis

Chapter 2

The structure of wood

This chapter is about the structure and basic features of wood. Some attention is also paid to the properties which control the transport of fluids (since this is one of the scopes of this thesis) within the wooden cell structure. Knowledge of the structure of wood is useful basically for the understanding of experimentally observed phenomena. The behavior of wood, that can be described on the macroscopic scale only by empirical relations, often turns out to be describable by more simple processes on the microscale. Moreover, the structure of wood serves as a physical justification for the model presented in this thesis.

The various wood species can be divided into two classes, normally referred to as softwood and hardwood. Although these names can be misleading, since some hardwoods are softer than some softwoods (for example: balsa is a hardwood), they are really useful since they specify two quite distinct types of cellular arrangements. In the following the structures of both kinds of wood (as related to transport phenomena) are discussed.

For the wood microstructure, five levels of organization [15] with different associated length scales can be distinguished (see also Figure 2.1):

- The macroscopic level, on which softwood and hardwood can be treated together (to a certain degree). A typical length scale is $2-4\,\mathrm{mm}$ (see Figure 2.1a).
- The microscopic or cell level, with the most clearly manifested distinctions between softwood and hardwood (see Figures 2.1c and 2.1b).
- A first ultra-structural level, on which the sequentially deposited layers of the cell walls are dealt with (Figure 2.1d).
- A second ultra-structural level for the cellulosic fibers in a non-cellulosic matrix, making up the cell wall layers (see Figure 2.1e).
- The molecular level, on which the chemical composition of the cell wall is dealt with: the cellulose chains (Figure 2.1f) and the matrix deposited in the spaces between the cellulose (Figure 2.1g shows the structure of hemicellulose, one of the matrix parts).

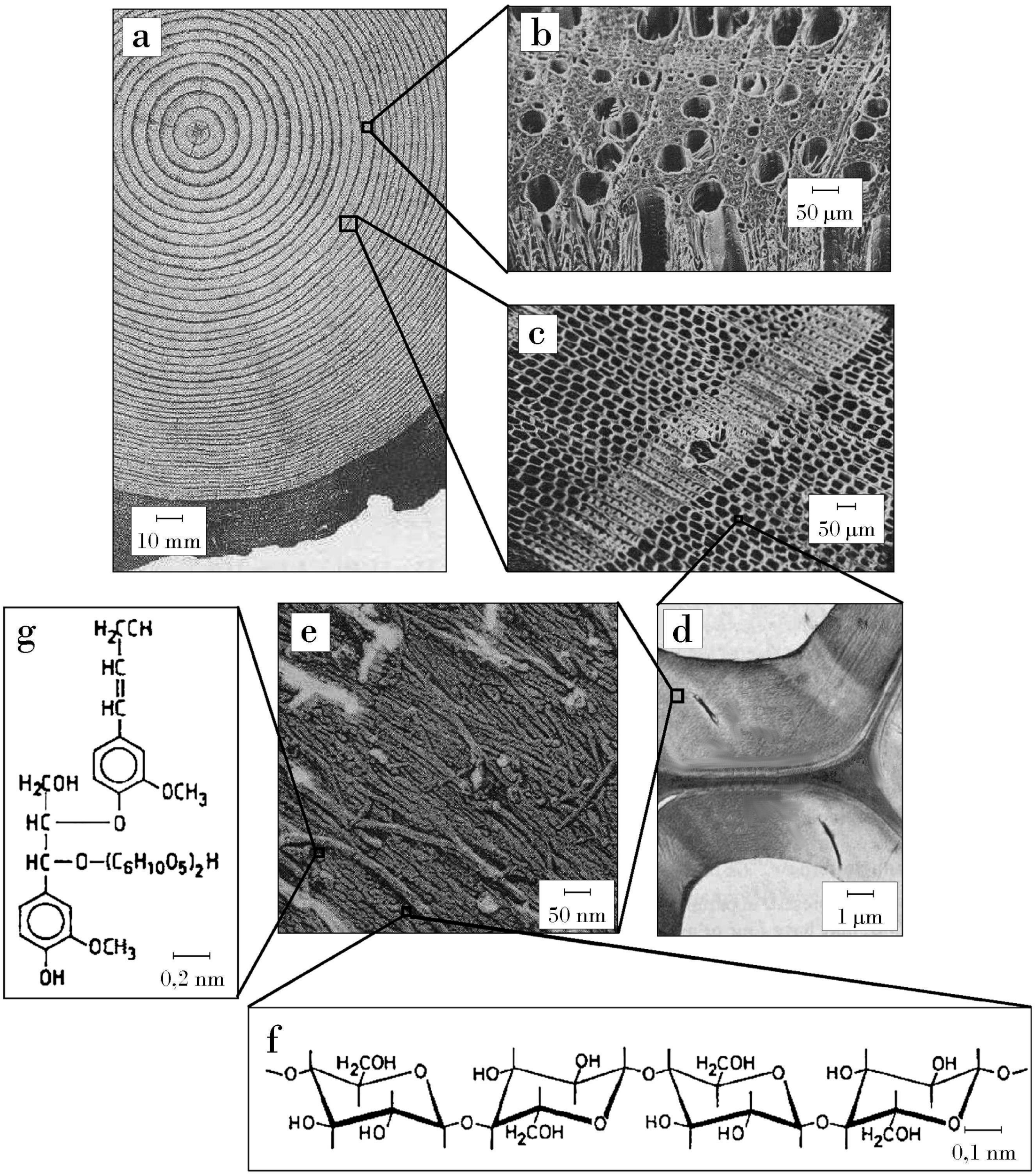

Figure 2.1: Hierarchical organization of wood

2.1 Structure on the macroscopic level

Before the cellular structures of softwood and hardwood are described, some common characteristics of all woods will be summarized. The trunk of a tree has three physical functions: it must support the crown, conduct minerals and water upwards from the roots to the crown, and store nutrients until they are needed. Whereas the entire trunk takes part in supporting the crown, only its outer regions contribute to conduction and storage. The wood located in this outer region is termed sapwood, the remaining part is referred to as heartwood. The width of the sapwood zone is usually much smaller than that of heartwood and mostly accounts for less than one third of the total width [18].

When the tree grows, former sapwood cells will gradually be transformed to heartwood cells. This transformation comes along with a number of chemical changes, which gives the heartwood a darker color than the sapwood (see Figure 2.2).

Figure 2.2: Cross section of a taxus tree [60]

With respect to the overall flow properties of the two kinds of wood, sapwood is usually much more permeable than heartwood. This is clear, since the two types of wood fulfill different functions in the living tree. In addition, the sapwood porosity is a bit higher than that of the heartwood. These factors affect the ability to water conduction of wood.

When a typical cross section of a tree (see Figure 2.2) is inspected further, the existence of a set of concentric rings with origin in the center of the tree can be noticed. These growth or annual rings are a consequence of the growing process during each season and result in the three principal material directions of wood - the longitudinal (L), radial (R), and tangential (T) direction. The longitudinal direction is that of the longitudinal axis of the trunk, which almost coincides with the direction of the tracheid cell axes. The radial direction points from the center of the trunk outwards, normal to the annual rings. The tangential direction is defined by the local tangent to the growth rings.

2.2 Structure on the microscopic level - softwood

The microscopic structure of a typical softwood tissue is shown in Figure 2.3. As can be seen, the cellular arrangement is one of long interconnected cells with ellipsoidal or square cross sections. These cells, named tracheids, account for 95 % of the mass of softwood tissues [31]. They are formed in the radial direction by the division of the same initial cell in the cambium [36]. Thus the cell walls are aligned in this direction. In the tangential direction, they are randomly arranged.

In softwood the cells do not form an unbroken pathway as longitudinal cylinders but have tapered ends, so that the cells form independent and relatively closed units, as seen in Figure 2.4. The conduction in the longitudinal direction thus takes place through holes in the cell walls, so-called pits, which interconnect neighboring cells. The resistance to flow through these pits makes up a mainly portion of the total resistance to longitudinal flow.

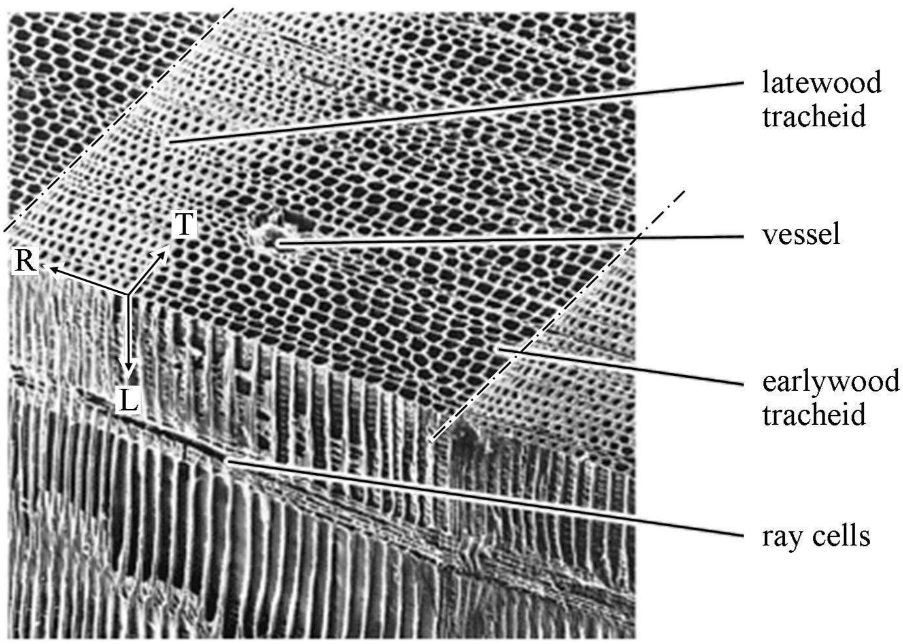

Figure 2.3: Structure of softwood (red pine) [39]

In the two other directions flow also takes place through interconnecting pits, and in the radial directions furthermore through ray cells as shown in Figure 2.3. This results in a slightly higher permeability in radial direction than in tangential direction, although most pits are located on the radial surfaces and thus support tangential flow [18].

2.2.1 Earlywood cells and latewood cells

The growth activity of trees varies within a year. Therefore the clearly visible growth rings are approximately linked to the seasons. In the beginning of the growing season in spring the tree will form cells whose primary function is conduction. Therefore, these cells are thin-walled and have more pits to increase connectivity. This wood named earlywood can be identified by its rather light color.

In contrast the darker part of an annual ring (the latewood) consists of cells with opposite features. Since the primary function is not longer conduction but mechanical support, the cells have thicker walls resulting in a much higher density and a lower number of interconnecting pits [18]. From earlywood to latewood, the tangential diameter is nearly constant (about $20 - 50\,\mu$m in softwood), while the radial diameter decreases, and the cell wall thickness ($2 - 20\,\mu$m) increases (see Figure 2.3). The cell length ranges between 2 and 10 mm [15].

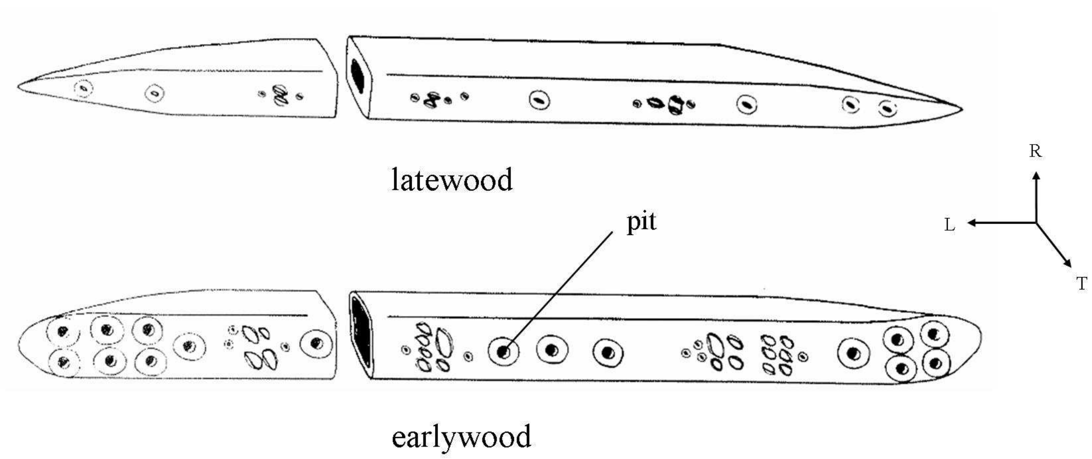

Figure 2.4: Earlywood and latewood tracheid cells [32]

2.2.2 Pit aspiration

As already mentioned, there is usually a distinct difference between the flow properties of green wood and dried wood. The higher porosity and the larger number of pits in earlywood motivate the assumption that the permeability of earlywood is much higher than that of latewood. This is the case, in fact, but only in the green state. The reason for the different behavior of dried wood can be found in a process named pit aspiration, that will be explained next.

The pits interconnecting the cells consist of an impermeable torus, that is held in position by surrounding margo strands as shown in Figure 2.5.

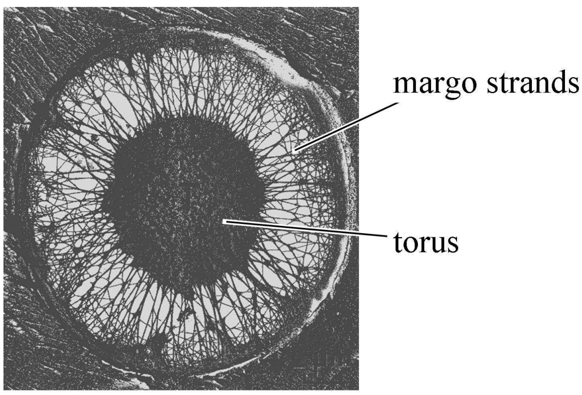

Figure 2.5: Unaspirated bordered pit in a sapwood tracheid [32]

In green wood, the pit torus is positioned in the middle of the pit chamber, so that flow through the pit is not really hindered. When water is removed, tension stresses because of water menisci will displace the torus like shown in Figure 2.6, resulting in an effectively closed pit. Afterwards, the torus is kept in the displaced position, so that pit aspiration is irreversible to the most extent. Rewetting with water will only cause partial reduction in the number of aspirated pits [18].

Pit aspiration takes place at relatively high moisture contents. According to Siau [32], the process of pit aspiration is already finished when the moisture content reaches the fiber saturation point (no liquid water in wood, see Section 5.1.3). All pits are closed under the fiber saturation point and, thus, can be neglected when modeling moisture transport in wood. The moisture transport is only affected by diffusion processes then, what considerably simplifies the modeling.

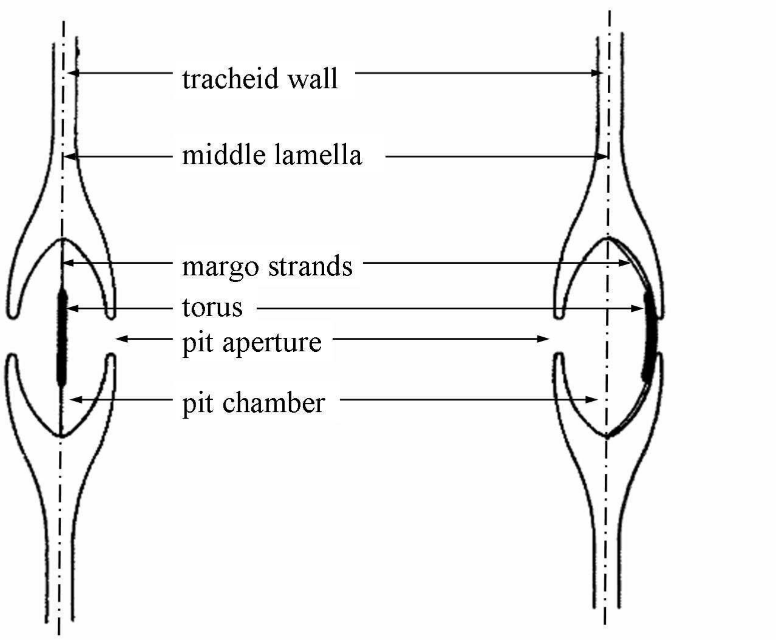

Figure 2.6: Cross section of a bordered pit in the unaspirated state (left) and the aspirated state (right) [18]

2.3 Structure on the microscopic level - hardwood

Although this diploma thesis deals only with softwood, also the structure of hardwood is described in order to point out why the modeling of hardwood is more complicated. The structure of hardwood is quite different from that of softwood, since hardwoods are younger species in biological evolution. Hardwood contains in contrast to softwood additional vessels wit a diameter up to 500 μm, that form continuous pathways in the cell assembly. Moreover, variability between several species is much greater for hardwood than for softwoods. In general, two types of hardwood can be differentiated: ring porous hardwood and diffusive porous hardwood. Figure 2.7 shows the microscopic structure of diffuse porous hardwood. In this type of wood, the cell sizes don't change throughout the growing season. This results in an even distribution of the large vessels, which are surrounded by cells with a much smaller diameter. These vessels cause the much higher longitudinal permeability of hardwood species compared to softwood tissues. Also the differences between the permeabilities of green and dried hardwood are much smaller, since the water flow through pits is only of minor importance [18]. In contrast to diffusive porous hardwood, the vessels are arranged according to the growth ring pattern in ring porous hardwood as is clearly visible in Figure 2.8. As can be easily understood, the differentiated structure of hardwood is much more difficult to model than that of softwood, which is more homogeneous.

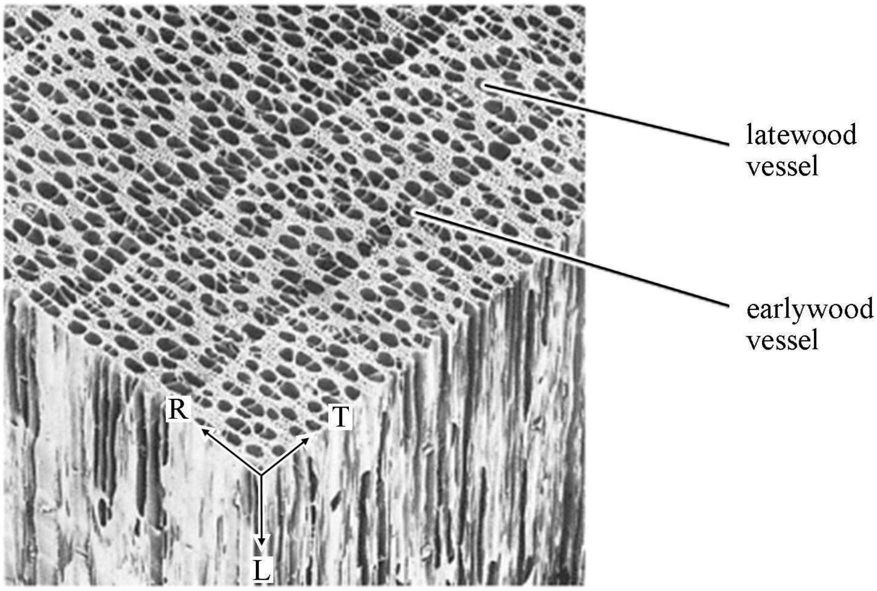

Figure 2.7: Structure of diffusive porous hardwood (aspen) [39]

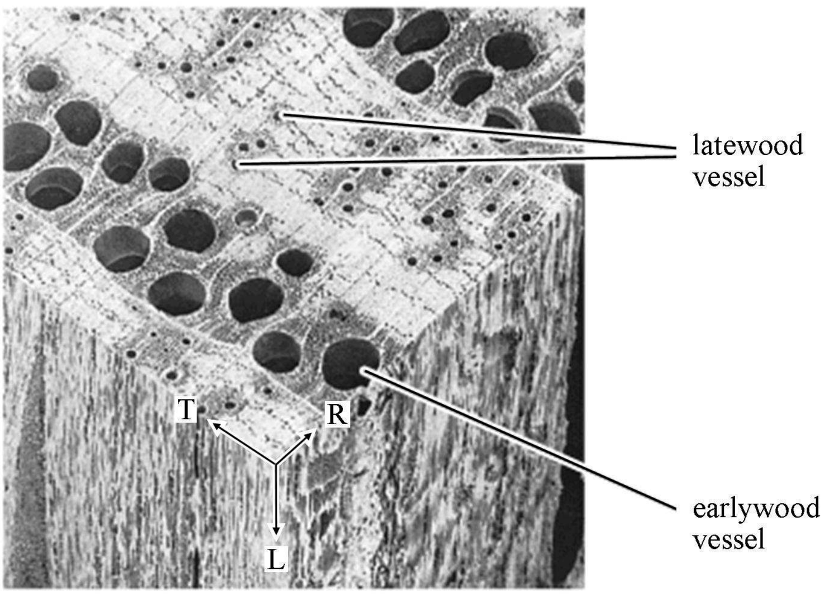

Figure 2.8: Structure of ring porous hardwood (red oak) [39]

2.4 Ultra- and molecular structure

The cell walls of wood consist of three polymers for the most part: cellulose, hemicellulose, and lignin. The relative shares of these three polymers vary between different species. Cellulose usually accounts for $40 - 50\,\%$ of the mass of the cell wall, while the rest is made up of hemicellulose and lignin in approximately equal shares [18]. The polymers are arranged as shown in Figure 2.9, which constitute the basic building blocks of the cell walls. Therein cellulosic microfibrils are sheathed by hemicellulose and finally connected by lignin. The long cellulosic threads with a typical length of about 5000 nm and a width of $10 - 20$ nm are shown in Figure 2.9 [15].

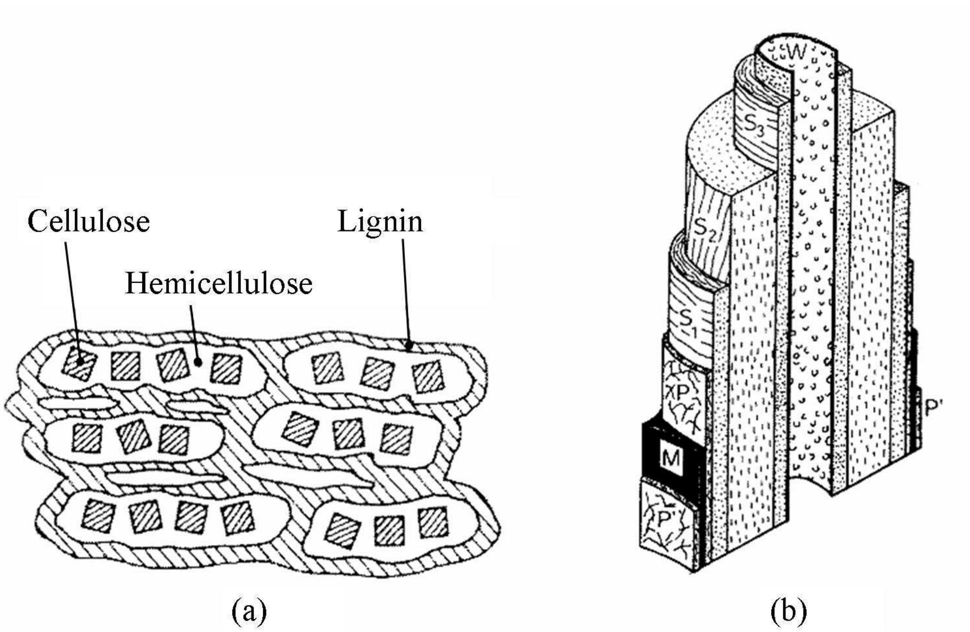

Figure 2.9: Cross section of a basic building block (a), and the layered structure of the cell wall (b) [18]

The cell walls are made up of several layers (denoted by P, S_1, S_2, S_3, W), which differ in the chemical composition and the orientation of the cellulose. The individual cells are bonded together by the middle lamella (M) to form the cellular microscopic honeycomb structure described before.

Since the different polymers each have different properties, for example different sorption isotherms, wood is in fact a composite material, where the overall behavior is a result of the features of the individual components and the arrangement of these components in the cell wall [18].

Chapter 3

Microscale transport model for wood

The aim of this diploma thesis is to predict the macroscopic transport behavior of wood from its microstructural characteristics. In contrast to previous research in this field, a new model for transport processes based on multiscale modeling is developed. The success of a similar model for the mechanical behavior of wood [15], developed at the Institute for Mechanics of Materials and Structures, Vienna University of Technology (my future place of employment), supports the research endeavor to apply such a model also to transport processes.

In this chapter a short introduction to the fundamentals of continuum modeling is given first. Since no analytical formulations for the components of the second order $\mathbb{P}$-tensor could be found in literature, this tensor is derived step-by-step in the second section. At last the model is applied to wood, and a summary of the resulting equations is given for use in a computer program.

3.1 Fundamentals of continuum modeling on the microscale

In microscale continuum modeling, a material is understood as a macro-homogeneous, but micro-heterogeneous body filling a representative volume element (RVE) with characteristic length ℓ, $\ell \gg d$, d standing for the characteristic length of inhomogeneities within the RVE (see Figure 3.1), and $\ell \gg \mathscr{L}$, $\mathscr{L}$ standing for the characteristic length of a structure built up by the material defined on the RVE. In general, the microstructure within the RVE is so complicated that it cannot be described in complete detail. Therefore, quasi-homogeneous sub-domains with known physical properties (such as volume fractions and diffusion coefficients) are reasonably chosen. They are called material phases. The homogenized behavior of the overall material, i.e. the relation between concentration gradients acting on the boundary of the RVE and resulting (average) fluxes, can then be estimated from the behavior of the homogeneous phases (representing the inhomogeneities within the RVE) as mentioned afore, their volume fractions within the RVE, their characteristic shapes, and their interactions. Based on solutions for matrix-inclusion problems, an estimate for the homogenized diffusion coefficient of the material reads as [38, 3]:

$$\mathbb{D}^{est} = \frac{\sum_r f_r \cdot \mathbb{D}_r \cdot \left[\mathbb{I} + \mathbb{P}^0_r \cdot (\mathbb{D}_r - \mathbb{D}^0)\right]^{-1}}{\sum_s f_s \cdot \left[\mathbb{I} + \mathbb{P}^0_s \cdot (\mathbb{D}_s - \mathbb{D}^0)\right]^{-1}} \tag{3.1}$$

where $\mathbb{D}_r$ and f_r denote the diffusion tensor and the volume fraction of phase r, respectively, and $\mathbb{I}$ is the second order unity tensor. The two sums are taken over all phases of the heterogeneous material in the RVE. The second order $\mathbb{P}$-tensor or Hill tensor, $\mathbb{P}^0_r$, accounts for the characteristic shape of phase r in a matrix with diffusion tensor $\mathbb{D}^0$. It is determined based on Eshelby's solution for matrix inclusion problems as outlined in Section 3.2. Choice of this diffusion tensor describes the interactions between the phases: For $\mathbb{D}^0$ corresponding to one of the phase diffusion tensors (Mori-Tanaka scheme), a composite material is represented (continuous matrix with inclusions); for $\mathbb{D}^0 = \mathbb{D}^{est}$ (self-consistent scheme), a dispersed arrangement of the phases is considered. If a single phase exhibits a heterogeneous microstructure itself, its behavior can be estimated by introduction of an RVE within this phase, with dimensions $\ell_2 \leq d$, comprising again smaller phases with characteristic length $d_2 \gg \ell_2$, and so on (see Figure 3.1).

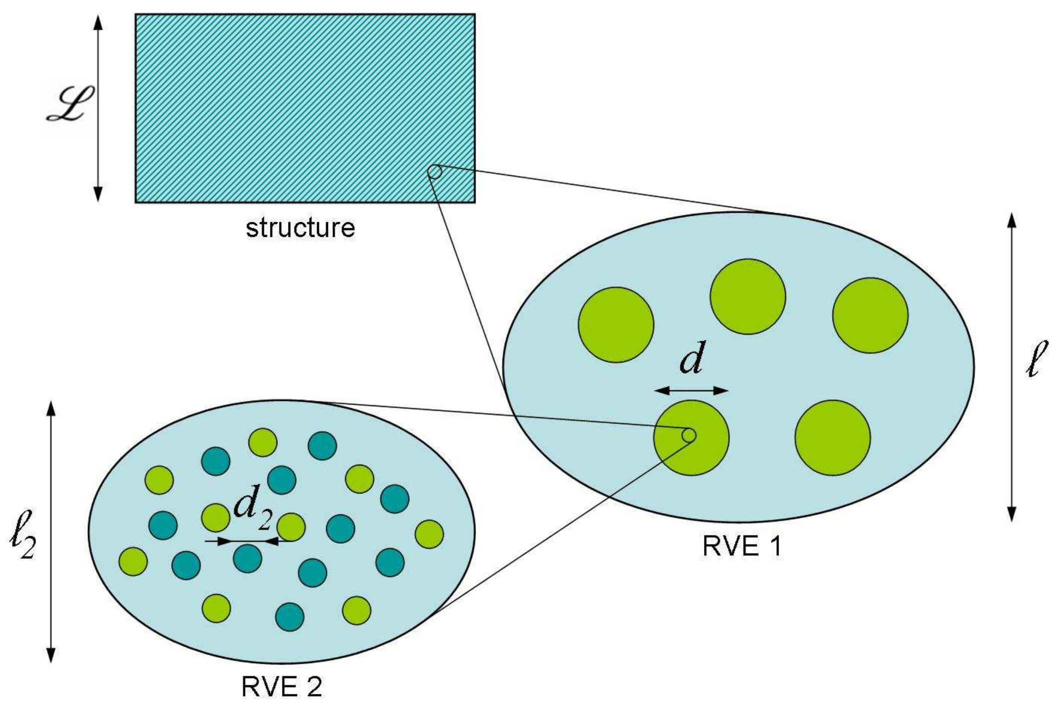

Figure 3.1: Multistep homogenization

This leads to a multistep homogenization scheme. Such a procedure should, in the end, provide access to universal phase properties of the structure, at a sufficiently low observation scale.

3.2 Eshelby's problem in linear diffusion

The following section presents the solution of Eshelby's problem in linear diffusion which delivers the components of the $\mathbb{P}$-tensor. The section is primarily according to two books by L. Dormieux [3, 4], but throughout the text the derivations in these books were amended for a better traceability. Furthermore, the $\mathbb{P}$-tensor was derived for ellipsoidal shape of the inclusions, which is not part of the mentioned books.

3.2.1 Introduction

The mathematical approach used for solving the homogenization problem for transport processes in the framework of this diploma thesis was first described by J. Eshelby in the year 1957, though for the mechanical behavior. For diffusion processes, a porous material (e.g. wood) is considered to be composed of a solid phase Ω^s (the cell walls) and a pore space Ω^p (the lumens), through which a diffusive flux occurs driven by a gradient in the solute concentration of substance γ. For this process a continuous description of the molecular diffusion throughout the porous material (the solid plus the connected pore space) can be given: the solute concentration ρ^γ and the diffusive flux $\underline{j}^\gamma$ are extended into the solid phase, while setting the diffusion coefficient to zero, $D^s = 0$. This is a simplified model since the cell walls in wood are not a completely impermeable solid phase. The physics of the molecular diffusion problem is then defined by the following set of equations:

- mass balance equation for the γ-component (a)
- Fick's law of diffusion [50] (b)
- boundary condition for concentration (c)

$$
\begin{aligned}
&\operatorname{div} \underline{j}^\gamma = 0 && \text{(a)}\\
&\underline{j}^\gamma = -D(\underline{z}) \cdot \underline{\operatorname{grad}}\, \rho^\gamma \quad \text{with} \quad D(\underline{z}) = \begin{cases} D^s = 0 & \text{for} \quad \underline{z} \in \Omega^s \\ D^\gamma & \text{for} \quad \underline{z} \in \Omega^p \end{cases} && \text{(b)}\\
&\rho^\gamma = \underline{H} \cdot \underline{z} \quad \text{when} \quad \underline{z} \in \partial\Omega && \text{(c)}
\end{aligned}
\qquad (3.2)
$$

where $\underline{H}$ denotes the macroscopic concentration gradient, prescribed at the boundary $\partial\Omega$ of the representative volume element. The solid phase is assumed being isotropic at first with diffusion coefficient D^γ, but the model will be extended to the more general anisotropic case later. The set of equations (3.2) defines a boundary value problem in a bounded domain Ω. Instead of solving it, it is more practical to reverse the problem and to define an auxiliary problem of a bounded inhomogeneity I embedded in an infinite homogeneous medium ω, the former representing a solid phase inclusion, the latter the pore space. The solution of the mechanical equivalent on the auxiliary problem was first derived by Eshelby [3]. Given the assumed infinity of ω, the boundary condition (3.2c) in the original problem needs to be replaced by a condition formulated at infinity. The set of equations that define this inhomogeneity problem is the following:

$$\begin{aligned}
&\operatorname{div} \underline{j}^{\gamma} = 0 && \text{(a)}\\
&\underline{j}^{\gamma} = -D(\underline{z}) \cdot \underline{\operatorname{grad}}\, \rho^{\gamma} \quad \text{with} \quad D(\underline{z}) = \begin{cases} D^{s} = 0 & \text{for} \quad \underline{z} \in I \\ D^{\gamma} & \text{for} \quad \underline{z} \in \omega \end{cases} && \text{(b)}\\
&\rho^{\gamma} \to \underline{H} \cdot \underline{z} \quad \text{when} \quad |\underline{z}| \to \infty && \text{(c)}
\end{aligned} \tag{3.3}$$

Further, by introducing $\delta D = D^{s} - D^{\gamma} = -D^{\gamma}$, (3.3b) can be written in the form:

$$\underline{j}^{\gamma} = -D^{\gamma} \cdot \underline{\operatorname{grad}}\, \rho^{\gamma} + \underline{j}^{p}(\underline{z}) \quad \text{with} \quad \underline{j}^{p}(\underline{z}) = -\delta D \cdot \chi_{I}(\underline{z}) \cdot \underline{\operatorname{grad}}\, \rho^{\gamma} \tag{3.4}$$

where $\underline{j}^{p}(\underline{z})$ is a fictitious flux that is non-zero only in the solid phase. Hereby χ_I denotes the characteristic function of the domain I.

For the purpose of analysis, it is assumed that $\underline{j}^{p}(\underline{z}) = \underline{j}^{I} \cdot \chi_{I}(\underline{z})$, where $\underline{j}^{I}$ is a constant vector. Hence, the problem defined by (3.3a), (3.3c), and (3.4) is:

$$\begin{aligned}
&\operatorname{div} \underline{j}^{\gamma} = 0 && \text{(a)}\\
&\underline{j}^{\gamma} = -D^{\gamma} \cdot \underline{\operatorname{grad}}\, \rho^{\gamma} + \underline{j}^{I} \cdot \chi_{I}(\underline{z}) && \text{(b)}\\
&\rho^{\gamma} \to \underline{H} \cdot \underline{z} \quad \text{when} \quad |\underline{z}| \to \infty && \text{(c)}
\end{aligned} \tag{3.5}$$

The equivalent mechanical set of equations is known as Eshelby's inclusion problem. An inclusion is a bounded domain with imposed concentration gradient (eigenstrains in mechanics) or diffusive flux (eigenstresses in the mechanical problem). In the following Eshelby's inclusion problem (3.5) is solved step-by-step. It will be seen, that the solution of this problem provides estimates for the homogenized diffusion tensor $\mathbb{D}_{hom}$, that captures, at the macroscopic scale, the overall effect of the microscopic physics of the molecular diffusion problem.

3.2.2 The inclusion problem

First the special case $\underline{H} = 0$ is considered. The combination of (3.5a) and (3.5b) gives [48]:

$$\begin{aligned}
\operatorname{div} \underline{j}^{\gamma} \;=\; 0 \;&=\; \operatorname{div}\left(-D^{\gamma} \cdot \underline{\operatorname{grad}}\, \rho^{\gamma} + \underline{j}^{I} \cdot \chi_{I}(\underline{z})\right) = \\
&= \operatorname{div}\left(-D^{\gamma} \cdot \underline{\operatorname{grad}}\, \rho^{\gamma}\right) + \operatorname{div}\left(\underline{j}^{I} \cdot \chi_{I}(\underline{z})\right) = \\
&= -D^{\gamma} \cdot \operatorname{div}\left(\underline{\operatorname{grad}}\, \rho^{\gamma}\right) + \left\langle \underline{\operatorname{grad}}\, \chi_{I}(\underline{z}) \,,\, \underline{j}^{I} \right\rangle + \chi_{I}(\underline{z}) \cdot \operatorname{div}\left(\underline{j}^{I}\right) = \\
&= -D^{\gamma} \cdot \triangle \rho^{\gamma} + \left\langle \underline{\operatorname{grad}}\, \chi_{I}(\underline{z}) \,,\, \underline{j}^{I} \right\rangle
\end{aligned} \tag{3.6}$$

with $\operatorname{div}\left(\underline{j}^{I}\right) = 0$ because the vector field $\underline{j}^{I}$ is solenoidal. The angle brackets $\langle\rangle$ in (3.6) denote the inner product of two vectors. According to the definition of the derivation of a distribution [47], it holds for any function ψ of $\mathcal{D}(\mathbb{R}^3)$ that:

$$\begin{aligned} \langle \underline{\mathrm{grad}}\, \chi_I(\underline{z}) \,,\, \psi \rangle &= -\langle \chi_I(\underline{z}) \,,\, \underline{\mathrm{grad}}\, \psi \rangle = -\int_{-\infty}^{\infty} \chi_I(\underline{z})\, \underline{\mathrm{grad}}\, \psi \,\mathrm{d}V = \\ &= -\int_I \underline{\mathrm{grad}}\, \psi \,\mathrm{d}V = -\int_{\partial I} \psi \cdot \underline{n} \,\mathrm{d}S \end{aligned} \tag{3.7}$$

In (3.7), $\underline{n}$ is the outward unit normal to I. Further the Dirac distribution $\delta_{\partial I}$ is introduced that is associated with the boundary of I and defined by:

$$\langle \delta_{\partial I} \,,\, \psi \rangle = \int_{\partial I} \psi \,\mathrm{d}S \tag{3.8}$$

From (3.7) and (3.8) it is seen that:

$$\underline{\mathrm{grad}}\, \chi_I(\underline{z}) = -\underline{n} \cdot \delta_{\partial I} \tag{3.9}$$

Thus, using (3.9) in (3.6) yields:

$$-D^\gamma \cdot \triangle \rho^\gamma - \underline{j}^I \cdot \underline{n} \cdot \delta_{\partial I} = 0 \tag{3.10}$$

The solution of such a partial differential equation can be gained by using the Green's function concept [54]. Technically, a Green's function $\mathcal{G}(\underline{z}, \underline{z}^{'})$ of a linear operator L acting on distributions over a manifold I is any solution of:

$$L\, \mathcal{G}(\underline{z}, \underline{z}^{'}) = \delta(\underline{z} - \underline{z}^{'}) \tag{3.11}$$

where $\delta(\underline{z} - \underline{z}^{'})$ is the Dirac delta function at point $\underline{z}^{'}$, defined by:

$$\int_I \delta(\underline{z} - \underline{z}^{'})\, f(\underline{z}^{'})\, \mathrm{d}\underline{z}^{'} = \int_I \delta(\underline{z}^{'} - \underline{z})\, f(\underline{z}^{'})\, \mathrm{d}\underline{z}^{'} = f(\underline{z}) \tag{3.12}$$

This technique can be used to solve differential equations of the form:

$$L\, u(\underline{z}) = f(\underline{z}) \tag{3.13}$$

In short, if such a function $\mathcal{G}(\underline{z}, \underline{z}^{'})$ can be found for the operator L, then multiplication of (3.11) by $f(\underline{z}^{'})$ and subsequent integration over $\underline{z}^{'}$ yields:

$$\int_I L\, \mathcal{G}(\underline{z}, \underline{z}^{'})\, f(\underline{z}^{'})\, \mathrm{d}\underline{z}^{'} = \int_I \delta(\underline{z} - \underline{z}^{'})\, f(\underline{z}^{'})\, \mathrm{d}\underline{z}^{'} = f(\underline{z}) \tag{3.14}$$

The result equals the right hand side of (3.13) which in turn equals $L\, u(\underline{z})$, so that:

$$L\, u(\underline{z}) = \int_I L\, \mathcal{G}(\underline{z}, \underline{z}^{'})\, f(\underline{z}^{'})\, \mathrm{d}\underline{z}^{'} \tag{3.15}$$

Because the operator L is linear and acts only on the variable $\underline{z}$ (and not on the variable of integration, $\underline{z}^{'}$), the operator L can be taken outside of the integration on the right hand side, resulting in:

$$L\, u(\underline{z}) = L \int\limits_I \mathcal{G}(\underline{z}, \underline{z}^{'})\, f(\underline{z}^{'})\, \mathrm{d}\underline{z}^{'} \tag{3.16}$$

This implies:

$$u(\underline{z}) = \int\limits_I \mathcal{G}(\underline{z}, \underline{z}^{'})\, f(\underline{z}^{'})\, \mathrm{d}\underline{z}^{'} \tag{3.17}$$

The solution of (3.13), $u(\underline{z})$, can be determined by the integral given in (3.17). Although the function $f(\underline{z})$ is known, this integration cannot be performed before the Green's function $\mathcal{G}(\underline{z}, \underline{z}^{'})$ is known too. The problem therefore is to find the Green's function $\mathcal{G}(\underline{z}, \underline{z}^{'})$ that satisfies (3.11). Rewriting (3.10) as:

$$-D^{\gamma} \cdot \triangle \rho^{\gamma} = \underline{j}^{I} \cdot \underline{n} \cdot \delta_{\partial I} \tag{3.18}$$

and comparing it with (3.13) shows:

$$\begin{aligned} L &= -D^{\gamma} \cdot \triangle && \text{(a)} \\ u(\underline{z}) &= \rho^{\gamma}(\underline{z}) && \text{(b)} \\ f(\underline{z}) &= \underline{j}^{I} \cdot \underline{n} \cdot \delta_{\partial I} && \text{(c)} \end{aligned} \tag{3.19}$$

Substituting (3.19a) in (3.11) gives:

$$-D^{\gamma} \cdot \triangle_{\underline{z}}\, \mathcal{G}(\underline{z}, \underline{z}^{'}) = \delta(\underline{z} - \underline{z}^{'}) \tag{3.20}$$

With (3.19a) and (3.19c), Equation (3.17) can be written as:

$$\rho^{\gamma}(\underline{z}) = \int\limits_I \mathcal{G}(\underline{z}, \underline{z}^{'}) \cdot \underline{j}^{I} \cdot \underline{n} \cdot \delta_{\partial I}\, \mathrm{d}V_{z'} = \int\limits_{\partial I} \mathcal{G}(\underline{z}, \underline{z}^{'}) \cdot \underline{j}^{I} \cdot \underline{n}\, \mathrm{d}V_{z'} \tag{3.21}$$

Using the divergence theorem [49], (3.21) changes to:

$$\rho^{\gamma}(\underline{z}) = \int\limits_{\partial I} \mathcal{G}(\underline{z}, \underline{z}^{'}) \cdot j_j^{I} \cdot n_j\, \mathrm{d}V_{z'} = \int\limits_I \frac{\partial}{\partial z_j^{'}} \left(\mathcal{G}(\underline{z}, \underline{z}^{'}) \right) j_j^{I}\, \mathrm{d}V_{z'} \tag{3.22}$$

Next, with the relation $\frac{\partial}{\partial z_j^{'}} \left(\mathcal{G}(\underline{z}, \underline{z}^{'}) \right) = -\frac{\partial}{\partial z_j} \left(\mathcal{G}(\underline{z}, \underline{z}^{'}) \right)$, one obtains:

$$\rho^{\gamma}(\underline{z}) = -\int\limits_I \frac{\partial}{\partial z_j} \left(\mathcal{G}(\underline{z}, \underline{z}^{'}) \right) j_j^{I}\, \mathrm{d}V_{z'} = -\frac{\partial}{\partial z_j} \left(\int\limits_I \mathcal{G}(\underline{z}, \underline{z}^{'})\, \mathrm{d}V_{z'} \right) j_j^{I} \tag{3.23}$$

An additional derivation gives the concentration gradient:

$$\frac{\partial}{\partial z_i} \left(\rho^{\gamma}(\underline{z}) \right) = -\frac{\partial^2}{\partial z_i \cdot \partial z_j} \left(\int\limits_I \mathcal{G}(\underline{z}, \underline{z}^{'})\, \mathrm{d}V_{z'} \right) j_j^{I} \tag{3.24}$$

which can be put in the form:

$$\underline{\operatorname{grad}}\, \rho^\gamma(\underline{z}) = \mathbb{P}(\underline{z}) \cdot \underline{j}^I \tag{3.25}$$

with:

$$P_{ij}(\underline{z}) = -\frac{\partial^2}{\partial z_i \cdot \partial z_j} \left(\int_I \mathcal{G}(\underline{z}, \underline{z}^{'})\, \mathrm{d}V_{z'} \right) \tag{3.26}$$

The solution (3.25) holds for $\underline{H} = 0$. However, since the problem (3.5) is linear with respect to $\underline{j}^I$ and $\underline{H}$, the concentration gradient $\underline{\operatorname{grad}}\, \rho^\gamma(\underline{z})$ in the general case ($\underline{H} \neq 0$) takes the form:

$$\underline{\operatorname{grad}}\, \rho^\gamma(\underline{z}) \quad = \quad \mathbb{P}(\underline{z}) \cdot \underline{j}^I + \underline{H} \tag{3.27}$$

In summary, provided that $\underline{j}^I$ is constant, the solution of Eshelby's inclusion problem (3.5) reduces to the determination of the expression of the $\mathbb{P}$-tensor defined by (3.26), which is shown next.

3.2.3 The second order $\mathbb{P}$-tensor

The presented derivation of the $\mathbb{P}$-tensor is based on isotropic diffusion behavior of the material at the microscale. Although the isotropic version of Fick's law applies here, it will turn out to be useful for multiscale homogenization to have an expression for the $\mathbb{P}$-tensor also for the case where the diffusion tensor at the microscale is anisotropic. Then the microscopic diffusive flux is related to the microscopic concentration gradient. Equation (3.3b) therefore changes to:

$$\underline{j}^\gamma = -\mathbb{D} \cdot \underline{\operatorname{grad}}\, \rho^\gamma \quad \text{with} \quad \mathbb{D} = D^\gamma_{ij}\, \underline{e}_i \otimes \underline{e}_j \tag{3.28}$$

With (3.28), Equation (3.20) for the Green's function changes to:

$$-D^\gamma_{ij} \cdot \mathcal{G}_{,ij}(\underline{z}, \underline{z}^{'}) = \delta(\underline{z} - \underline{z}^{'}) \tag{3.29}$$

where the subscripts $,i$ refers to the derivation with respect to z_i. A solution for the Green's function is obtained in the following. For a given value of $\underline{z}$ with $r = |\underline{z}|$, the following equation holds:

$$\frac{2 \cdot \pi}{r} = \int\limits_{|\underline{\xi}|=1} \delta(\underline{\xi} \cdot \underline{z})\, dS_\xi \tag{3.30}$$

Therein, integration is performed over the surface of the unit sphere, where $|\underline{\xi}| = 1$. In order to prove Equation (3.30), it is first re-formulated in spherical coordinates (see Figure 3.2). Then let $\underline{z}$ be parallel to the $\theta = 0$ axis. By substitution of $\zeta = \underline{\xi} \cdot \underline{z} = r \cdot \cos\, \theta$ on the right hand side of (3.30), the integral over the surface of the unit sphere can be evaluated:

$$\int\limits_{|\underline{\xi}|=1} \delta(\underline{\xi} \cdot \underline{z})\, \mathrm{d}S_\xi = \int\limits_0^{2\pi} \int\limits_0^{\pi} \delta(r \cdot \cos\, \theta)\, \mathrm{d}\theta\, \mathrm{d}\varphi = \int\limits_0^{2\pi} \mathrm{d}\varphi \int\limits_{-r}^{+r} \delta(\zeta)\, \frac{\mathrm{d}\zeta}{r} = \frac{2 \cdot \pi}{r} \tag{3.31}$$

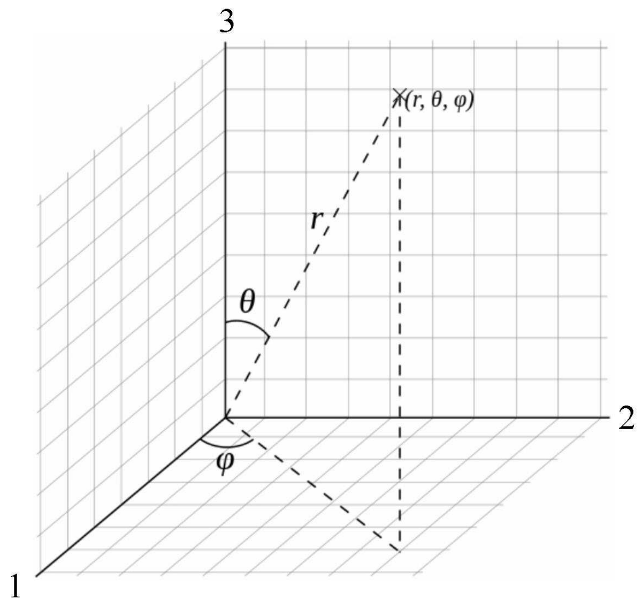

Figure 3.2: Spherical coordinate system

By use of the chain rule, it can be observed that:

$$\frac{\partial}{\partial z_i}\left(\delta(\underline{\xi} \cdot \underline{z})\right) = \xi_i \cdot \delta^{'}(\underline{\xi} \cdot \underline{z}) \tag{3.32}$$

where $\delta^{'}(\underline{\xi} \cdot \underline{z})$ denotes the first derivation of the Dirac delta function with respect to its argument $(\underline{\xi} \cdot \underline{z})$. Further, recalling that $\left|\underline{\xi}\right| = 1$, the Laplacian is taken of both sides in (3.31):

$$\delta(\underline{z}) = -\frac{1}{8 \cdot \pi^2} \int\limits_{\left|\underline{\xi}\right|=1} \delta^{''}(\underline{\xi} \cdot \underline{z})\, \mathrm{d}S_{\xi} \tag{3.33}$$

Inserting this result in (3.29) yields:

$$-D^{\gamma}_{kl} \cdot \mathcal{G}_{,kl}(\underline{z}, \underline{z}^{'}) = -\frac{1}{8 \cdot \pi^2} \int\limits_{\left|\underline{\xi}\right|=1} \delta^{''}(\underline{\xi} \cdot \underline{z} - \underline{\xi} \cdot \underline{z}^{'})\, \mathrm{d}S_{\xi} \tag{3.34}$$

For a given value of $\underline{\xi}$ on the unit sphere, relation (3.34) motivates a search for the solution $\mathcal{G}^{\xi}(\underline{z}, \underline{z}^{'})$ of:

$$D^{\gamma}_{kl} \cdot \mathcal{G}^{\xi}_{,kl}(\underline{z}, \underline{z}^{'}) = \delta^{''}(\underline{\xi} \cdot \underline{z} - \underline{\xi} \cdot \underline{z}^{'}) = \delta^{''}(\underline{\xi} \cdot (\underline{z} - \underline{z}^{'})) \tag{3.35}$$

An immediate solution is:

$$\mathcal{G}^{\xi}(\underline{z}, \underline{z}^{'}) = \delta(\underline{\xi} \cdot (\underline{z} - \underline{z}^{'})) \cdot (D^{\gamma}_{kl} \cdot \xi_k \cdot \xi_l)^{-1} \tag{3.36}$$

By superposition of (3.34) and (3.36), one obtains the Green's function in the form:

$$\mathcal{G}(\underline{z}, \underline{z}^{'}) = \frac{1}{8 \cdot \pi^2} \int\limits_{\left|\underline{\xi}\right|=1} \delta(\underline{\xi} \cdot (\underline{z} - \underline{z}^{'})) \cdot (D^{\gamma}_{kl} \cdot \xi_k \cdot \xi_l)^{-1}\, \mathrm{d}S_{\xi} \tag{3.37}$$

Now the components of the $\mathbb{P}$-tensor can be derived. Substituting:

$$\frac{\partial^2}{\partial z_i \cdot \partial z_j}\mathcal{G}(\underline{z}, \underline{z}^{'}) = \frac{1}{8 \cdot \pi^2} \int\limits_{|\underline{\xi}|=1} \xi_i \cdot \xi_j \cdot \delta^{''}(\underline{\xi} \cdot (\underline{z} - \underline{z}^{'}))\, (D^{\gamma}_{kl} \cdot \xi_k \cdot \xi_l)^{-1} \, \mathrm{d}S_{\xi} \tag{3.38}$$

in (3.26) yields:

$$\begin{aligned} P_{ij}(\underline{z}) &= -\frac{1}{8 \cdot \pi^2} \int\limits_{I} \int\limits_{|\underline{\xi}|=1} \xi_i \cdot \xi_j \cdot \delta^{''}(\underline{\xi} \cdot (\underline{z} - \underline{z}^{'}))\, (D^{\gamma}_{kl} \cdot \xi_k \cdot \xi_l)^{-1} \, \mathrm{d}S_{\xi}\, \mathrm{d}V_{z'} = && (3.39) \\ &= -\frac{1}{8 \cdot \pi^2} \int\limits_{|\underline{\xi}|=1} \xi_i \cdot \xi_j \cdot (D^{\gamma}_{kl} \cdot \xi_k \cdot \xi_l)^{-1} \left(\int\limits_{I} \delta^{''}(\underline{\xi} \cdot (\underline{z} - \underline{z}^{'}))\, \mathrm{d}V_{z'} \right) \mathrm{d}S_{\xi} && (3.40) \end{aligned}$$

What is still missing is to determine the value of the integral over I in (3.40). For this purpose, the function $\mathcal{I}(\zeta)$ and its second derivative $\mathcal{I}''(\zeta)$ with respect to ζ, which depend on the shape of the inclusion I (for example spherical or ellipsoidal inclusions), are introduced:

$$\mathcal{I}^{''}(\zeta) = \int\limits_{I} \delta^{''}(\zeta - \underline{\xi} \cdot \underline{z}^{'})\, \mathrm{d}V_{z'} \quad \text{with} \quad \mathcal{I}(\zeta) = \int\limits_{I} \delta(\zeta - \underline{\xi} \cdot \underline{z}^{'})\, \mathrm{d}V_{z'} \tag{3.41}$$

Equation (3.40) thus can be recast in the form:

$$P_{ij}(\underline{z}) = -\frac{1}{8 \cdot \pi^2} \int\limits_{|\underline{\xi}|=1} \xi_i \cdot \xi_j \cdot (D^{\gamma}_{kl} \cdot \xi_k \cdot \xi_l)^{-1}\, \mathcal{I}^{''}(\underline{\xi} \cdot \underline{z})\, \mathrm{d}S_{\xi} \tag{3.42}$$

Expression (3.42) provides a relation for the components of the $\mathbb{P}$-tensor, which is particularly efficient for numerical implementation. For the application to wood, the case of an ellipsoidal inclusion shape is considered. In order to simplify the integration over the volume of the inclusion, this ellipsoid is mapped onto a unit sphere:

$$\underline{z} \rightarrow \underline{\hat{z}} \tag{3.43}$$

by:

$$\hat{z}_i = \frac{z_i}{a_i} \quad \text{and} \quad z_i = \hat{z}_i \cdot a_i \tag{3.44}$$

where a_i, $i = 1, 2, 3$, denote the radii of the ellipsoid. The differential volume dV_z thus changes to:

$$\begin{aligned} \mathrm{d}V_z &= \mathrm{d}z_1 \cdot \mathrm{d}z_2 \cdot \mathrm{d}z_3 = \\ &= \mathrm{d}\hat{z}_1 \cdot a_1 \cdot \mathrm{d}\hat{z}_2 \cdot a_2 \cdot \mathrm{d}\hat{z}_3 \cdot a_3 = \\ &= \mathrm{d}V_{\hat{z}} \cdot a_1 \cdot a_2 \cdot a_3 \end{aligned} \tag{3.45}$$

Further, also $\underline{\xi}$ has to be transformed by an inverse map to:

$$\underline{\xi} \rightarrow \underline{\hat{\xi}} \tag{3.46}$$

with:

$$\hat{\xi}_i = \xi_i \cdot \frac{z_i}{\hat{z}_i} = \xi_i \cdot \frac{z_i \cdot a_i}{z_i} = \xi_i \cdot a_i \tag{3.47}$$

$$\xi_i = \frac{\hat{\xi}_i}{a_i} \tag{3.48}$$

Applying (3.44) and (3.48) to (3.41) yields:

$$\begin{aligned} \mathcal{I}(\underline{\xi} \cdot \underline{z}) &= \int\limits_I \delta(\underline{\xi} \cdot \underline{z} - \underline{\xi} \cdot \underline{z}^{'})\,\mathrm{d}V_z = \\ &= \int\limits_I \delta(\underline{\xi} \cdot (\underline{z} - \underline{z}^{'})\,\mathrm{d}V_z = \\ &= \int\limits_S \delta(\frac{\hat{\xi}_i}{a_i} \cdot ((\hat{z}_i \cdot a_i - \hat{z}_i^{'} \cdot a_i)) \cdot a_1 \cdot a_2 \cdot a_3\,\mathrm{d}V_{\hat{z}} = \\ &= a_1 \cdot a_2 \cdot a_3 \cdot \int\limits_S \delta(\hat{\xi}_i \cdot \hat{z}_i - \hat{\xi}_i \cdot \hat{z}_i^{'})\,dV_{\hat{z}} = \\ &= a_1 \cdot a_2 \cdot a_3 \cdot \mathcal{I}(\hat{\zeta}) \end{aligned} \tag{3.49}$$

Now $\mathcal{I}(\hat{\zeta})$ represents a spherical inclusion $S(O, a)$ with radius a and the origin O. $(\hat{r}^{'}, \hat{\theta}^{'}, \hat{\varphi}^{'})$ denote the spherical coordinates of $\underline{\hat{z}}^{'}$ in $S(O, a)$. $\mathcal{I}(\hat{\zeta})$ does not depend on the orientation of the unit vector $\underline{\hat{\xi}}$. It is therefore possible to assume that $\underline{\hat{\xi}}$ is parallel to the $\hat{\theta}^{'} = 0$ axis, so that $\underline{\hat{\xi}} \cdot \underline{\hat{z}}^{'} = \hat{r}^{'} \cdot \cos\hat{\theta}$. By using the substitution $\hat{\zeta}^{'} = \hat{\zeta} - \hat{r}^{'} \cdot \cos\hat{\theta}^{'}$ the term $\mathcal{I}(\hat{\zeta})$ converts to:

$$\begin{aligned} \mathcal{I}(\hat{\zeta}) &= \int\limits_0^{2\pi}\int\limits_0^{a}\int\limits_0^{\pi} \delta(\hat{\xi}_i \cdot \hat{z}_i - \hat{\xi}_i \cdot \hat{z}_i^{'})\,\mathrm{d}\hat{\theta}^{'}\,\mathrm{d}\hat{r}^{'}\,\mathrm{d}\hat{\varphi}^{'} = \\ &= \int\limits_0^{2\pi}\int\limits_0^{a}\int\limits_0^{\pi} \delta(\hat{\zeta} - \hat{r}^{'} \cdot \cos\hat{\theta}^{'})\,\mathrm{d}\hat{\theta}^{'}\,\mathrm{d}\hat{r}^{'}\,\mathrm{d}\hat{\varphi}^{'} = \\ &= \int\limits_0^{2\pi}\int\limits_0^{a}\int\limits_0^{\pi} \delta(\hat{\zeta}^{'})\,\mathrm{d}\hat{\theta}^{'}\,\mathrm{d}\hat{r}^{'}\,\mathrm{d}\hat{\varphi}^{'} = \\ &= \int\limits_0^{2\pi}\int\limits_0^{a}\int\limits_{\hat{\zeta}-\hat{r}^{'}}^{\hat{\zeta}+\hat{r}^{'}} \hat{r}^{'}\,\delta(\hat{\zeta}^{'})\,\mathrm{d}\hat{\zeta}^{'}\,\mathrm{d}\hat{r}^{'}\,\mathrm{d}\hat{\varphi}^{'} = \\ &= \int\limits_0^{2\pi}\mathrm{d}\hat{\varphi}^{'}\int\limits_0^{a}\hat{r}^{'}\,\mathrm{d}\hat{r}^{'}\int\limits_{\hat{\zeta}-\hat{r}^{'}}^{\hat{\zeta}+\hat{r}^{'}} \delta(\hat{\zeta}^{'})\,\mathrm{d}\hat{\zeta}^{'} \end{aligned} \tag{3.50}$$

For the case that $\left|\hat{\zeta}\right| < a$, this yields:

$$\mathcal{I}(\hat{\zeta}) = \int\limits_{0}^{2\pi} \mathrm{d}\hat{\varphi}' \int\limits_{|\hat{\zeta}|}^{a} \hat{r}' \, \mathrm{d}\hat{r}' = \pi \cdot \left(a^2 - \hat{\zeta}^2\right) \quad \Rightarrow \quad \mathcal{I}''(\hat{\zeta}) = -2 \cdot \pi \tag{3.51}$$

which together with (3.49) gives:

$$\forall \hat{\underline{z}} \in I = S(O, a) \qquad \mathcal{I}''(\underline{\xi} \cdot \underline{z}) = -a_1 \cdot a_2 \cdot a_3 \cdot 2 \cdot \pi \tag{3.52}$$

Finally, returning to (3.42), the $\mathbb{P}$-tensor for ellipsoidal inclusions can be calculated as:

$$P_{ell,ij}(\underline{z}) = \frac{1}{4 \cdot \pi} \cdot a_1 \cdot a_2 \cdot a_3 \int\limits_{|\underline{\xi}|=1} \xi_i \cdot \xi_j \cdot \left(D^{\gamma}_{kl} \cdot \xi_k \cdot \xi_l\right)^{-1} \mathrm{d}S_\xi \tag{3.53}$$

A further simplification is possible: First, a transformation to the unit sphere is performed, whose coordinates are then expressed in spherical coordinates (see Figure 3.2). With

$$\sin \hat{\theta} = \sqrt{1 - \left(\cos \hat{\theta}\right)^2} = \sqrt{1 - \left(\hat{\xi}_3\right)^2} \tag{3.54}$$

and $\hat{r} = 1$, the values for $\hat{\xi}_i$ can be calculated as follows:

$$\begin{aligned} \hat{\xi}_1 &= \hat{r} \cdot \sin \hat{\theta} \cdot \cos \hat{\varphi} = \sin \hat{\theta} \cdot \cos \hat{\varphi} = \sqrt{1 - \left(\hat{\xi}_3\right)^2} \cdot \cos \hat{\varphi} \\ \hat{\xi}_2 &= \hat{r} \cdot \sin \hat{\theta} \cdot \sin \hat{\varphi} = \sin \hat{\theta} \cdot \sin \hat{\varphi} = \sqrt{1 - \left(\hat{\xi}_3\right)^2} \cdot \sin \hat{\varphi} \\ \hat{\xi}_3 &= \hat{r} \cdot \cos \hat{\theta} = \cos \hat{\theta} = \hat{\xi}_3 \end{aligned} \tag{3.55}$$

The values of ξ_i are therefore:

$$\begin{aligned} \xi_1 &= \frac{\hat{\xi}_1}{a_1} = \frac{\sqrt{1 - \hat{\xi}_3^2} \cdot \cos \hat{\varphi}}{a_1} \\ \xi_2 &= \frac{\hat{\xi}_2}{a_2} = \frac{\sqrt{1 - \hat{\xi}_3^2} \cdot \sin \hat{\varphi}}{a_2} \\ \xi_3 &= \frac{\hat{\xi}_3}{a_3} \end{aligned} \tag{3.56}$$

By use of the matrix notation for the cross product with the unit vectors $\hat{\underline{\xi}}_1$, $\hat{\underline{\xi}}_2$ and $\hat{\underline{\xi}}_3$, the differential $\mathrm{d}S_\xi$ can be expressed as:

$$\mathrm{d}S_\xi = \mathrm{d}\underline{\xi}_{\mathrm{I}} \times \mathrm{d}\underline{\xi}_{\mathrm{II}} = \frac{\mathrm{d}\hat{\underline{\xi}}_{\mathrm{I}} \times \mathrm{d}\hat{\underline{\xi}}_{\mathrm{II}}}{a_1 \cdot a_2 \cdot a_3} = \frac{\mathrm{d}S_{\hat{\xi}}}{a_1 \cdot a_2 \cdot a_3} \tag{3.57}$$

With (3.57), Equation (3.53) can therefore be written as:

$$P_{ell,ij}(\underline{z}) = \frac{1}{4\cdot\pi} \int\limits_{|\underline{\xi}|=1} \xi_i \cdot \xi_j \cdot \left(D^{\gamma}_{kl} \cdot \xi_k \cdot \xi_l\right)^{-1} \, \mathrm{d}S_{\underline{\xi}} \tag{3.58}$$

By use of the values of ξ_i according to Equation (3.56) as functions of $\hat{\varphi}$ and $\hat{\xi}_3$, the components of the $\mathbb{P}$-tensor for ellipsoidal inclusion shape can be calculated as following:

$$P_{ell,ij}(\underline{z}) = \frac{1}{4\cdot\pi} \int\limits_{-1}^{+1} \int\limits_{0}^{2\pi} \xi_i \cdot \xi_j \cdot \left(D^{\gamma}_{kl} \cdot \xi_k \cdot \xi_l\right)^{-1} \, \mathrm{d}\hat{\varphi} \, \mathrm{d}\hat{\xi}_3 \tag{3.59}$$

3.3 Application of the homogenization scheme to wood

In this section the homogenization model developed in the previous sections will be applied to wood. According to Chapter 2, five levels of organization may be distinguished. For each of the hierarchical levels of wood homogenization techniques can be used to gain input parameters for the next higher level. So the overall macroscopic behavior can be derived with a multistep homogenization model from the behavior of elementary constituents of wood at the molecular level. This strategy pursued in the micromechanical model for wood [15] can also be applied to the modeling of transport processes, for example heat conduction or water vapor diffusion. This diploma thesis focuses on the homogenization step at the cell level, starting from given input values for the cell walls and the lumens. For comparability with measured values, another simplified homogenization step is performed in order to take the variation of the density and the cell shape between latewood and earlywood into account. Further refinement of the model is possible by introducing homogenization steps also at the other levels described before.

The main task of this diploma thesis is therefore to determine overall transport properties for a wood tissue from corresponding values for lumens and cell walls. This homogenization procedure is done by means of the Mori-Tanaka scheme (see Equation (3.1)), with the cell wall material as matrix material and the lumens as ellipsoidal inclusions. What remains to be specified is an equation for the $\mathbb{P}$-tensor for ellipsoidal inclusions — it is derived in Section 3.2. To check the results of this homogenization method, the results are compared with corresponding values obtained by means of the unit cell method as described in Chapter 4.

3.3.1 Calculation of the geometric parameters

For the calculation of the $\mathbb{P}$-tensor for the cell assembly of wood and, thereon, the homogenized diffusion tensor, geometric parameters of the cell structure are needed.

The volume fractions

Since there are two phases (cell walls and lumens) used in the homogenization step, their volume fractions ($f_{cellwall}$ and f_{lumen}) have to be specified. The volume fraction of the cell walls can be calculated as the ratio of the specific oven-dry wood density $\varrho_{ovendry}$ to the density of the oven-dry cell walls ϱ_0. The latter density can be taken as $1530\,\mathrm{kg/m^3}$ according to Siau [31]. The volume fraction of the cell walls therefore is:

$$f_{cellwall} = \frac{\varrho_{ovendry}}{\varrho_0} \tag{3.60}$$

The volume fraction of the lumens is the difference to 100 %:

$$f_{lumen} = 1 - f_{cellwall} \tag{3.61}$$

The cell dimensions

Turner [36] developed a model for the average tracheid shape depending on the local density. Because of the alignment of the cells in radial direction, the tangential dimension is chosen as a constant value with:

$$a_{tang} = 50 \cdot 10^{-6}\,\mathrm{m} \tag{3.62}$$

The length of the tracheids is also required for the evaluation of the longitudinal diffusivity. Tracheids in softwood have lengths between 3 and 5 mm [37]. Because of overlapping, the mean distance between two consecutive tracheids is less. The value used for the tracheid dimension in longitudinal direction is:

$$a_{long} = 1.8 \cdot 10^{-3}\,\mathrm{m} \tag{3.63}$$

The radial dimension of a tracheid, a_{rad}, varies according to the position within the annual ring and, thus, with density. Turner [36] assumes this variation to be linear. Assuming that $a_{rad,200} = 50 \cdot 10^{-6}$ m at $\varrho_{ovendry} = 200$ kg/m^3 and $a_{rad,1000} = 20 \cdot 10^{-6}$ m at $\varrho_{ovendry} = 1000$ kg/m^3, the radial dimension can be calculated as:

$$c_1 = \frac{1}{1000\,\mathrm{kg/m^3} - 200\,\mathrm{kg/m^3}} \left(a_{rad,1000}\,[\mathrm{m}] - a_{rad,200}\,[\mathrm{m}]\right) \tag{3.64}$$

$$c_2 = a_{rad,200}\,[\mathrm{m}] - c_1 \cdot 200\,\mathrm{kg/m^3} \tag{3.65}$$

$$a_{rad} = c_2 + c_1 \cdot \varrho_{ovendry}\,[\mathrm{kg/m^3}] \tag{3.66}$$

Based on the radial and tangential dimensions and the volume fraction of the cell wall, the cell wall thickness can be calculated by solving the following equation for $a_{cellwall}$:

$$f_{cellwall} = 1 - \frac{\left(a_{rad} - 2 \cdot a_{cellwall}\right)\left(a_{tang} - 2 \cdot a_{cellwall}\right)}{a_{rad} \cdot a_{tang}} \tag{3.67}$$

In the following, the lumens are considered as ellipsoidal inclusions. For their calculation the three principal ellipsoidal radii are needed:

$$2 \cdot a_1 = a_{rad} - 2 \cdot a_{cellwall} \tag{3.68}$$

$$2 \cdot a_2 = a_{tang} - 2 \cdot a_{cellwall} \tag{3.69}$$

$$2 \cdot a_3 = a_{long} \tag{3.70}$$

With these values the further calculations can be accomplished.

3.3.2 Homogenization step 1: Diffusion coefficients of the cell assembly

Now the developed equations are assembled for use in the homogenization step described in Section 3.2. At first the volume fractions and the dimensions of the lumens are calculated as shown in the previous Section 3.3.1. Next the components of the $\mathbb{P}$-tensor are calculated by Equations (3.56), and (3.59):

$$P_{ell,ij}(\underline{z}) = \frac{1}{4\cdot\pi}\int_{-1}^{+1}\int_{0}^{2\pi} \xi_i \cdot \xi_j \cdot \left(D^{\gamma}_{kl}\cdot\xi_k\cdot\xi_l\right)^{-1}\,\mathrm{d}\hat{\varphi}\,\mathrm{d}\hat{\xi}_3 \tag{3.71}$$

with

$$\begin{aligned} \xi_1 &= \frac{\hat{\xi}_1}{a_1} = \frac{\sqrt{1-\hat{\xi}_3^2}\cdot\cos\hat{\varphi}}{a_1} \\ \xi_2 &= \frac{\hat{\xi}_2}{a_2} = \frac{\sqrt{1-\hat{\xi}_3^2}\cdot\sin\hat{\varphi}}{a_2} \\ \xi_3 &= \frac{\hat{\xi}_3}{a_3} = \frac{\hat{\xi}_3}{a_3} \end{aligned} \tag{3.72}$$

Specifying Equation (3.1) for two phases, namely the cell walls and lumens, and choosing the cell walls as matrix material, the Mori-Tanaka scheme takes the form:

$$\mathbb{D}_{hom1} = \frac{f_{cellwall}\cdot\mathbb{D}_{cellwall} + f_{lumen}\cdot\mathbb{D}_{lumen}\cdot\left[\mathbb{I}+\mathbb{P}_{ell}\cdot(\mathbb{D}_{lumen}-\mathbb{D}_{cellwall})\right]^{-1}}{f_{cellwall}\cdot\mathbb{I} + f_{lumen}\cdot\left[\mathbb{I}+\mathbb{P}_{ell}\cdot(\mathbb{D}_{lumen}-\mathbb{D}_{cellwall})\right]^{-1}} \tag{3.73}$$

$$\mathbb{D}_{hom1} = \begin{bmatrix} D_{hom1,rad} & 0 & 0 \\ 0 & D_{hom1,tang} & 0 \\ 0 & 0 & D_{hom1,long} \end{bmatrix} \tag{3.74}$$

with $\mathbb{I}$ denoting the second order unity tensor, and $f_{cellwall}$ and f_{lumen} the volume fractions of cell walls and lumens. $\mathbb{D}_{hom1}$ is the homogenized diffusion tensor of the cell matrix for a constant density, with components for the radial, tangential, and longitudinal direction.

3.3.3 Homogenization Step 2: Diffusion coefficients of a whole sample

$\mathbb{D}_{hom1}$ is the homogenized diffusion tensor of the cell matrix for a constant density. Because of the density variation within the annual rings, a second homogenization step is needed to allow comparison with measured values. The actually continuous density distribution over an annual ring was approximated by two sections with constant density: $\rho_{earlywood}$ as average density of earlywood and $\rho_{latewood}$ as average density of latewood. For a given value of density $\rho_{ovendry}$, the volume fractions of earlywood and latewood can be calculated as follows:

$$f_{earlywood} = \frac{\varrho_{ovendry} - \varrho_{earlywood}}{\varrho_{earlywood} - \varrho_{latewood}} \tag{3.75}$$

$$f_{latewood} = 1 - f_{earlywood} \tag{3.76}$$

In longitudinal and tangential direction earlywood and latewood are arranged in parallel, while they are arranged in series in the radial direction. Therefore, with a grading in only two densities, the homogenized diffusion tensor for a whole wood sample can be written as:

$$D_{hom2,rad} = \left(\frac{f_{earlywood}}{D_{hom1,rad,earlywood}} + \frac{f_{latewood}}{D_{hom1,rad,latewood}} \right)^{-1} \tag{3.77}$$

$$D_{hom2,tang} = D_{hom1,tang,earlywood} \cdot f_{earlywood} + D_{hom1,tang,latewood} \cdot f_{latewood} \tag{3.78}$$

$$D_{hom2,long} = D_{hom1,long,earlywood} \cdot f_{earlywood} + D_{hom1,long,latewood} \cdot f_{latewood} \tag{3.79}$$

$$\mathbb{D}_{hom2} = \begin{bmatrix} D_{hom2,rad} & 0 & 0 \\ 0 & D_{hom2,tang} & 0 \\ 0 & 0 & D_{hom2,long} \end{bmatrix} \tag{3.80}$$

Chapter 4

The unit cell method

To evaluate the homogenization scheme developed in the previous chapter, a test series with different volume fractions and diffusivity ratios of cell walls and cell lumens, respectively, was made. The resulting effective conductivities were compared to corresponding values computed with the unit cell method, an alternative homogenization method.

4.1 Introduction

Unit cell computational homogenization methods typically involve constructing a continuum model of a periodic material microstructure with uniform repeating basic elements, so-called unit cells (see Figure 4.1). After that a predefined macroscopic flux or imposed concentration gradient is applied to this element. By solving the resulting boundary value problem, the unit cell method provides a link between the properties of the microstructure and those of the macrostructure. The relation between the overall flux and the concentration gradient on the boundary of the unit cell yields an effective diffusion coefficient of the material.

For simple microstructures the unit cell problem can sometimes be solved analytically, but often only a numerical solution is possible. The method used for this diploma thesis was the finite element method (FEM). The computations were done by the FEM-program Abaqus Version 6.7-3.

Similar to mechanical investigations, the unit cell method provides different results for the effective material properties depending on the type of boundary conditions. Applying a constant concentration gradient in terms of a constant concentration on one side of the unit cell, and a different but also constant concentration on the other side results in an overestimation of the homogenized diffusion coefficient. On the other hand, when a constant flux is applied, the homogenized diffusion coefficient will be somewhat too low. However, these two methods can be used to calculate strict upper and lower bounds for the real diffusion coefficient. In most cases the result gained by applying constant

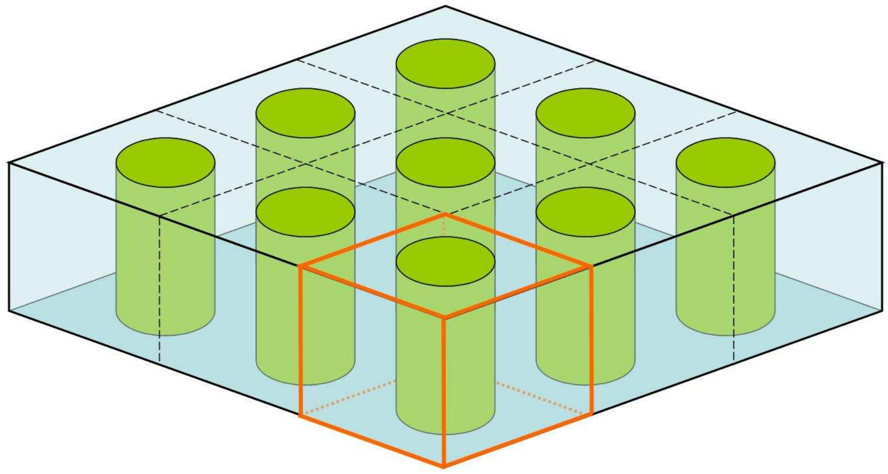

Figure 4.1: Periodic material microstructure with unit cell

concentration is closer to the real result. The best results can be gained by use of periodic boundary conditions for both the flux and the concentration gradient. Because of their complexity (a further computer program is needed to calculate the required couplings of degrees of freedom of the FEM model), in this diploma thesis only the first two types of boundary conditions were used to calculate bounds. They are accurate enough to compare the behavior of the two homogenization schemes based on microscale continuum modeling and the unit cell method, respectively.

4.2 Basics of the comparison

To check the different behaviors of the Mori-Tanaka scheme and the unit cell method at varied conditions, several numerical test series were made. To investigate the influence of volume fractions and cell dimensions, one series was made for a sample of earlywood ($\varrho_{ovendry} = 200\text{kg/m}^3$) and another series for a sample of latewood ($\varrho_{ovendry=1000}\text{kg/m}^3$). The effect of different ratios of the diffusion coefficients of cell walls and lumens, respectively, was checked by three varied diffusivity ratios that are typical of transport processes in wood (Table 4.1):

$D_{cellwall}$	D_{lumen}	appearance in transport processes
1	10	water diffusion
1	100	water diffusion
10	1	heat conduction

Table 4.1: Diffusion coefficient ratios used in the comparison of the homogenization models

For these six different conditions (two geometries and three ratios) the diffusion coefficients for the three principal material directions of wood were calculated and compared.

4.3 Comparison 1: The unit cell for earlywood

4.3.1 Dimensions of the unit cell

The first comparison was made for a sample of earlywood with a density of $\varrho_{ovendry} = 200\,\mathrm{kg/m^3}$. According to Subsection 3.3.1 the volume fractions and cell dimensions were set to:

$$\begin{array}{lcll} f_{cellwall} & = & 0.130719 & \text{(a)} \\ f_{lumen} & = & 0.869281 & \text{(b)} \\ a_{rad} & = & 50 \cdot 10^{-6}\,\mathrm{m} & \text{(c)} \\ a_{tang} & = & 50 \cdot 10^{-6}\,\mathrm{m} & \text{(d)} \\ a_{long} & = & 3000 \cdot 10^{-6}\,\mathrm{m} & \text{(e)} \end{array} \tag{4.1}$$

The calculation was made by one unit cell for the transversal direction and one for the longitudinal direction, in order to optimize the computational effort. Because of the negligible influence of the cell tails in the transversal directions (about $\pm 0,5\,\%$), the transversal diffusivity can be described by a 2-dimensional model. According to an existing unit cell model for the cell matrix of wood [15], the angle between radial and tangential cell walls was chosen as 70°. Because of the tapered ends of the tracheids in longitudinal direction, an angle of 20° is chosen for the separating cell wall. The resulting geometries of the unit cells for softwood are shown in Figures 4.2 and 4.3.

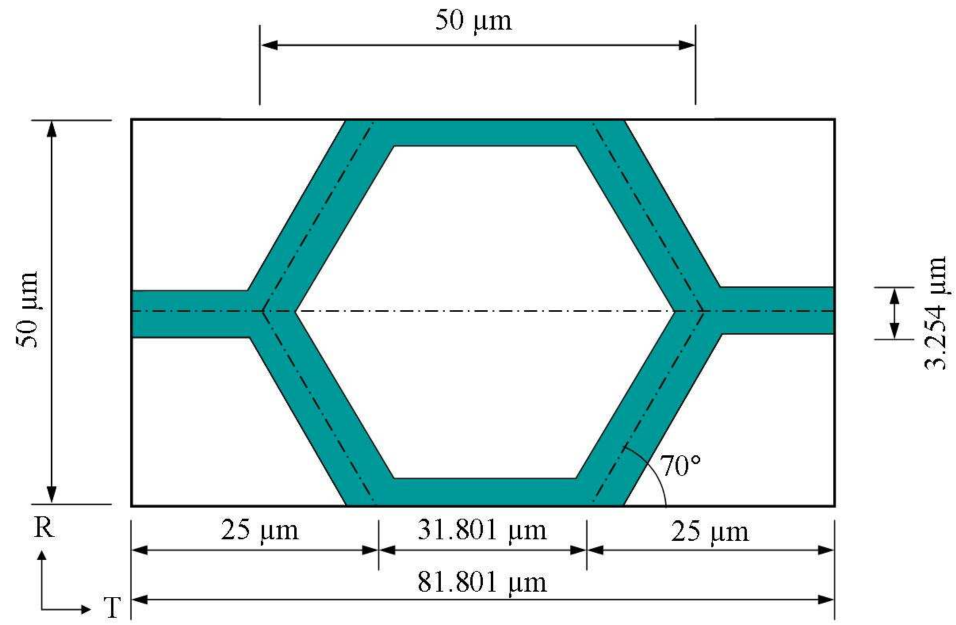

Figure 4.2: Geometry of the transversal unit cell for earlywood

4.3.2 Results and comparison

The results of the calculations are assembled in Table 4.2. As can be seen, the two homogenization models agree quite well. The higher deviations at ratio 1 : 100 of the diffusivities of

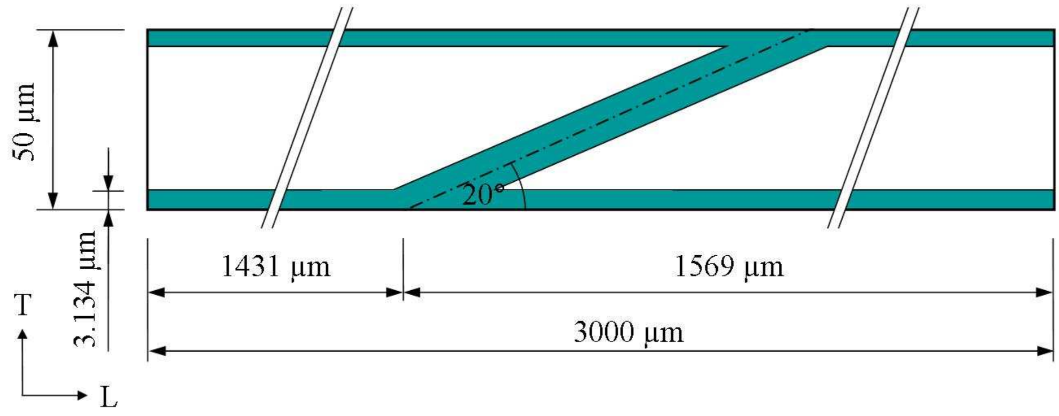

Figure 4.3: Geometry of the longitudinal unit cell for earlywood

cell wall and lumen, respectively, can be explained by the different geometries (ellipsoidal cross section of the inclusions in the Mori-Tanaka scheme compared with hexagonal cross section of the inclusions in the unit cell method).

Homogenization method	$D_{cellwall}$ m^2/s	D_{lumen} m^2/s	$D_{hom,rad}$ m^2/s	$D_{hom,tang}$ m^2/s	$D_{hom,long}$ m^2/s
Mori-Tanaka scheme	1	10	5.9300	5.9300	8.8029
Unit cell, constant flux	1	10	6.0949	5.7183	8.7491
			+2.78 %	−3.57 %	−0.61 %
Unit cell, constant concentration	1	10	6.1718	5.7574	8.7634
			+4.08 %	−2.91 %	−0.45 %
Mori-Tanaka scheme	1	100	12.5421	12.5421	84.6269
Unit cell, constant flux	1	100	13.7227	11.5027	79.7829
			+9.41 %	−8.29 %	−5.72 %
Unit cell, constant concentration	1	100	14.0567	11.6628	80.9773
			+12.08 %	−7.01 %	−4.31 %
Mori-Tanaka scheme	10	1	1.6887	1.6887	2.1744
Unit cell, constant flux	10	1	1.6083	1.3740	2.1462
			−4.76 %	−18.64 %	−1.30 %
Unit cell, constant concentration	10	1	1.7386	1.6222	2.1560
			+4.99 %	−3.94 %	−0.85 %

Table 4.2: Comparison of unit cell method to Mori-Tanaka scheme, $\varrho_{ovendry} = 200\,\mathrm{kg/m^3}$

4.4 Comparison 2: The unit cell for latewood

4.4.1 Dimensions of the unit cell

The second comparison was made for a sample of latewood with a density of $\rho_{ovendry} = 1000\,\mathrm{kg/m^3}$. Again according to Subsection 3.3.1 the volume fractions and cell dimensions were calculated as:

$$
\begin{aligned}
f_{cellwall} &= 0.653595 && \text{(a)} \\
f_{lumen} &= 0.346405 && \text{(b)} \\
a_{rad} &= 20 \cdot 10^{-6}\,\mathrm{m} && \text{(c)} \\
a_{tang} &= 50 \cdot 10^{-6}\,\mathrm{m} && \text{(d)} \\
a_{long} &= 3000 \cdot 10^{-6}\,\mathrm{m} && \text{(e)}
\end{aligned}
\qquad (4.2)
$$

Similar to the calculation for softwood two 2-dimensional unit cells for the transversal and the longitudinal direction were used. Using the same angles between radial and tangential cell walls (70°) and for the tapered ends (20°) results in the geometries of the unit cells for latewood shown in Figures 4.4 and 4.5.

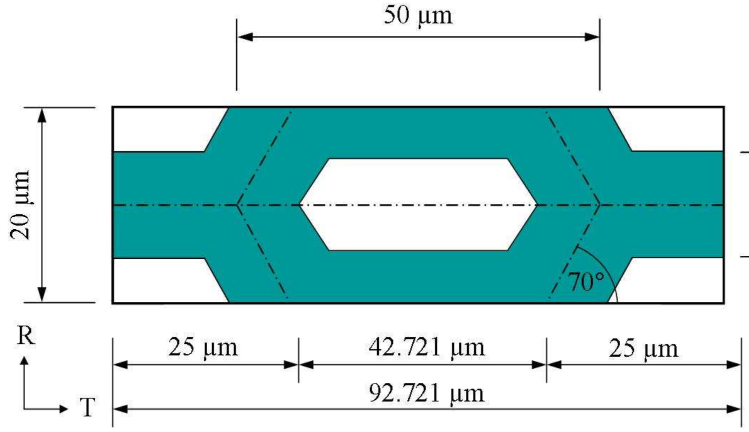

Figure 4.4: Geometry of the transversal unit cell for latewood

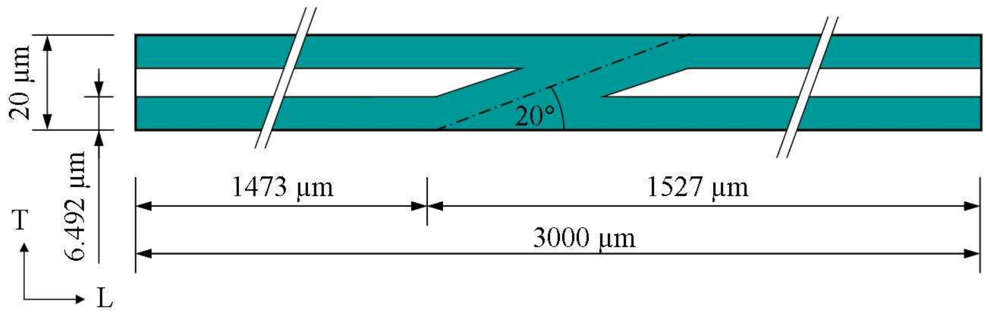

Figure 4.5: Geometry of the longitudinal unit cell for latewood

4.4.2 Results and comparison

The results of the calculations are assembled in Table 4.3. Like for softwood, also the results for latewood obtained with the two homogenization methods agree well, especially for the case of a constant concentration gradient used in the calculation of the unit cell. The comparisons for both earlywood and latewood depict the similarity of the two homogenization models. Differences can be explained by the different inclusion geometries (ellipsoidal and hexagonal), which are both abstractions of the real structure of wood.

The advantage of the Mori-Tanaka scheme over the unit cell method is the simple adaptivity to different geometries because of the analytical formulation of this scheme. When using the fully parametrized Mori-Tanaka scheme, a change in geometry can be easily taken into account by changing the geometrical parameters, while the use of the unit cell method requires the generation of a completely new unit cell.

Homogenization method	$D_{cellwall}$ m^2/s	D_{lumen} m^2/s	$D_{hom,rad}$ m^2/s	$D_{hom,tang}$ m^2/s	$D_{hom,long}$ m^2/s
Mori-Tanaka scheme	1	10	1.5389	2.4886	4.1098
Unit cell, constant flux	1	10	1.5378 −0.07 %	2.3364 −6.12 %	4.0059 −2.53 %
Unit cell, constant concentration	1	10	1.5583 +1.26 %	2.4616 −1.08 %	4.0228 −2.12 %
Mori-Tanaka scheme	1	100	1.6393	3.6302	34.3671
Unit cell, constant flux	1	100	1.6465 +0.72 %	3.2245 −11.18 %	26.0952 −23.46 %
Unit cell, constant concentration	1	100	1.6732 +2.07 %	3.5980 −0.89 %	27.1823 −20.91 %
Mori-Tanaka scheme	10	1	4.0213	6.4992	6.8816
Unit cell, constant flux	10	1	3.1893 −20.69 %	5.8074 −10.64 %	6.8592 −3.26 %
Unit cell, constant concentration	10	1	4.1059 +2.10 %	6.4539 −0.70 %	6.8698 −0.17 %

Table 4.3: Comparison of unit cell method to Mori-Tanaka scheme, $\rho_{ovendry} = 1000\,\mathrm{kg/m^3}$

4.5 Further results of the unit cell method

Since the unit cell method resolves the microscopic flux and concentration fields, and the calculation is done by a FEM-program with many graphical illustration facilities, further insight into the diffusion processes on the cell level can be gained.

Figures 4.6 and 4.7 show the concentration distribution and the resulting fluxes in radial direction for the earlywood unit cell and a diffusivity ratio of 10 : 1. This ratio appears in heat transfer modeling.

Figures 4.8 and 4.9 show the concentration distribution and the resulting fluxes in tangential direction for the latewood unit cell and a diffusivity ratio of 1 : 10. Figure 4.8 also depicts the mesh of the used FEM-model.

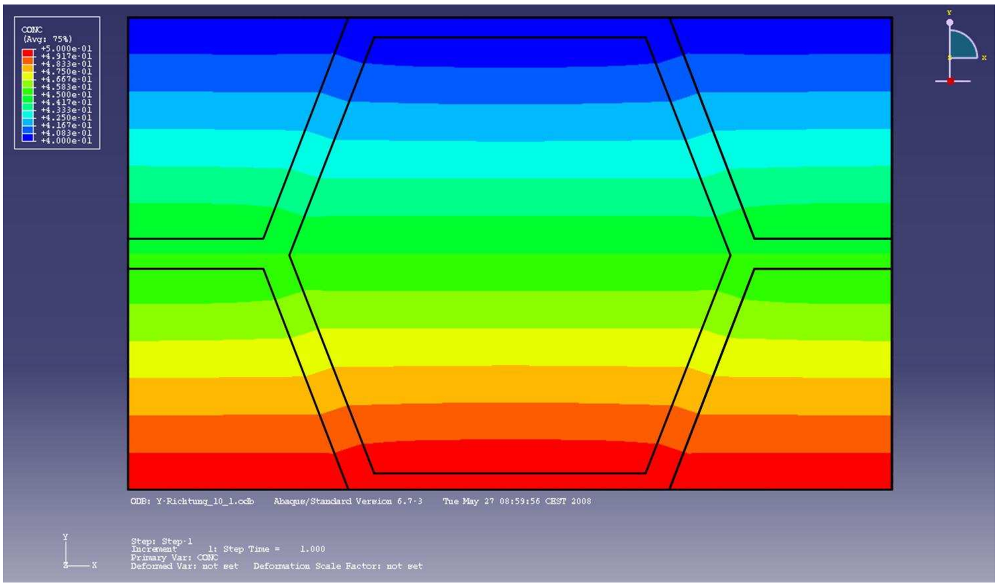

Figure 4.6: Temperature distribution in earlywood resulting from a radial temperature gradient

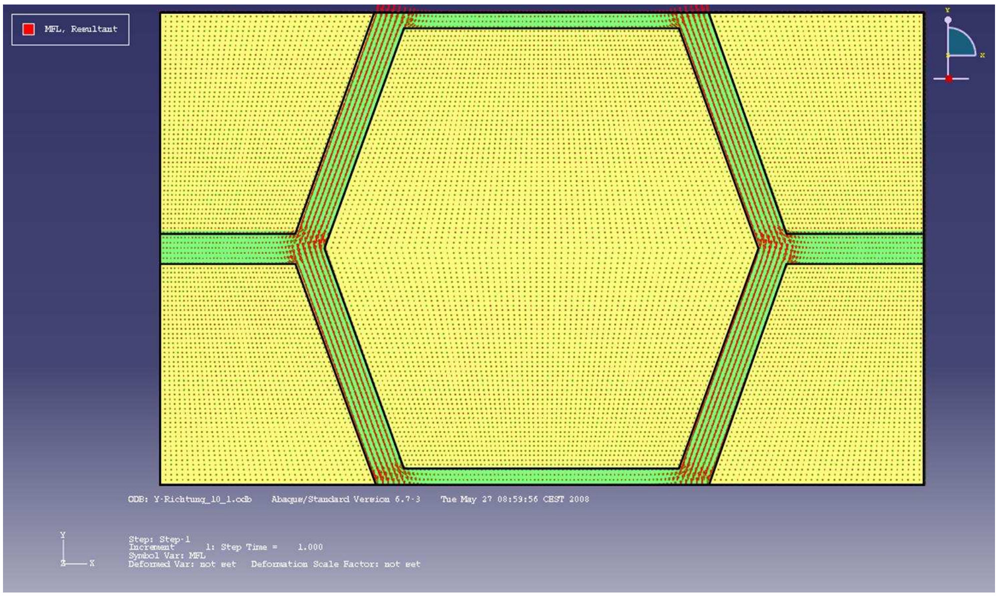

Figure 4.7: Heat flux distribution in earlywood resulting from a radial temperature gradient

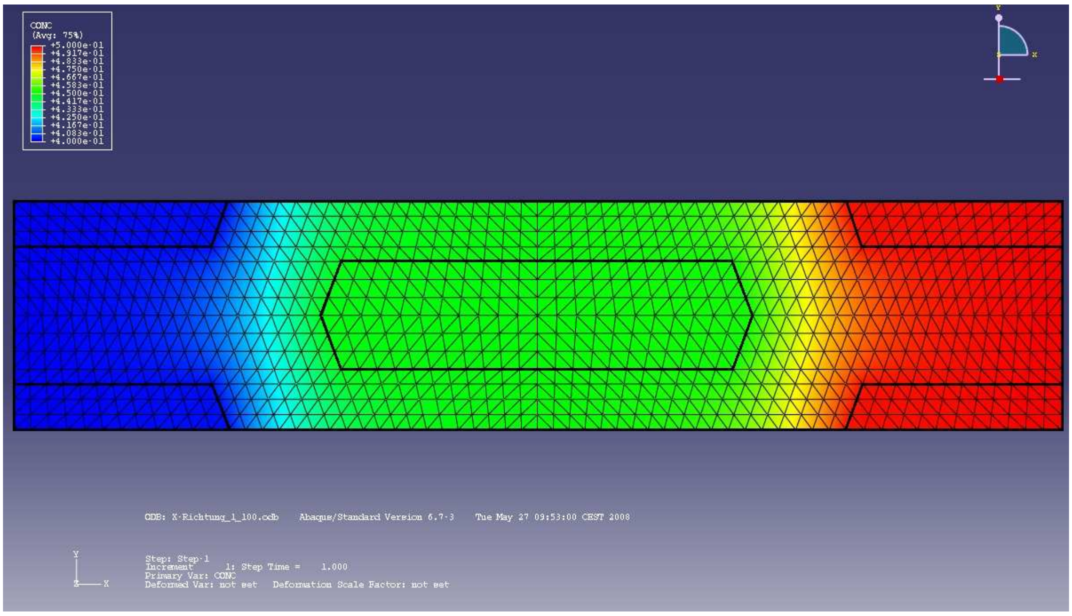

Figure 4.8: Concentration distribution in latewood resulting from a tangential concentration gradient

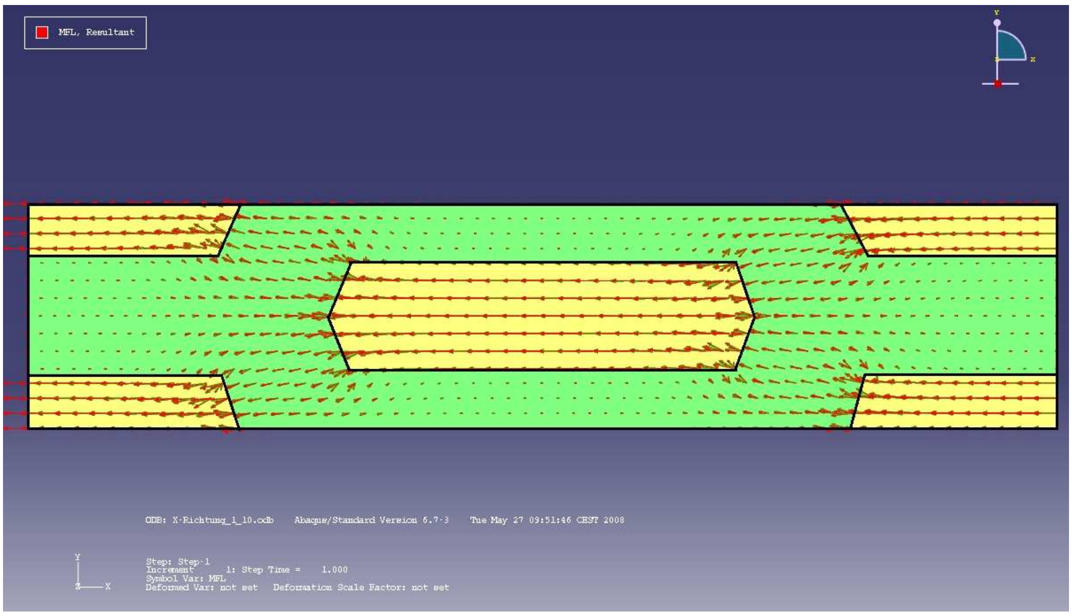

Figure 4.9: Distribution of fluxes in latewood resulting from a tangential concentration gradient

Chapter 5

Evaluation of the model for moisture diffusion

In this chapter the developed model is applied to moisture diffusion in wood and evaluated for the first time. First definitions for a few basic terms are given, that are important for the topic "water diffusion". Thereafter some constants and properties of water and steam are defined. After deriving values for the diffusivities of both cell walls and water, homogenized diffusivities obtained with the homogenization model are compared with corresponding measured values.

5.1 Basics

5.1.1 Moisture content

Moisture content (mc) is the mass of moisture in wood, expressed as a percentage of oven-dry mass. The latter is defined as the constant mass obtained after drying in an air oven maintained at $102 \pm 3\,^{\circ}\mathrm{C}$ [31]. The moisture content is computed as:

$$mc = \frac{m_{green} - m_{ovendry}}{m_{ovendry}} \tag{5.1}$$

where m_{green} is the green or moist mass, and $m_{ovendry}$ the oven-dry mass. The moisture in wood has two forms: bound or hygroscopic water, and free or capillary water. Bound water is found in the cell wall and is believed to be hydrogen bonded to the hydroxyl groups of primarily cellulose and hemicellulose, and to a lower extent also to the hydroxyl groups of lignin. The bound water moisture content is limited by the number of available sorption sites and by the number of molecules of water which can be held on a sorption site.

The moisture content of green wood varies considerably between different wood species, between heartwood and sapwood in the same tree, and even between logs cut from different heights in the tree. For example, the reported average moisture content of a conifer sapwood was 148.9 %, ranging from 98 % up to 249 %. This was almost three times higher than the heartwood mean value of 55.4 %, with a variation from 30 % to 121 % [33].

5.1.2 The equilibrium moisture content

Wood in a living tree generally has a moisture content well above 30 %. At this state the cell walls are fully saturated, and the cell lumens generally contain some water as shown in Figure 5.1. When the tree is felled, and the green wood is exposed to atmospheric conditions, moisture is lost until a moisture content is reached that is in equilibrium with the ambient atmosphere [33]. The moisture content mc in equilibrium with a given relative humidity φ of the environmental air is called the *equilibrium moisture content* (EMC).

Although relative humidity is the most important variable affecting the EMC, other influencing factors are: mechanical stress, the drying history of the wood tissue, the species and the specific gravity of the wood, the extractive content, and the temperature. These other factors are discussed in detail for example by Skaar [33]. In general, an increase in compressive stress decreases the EMC.

The EMC of never-dried wood is higher than that of wood that has undergone drying. In addition, the EMC is higher during desorption than during adsorption. These effects can be explained by an incomplete rehydration of sorption sites during a subsequent adsorption cycle and by the effect of compressive stresses during swelling. This hysteresis phenomenon has been discussed by several authors like Skaar [33], Frandsen [10], and Krabbenhoft [19].

5.1.3 The fiber saturation point

Conceptually, the moisture content at which only the cell walls are completely saturated with bound water and no free water exists in the cell lumens, is called the *fiber saturation point* (FSP, see Figure 5.1).

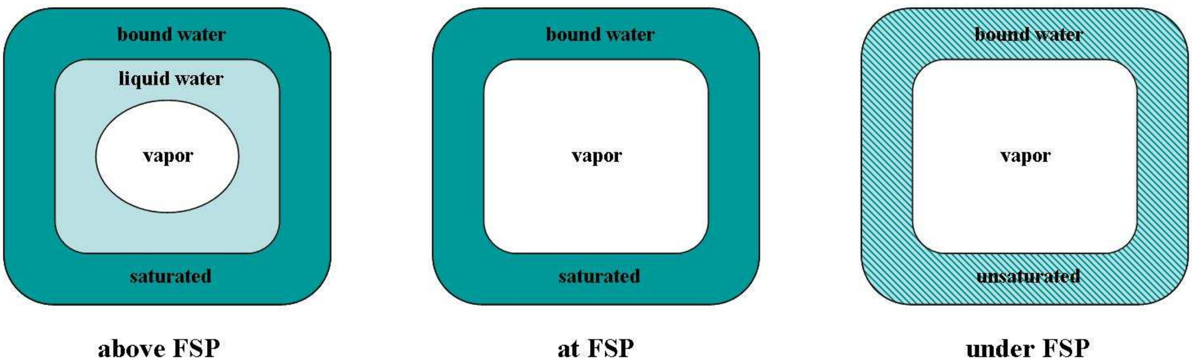

Figure 5.1: Schematic diagram showing the different moisture distributions in the cell wall and the lumen in a wood cell cross-section

At the fiber saturation point abrupt changes in the behavior of the physical properties of wood such as shrinkage, mechanical strength, and electrical conductivity are observed. While being a useful concept, the term fiber saturation point is not very precise. Conceptually, it distinguishes between the two ways water is held in wood. But, in reality, it is possible that a cell wall will begin to dry before all the water has left the lumen of the same cell. The fiber saturation point of wood is on average at a moisture content of about 30 % [34], but there are considerable variations across species, with values extending from 21 % for *Thuja plicata* up to 32 % for *Tilia americana* [31]. The FSP is also temperature-dependent and increases with decreasing temperature.

5.1.4 The sorption isotherm

The relationship between EMC and relative humidity under the FSP at a given temperature (between the freezing and boiling points) is called the sorption isotherm. In this diploma thesis the data for EMC, FSP (equivalent to the moisture content at 100 % relative humidity), and the sorption isotherms were taken from the Wood Handbook [34] of the USDA Forest Products Society. The sorption isotherms describe an average for sorption and desorption data suitable for several wood species. Although significant deviations from these values may occur in specific wood tissues as noted above, this data is very useful for many practical applications where the sorption isotherm for a particular wood tissue is not available. According to the Wood Handbook [34], the EMC can be approximated by the following relation:

$$mc = \frac{18}{W}\left[\frac{K \cdot \varphi}{1 - K \cdot H} + \frac{K_1 \cdot K \cdot \varphi + 2 \cdot K_1 \cdot K_2 \cdot K^2 \cdot \varphi^2}{1 + K_1 \cdot K \cdot \varphi + K_1 \cdot K_2 \cdot K^2 \cdot \varphi^2}\right] \tag{5.2}$$

with

$$\begin{aligned} W &= 349 + 1.29 \cdot T + 0.0135 \cdot T^2 \\ K &= 0.805 + 0.000736 \cdot T + 0.00000273 \cdot T^2 \\ K_1 &= 6.27 - 0.00938 \cdot T + 0.000303 \cdot T^2 \\ K_2 &= 1.91 + 0.0407 \cdot T + 0.000293 \cdot T^2 \end{aligned} \tag{5.3}$$

where φ is the relative humidity, mc the equilibrium moisture content, and T the temperature in [K].

Figure 5.2 shows sorption isotherms at five different temperatures according to Equation (5.2).

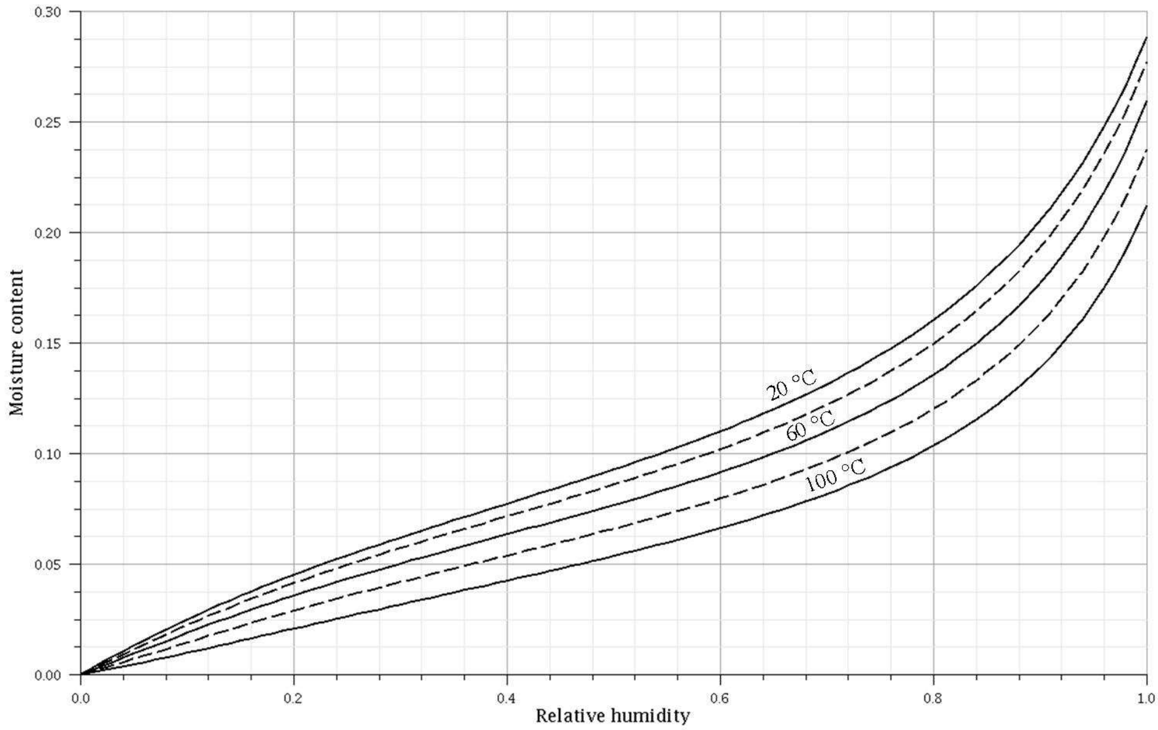

Figure 5.2: Mean sorption isotherms of wood at five temperatures calculated from (5.2)

5.2 Constants

5.2.1 The universal gas constant

The universal gas constant (usually denoted by R) is a physical constant which is needed in several equations in the following section. Its value is [51]:

$$R = 8.314472 \, \frac{\mathrm{J}}{\mathrm{mol\,K}} \tag{5.4}$$

5.2.2 The Avogadro constant

The Avogadro constant is the number of entities (atoms, molecules, elementary particles) contained in one mole of a substance. It is also a physical constant with a value of [43]:

$$N_A = 6.02214179 \cdot 10^{23} \, \frac{1}{\mathrm{mol}} \tag{5.5}$$

5.2.3 The density of the cell wall

According to Siau [31], the density of the cell wall is taken as:

$$\varrho_0 = 1530 \, \frac{\mathrm{kg}}{\mathrm{m}^3} \tag{5.6}$$

5.2.4 The molar mass of water

Molar mass is the mass of one mole of a substance. The molar mass of water is [59]:

$$M = 18.01524 \, \frac{\mathrm{g}}{\mathrm{mol}} \tag{5.7}$$

5.3 Properties of steam and water

In several equations in the following chapter values of water and steam properties are needed:

- the saturation vapor pressure p_0,
- the density of water ϱ_w,
- the heat of evaporation Q_v,
- the viscosity of water η_w,
- and the specific heat of steam at constant pressure $c_{p,v}$.

Because of their importance in chemistry and physics there exist comprehensive tables for these properties across a wide range of temperatures and pressures [11, 30]. The values for the relevant temperature range for transport processes in wood (from the freezing up to the boiling point) are specified in Appendix A. In this section equations for the different values are evolved for the later use in a computer program.

5.3.1 The saturation vapor pressure

The saturation vapor pressure is the pressure at which air is saturated with water vapor. Thus, at saturation vapor pressure, air has a relative humidity of 100 % and condensation occurs at any increase of water vapor content or reduction in temperature. Therefore the saturation vapor pressure is temperature-dependent, an increase in temperature comes along with an increase in the adsorption capacity of air. There exist many different formulas for the saturation vapor pressure like the Goff-Gratch equation or the Arden Buck equation [58]. In this diploma thesis the equation given by the "International Association for the Properties of Steam" was used [30]:

$$ln\left(\frac{p_0}{p_c}\right) = \left(\frac{T_c}{T}\right)\left(b_1\tau + b_2\tau^{1.5} + b_3\tau^3 + b_4\tau^{3.5} + b_5\tau^4 + b_6\tau^{7.5}\right) \tag{5.8}$$

with:

$$\tau = 1 - \frac{T}{T_c} \qquad T_c = 647.14\,\mathrm{K} \qquad p_c = 220.64\,\mathrm{bar} \tag{5.9}$$

and:

$$
\begin{aligned}
b_1 &= -7.85823 \\
b_2 &= +1.83991 \\
b_3 &= -11.7811 \\
b_4 &= +22.6705 \\
b_5 &= -15.9393 \\
b_6 &= +1.77516
\end{aligned}
\tag{5.10}
$$

By inserting (5.9) and (5.10) into (5.8) and converting the formula to p_0 one gains the desired equation. Figure 5.3 shows the saturation vapor pressure over the temperature range of interest from the freezing up to the boiling point.

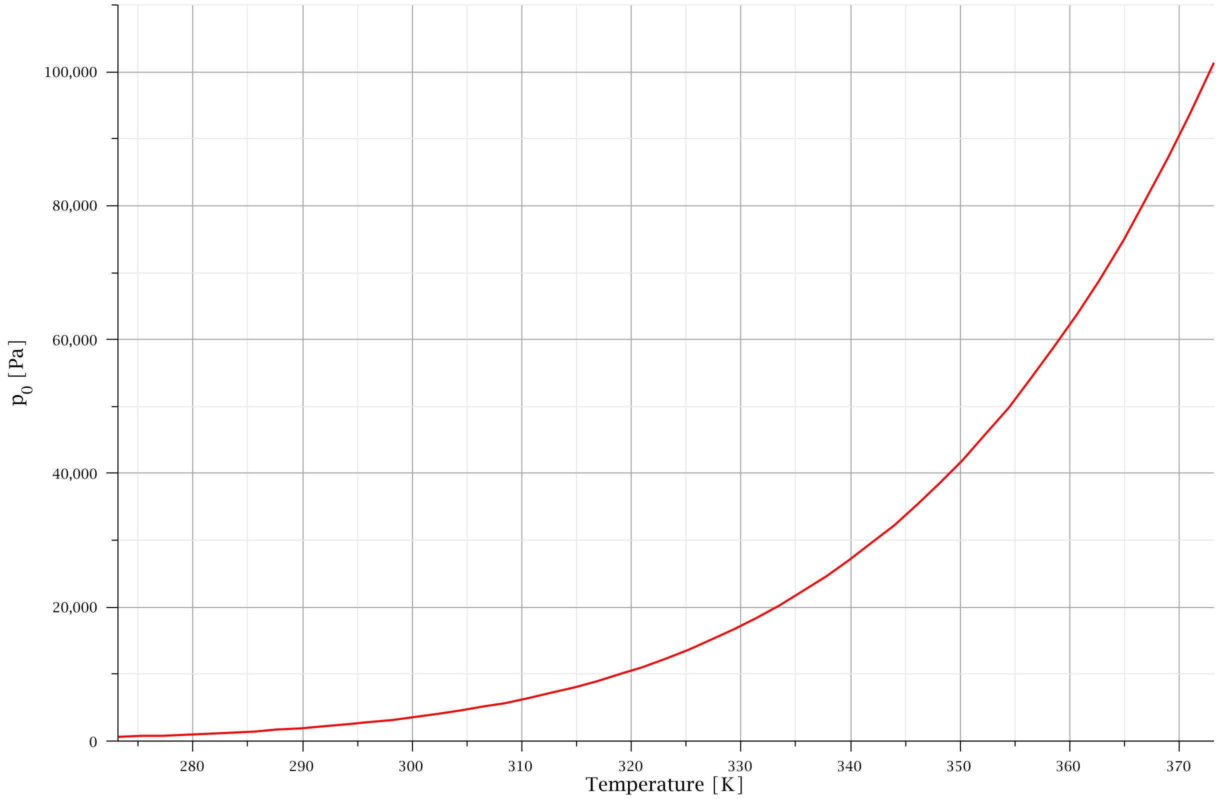

Figure 5.3: Saturation vapor pressure from 273.15 to 373.15 K

5.3.2 The density of water

The values for the density of water used in this diploma thesis were taken from steam tables [11] and fitted (see Section B.1.1) by the polynomial (5.11). Figure 5.4 shows the density of water over the temperature range from the freezing up to the boiling point.

$$\begin{aligned}\varrho_w = &- 1.390021658\,10^{-7}\,T^4 + 0.1956853951\,10^{-3}\,T^3 - 0.1058224883\,T^2 \\ &+ 25.39735328\,T - 1256.217406\,\left[\frac{\mathrm{kg}}{\mathrm{m}^3}\right]\end{aligned} \tag{5.11}$$

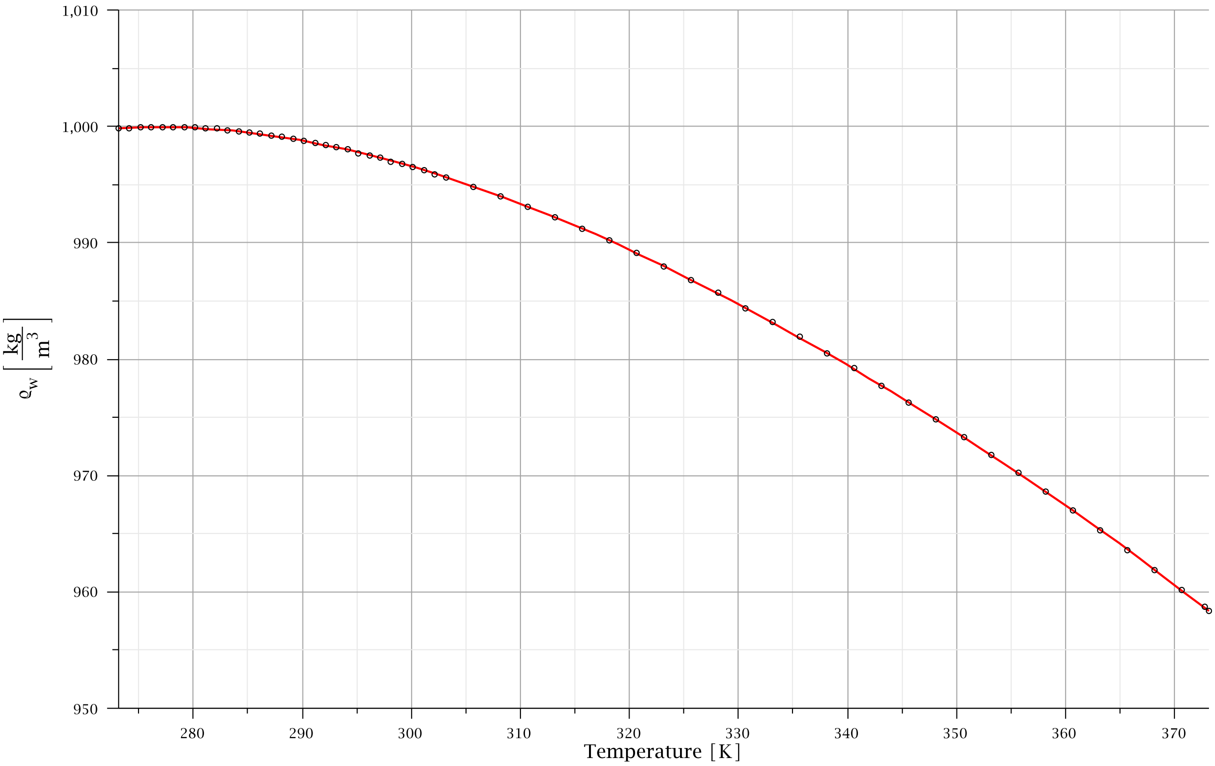

Figure 5.4: Density of water from 273.15 to 373.15 K

5.3.3 The heat of evaporation

The heat of evaporation of water, also known as enthalpy of vaporization, is the energy required to transform a given quantity of liquid water into gas (vapor). The values for the heat of evaporation of water used in this diploma thesis were taken from steam tables [11] and fitted (see Section B.1.2) by a polynomial reading as:

$$Q_v = -0.1278794562\,10^{-2}\,T^2 - 1.601883570\,T + 3033.019010\ \left[\frac{\mathrm{kJ}}{\mathrm{kg}}\right] \tag{5.12}$$

Figure 5.5 shows the heat of evaporation of water over the temperature range from freezing to boiling point.

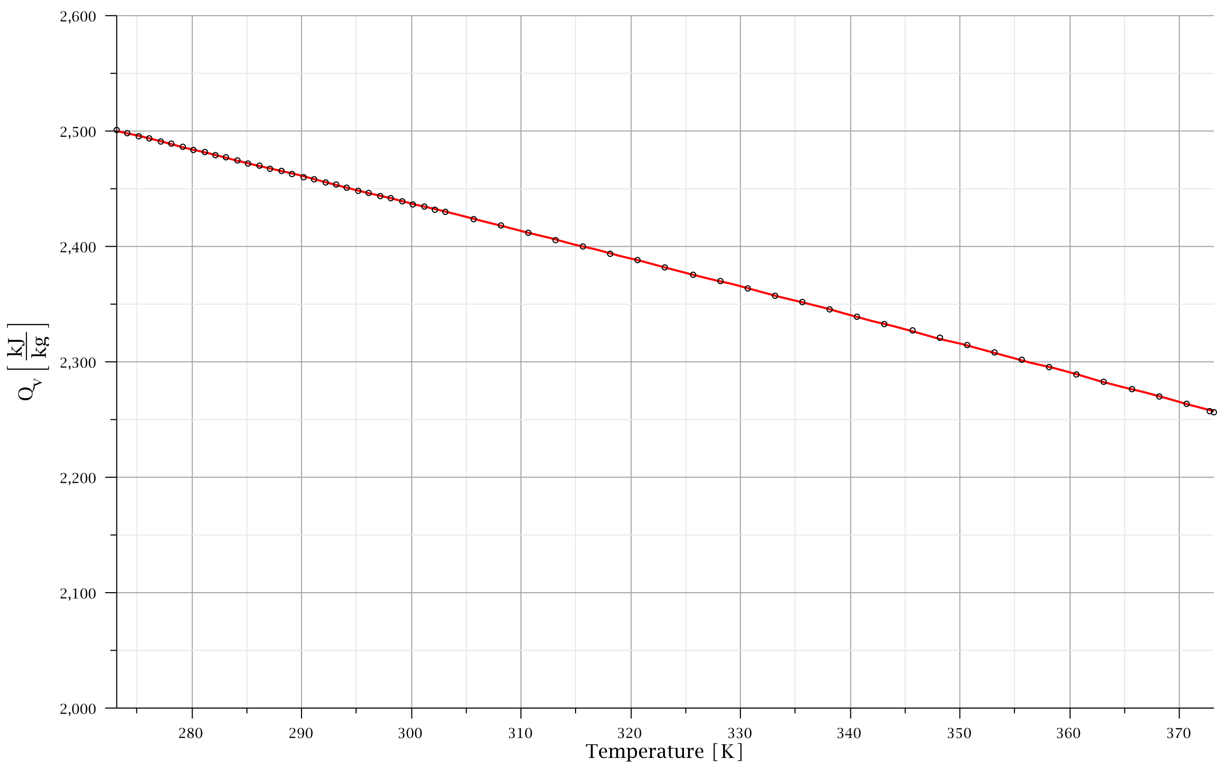

Figure 5.5: Heat of evaporation of water from 273.15 to 373.15 K

5.3.4 The viscosity of water

The viscosity of water is a measure of the resistance of water to being deformed either by shear stress or extensional stress. The values for the viscosity of water were also taken from steam tables [11] and fitted (see Section B.1.3) by a polynomial:

$$\begin{aligned}\eta_w = &- 4.239227084\,10^{-7}\,T^5 + 0.7171886828\,10^{-3}\,T^4 - 0.4855992853\,T^3 \\ &+ 164.5725238\,T^2 - 27937.97821\,T + 1.902803765\,10^6\ [\mu\text{Pa s}]\end{aligned} \tag{5.13}$$

Figure 5.6 shows the viscosity of water over the temperature range from freezing to boiling point.

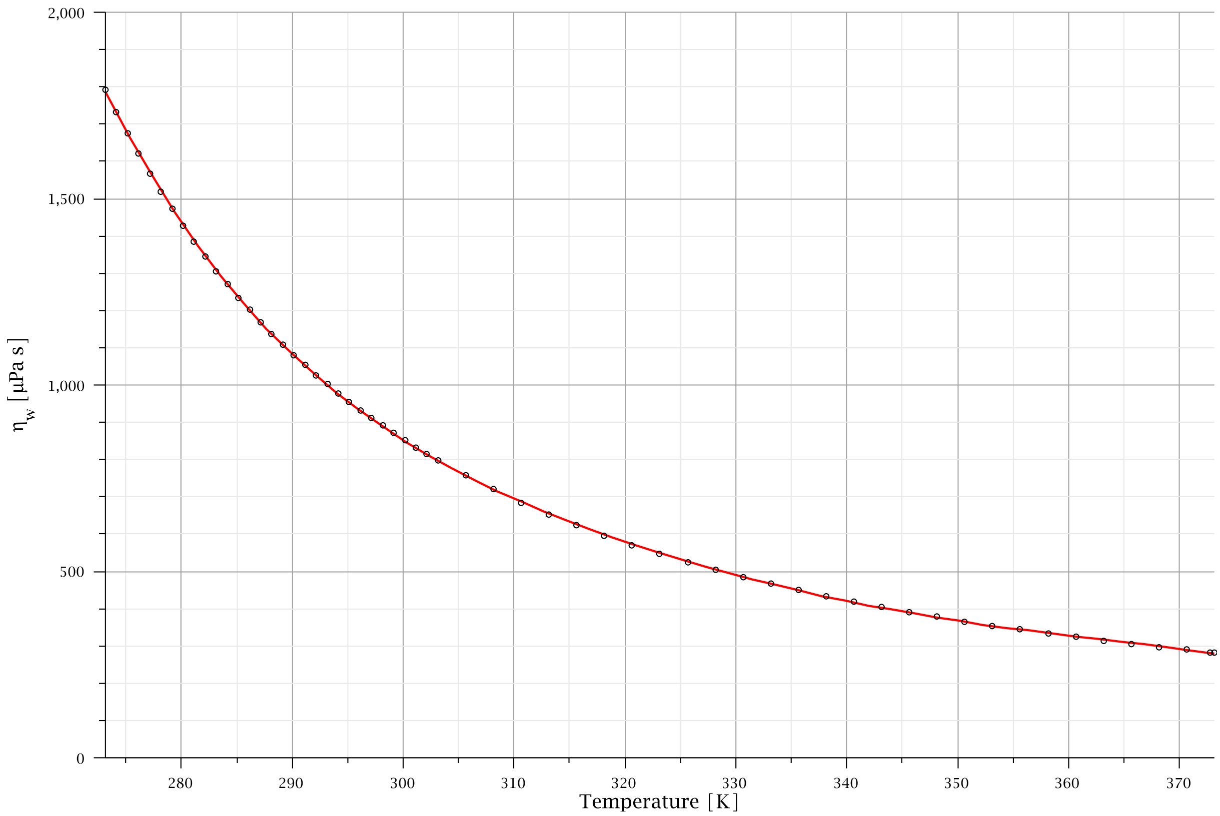

Figure 5.6: Viscosity of water from 273.15 to 373.15 K

5.3.5 The specific heat at constant pressure of steam

The specific heat or specific heat capacity is the measure of the heat energy required to increase the temperature of a unit quantity of a substance by a certain temperature interval [56]. Again the values for the specific heat at constant pressure of steam were taken from steam tables [11] and fitted (see Section B.1.4) by a polynomial:

$$\begin{aligned} c_{p,v} = & \, 5.407142991\,10^{-8}\,T^3 - 0.3784676236\,10^{-4}\,T^2 + 0.9149548711\,10^{-2}\,T \\ & + 1.090125256 \left[\frac{\text{kJ}}{\text{kg K}}\right] \end{aligned} \tag{5.14}$$

Figure 5.7 shows the specific heat at constant pressure of steam over the temperature range from freezing to boiling point.

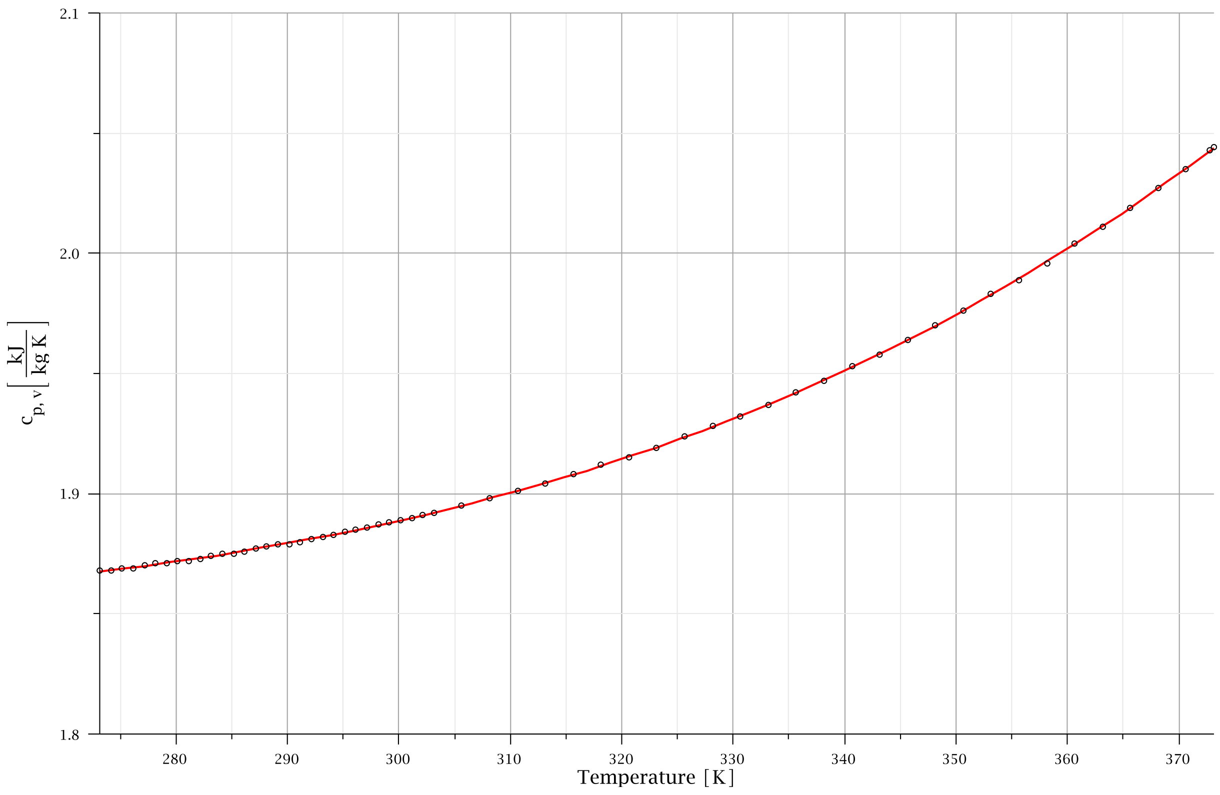

Figure 5.7: Specific heat at constant pressure of steam from 273.15 to 373.15 K

5.4 The diffusion tensor of the lumen

In this section the diffusion tensor of the lumen, $\mathbb{D}_{lumen}$, is calculated for use in Equation (3.73)

5.4.1 The diffusion coefficient of air

In order to be able to calculate homogenized diffusion properties of wood, it is necessary to know the coefficient for the transport of water vapor through the air in the lumens. This may be calculated from the inter-diffusion coefficient of water vapor in air, which describes the diffusive transport of water vapor in bulk air. A semi-empirical equation for this coefficient can be taken from Siau [31]:

$$D_a = 2.2 \cdot 10^{-5} \cdot \left(\frac{p_0}{p}\right) \cdot \left(\frac{T}{273.15}\right)^{1.75} \left[\frac{\mathrm{m}^2}{\mathrm{s}}\right] \tag{5.15}$$

with D_a denoting the inter-diffusion coefficient of the water vapor in air, p the total pressure, p_0 the saturation vapor pressure, and T the temperature in [K].

5.4.2 The diffusion coefficient of the lumen

Diffusion in wood is usually described by the moisture flux resulting from a spatial gradient of the moisture content in wood. Since the diffusion coefficient of water vapor in air, D_a, is based on a concentration gradient of moisture in air, it must be converted to a basis of concentration of moisture in the cell wall substance, which is in equilibrium with the relative humidity of the surrounding air. This requires knowledge of the sorption isotherm, which describes the cell wall moisture content associated with a specific water-vapor concentration in the lumens. Moisture is diffusing from one side (1) of the lumen to the opposite side (2) if $mc_1 > mc_2$ and $\varphi_1 > \varphi_2$ (see Figure 5.8). Therefore the relative humidity gradient in the lumen must correspond to a moisture gradient in the cell wall substance as defined by the sorption isotherm. When D_a is converted to a gradient of moisture concentration in the cell wall, it is generally designated as D_v, the water-vapor diffusion coefficient of air in the lumens of wood. Formulating Fick's Law on the basis of concentration gradients in air and in the cell wall substance, respectively, yields:

$$j^\gamma = -D_a \cdot \operatorname{grad}_a \rho^\gamma \tag{5.16}$$

$$j^\gamma = -D_v \cdot \operatorname{grad}_v \rho^\gamma \tag{5.17}$$

$$D_v = D_a \cdot \frac{\operatorname{grad}_a \rho^\gamma}{\operatorname{grad}_v \rho^\gamma} \tag{5.18}$$

The pressure gradient to be used with D_a may be calculated from the ideal gas law [52]:

$$p \cdot V = n \cdot R \cdot T \tag{5.19}$$

with p denoting the partial water-vapor pressure in the lumen, n the number of moles of water vapor, R the universal gas constant, and T the temperature.

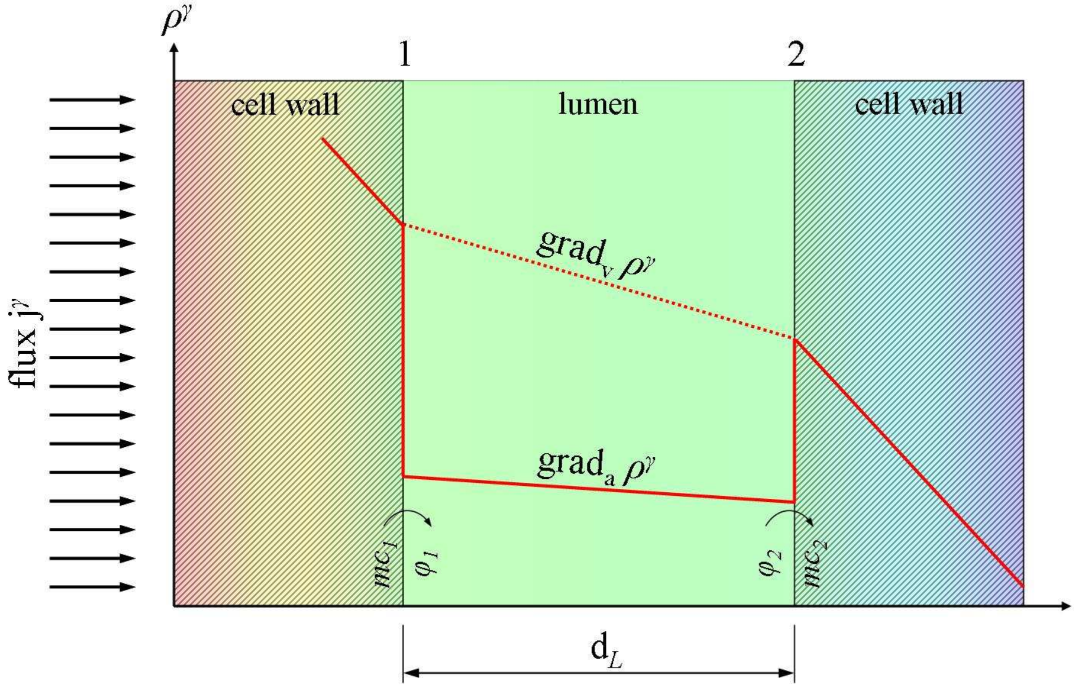

Figure 5.8: Illustration of the corresponding moisture concentration gradients in the cell wall and in the lumen

The value of n can be calculated by dividing the mass of water vapor in the volume, V, through the molecular weight of water, M:

$$n = \frac{m}{M} \tag{5.20}$$

The water-vapor pressure is related to the relative humidity φ by:

$$\varphi = \frac{p}{p_0} \tag{5.21}$$

Equation (5.21) can also be written as:

$$p = \varphi \cdot p_0 \tag{5.22}$$

With (5.20) and (5.22), Equation (5.19) yields the concentration of water vapor in the lumen as:

$$\frac{m}{V} = \frac{M \cdot p}{R \cdot T} = \frac{M \cdot p_0 \cdot \varphi}{R \cdot T} \tag{5.23}$$

Thus the concentration gradient is:

$$\mathrm{grad}_a\, \rho^\gamma = \frac{M \cdot p_0 \cdot \mathrm{d}\varphi}{R \cdot T \cdot \mathrm{d}_L} \tag{5.24}$$

with $\mathrm{d}\varphi = \varphi_1 - \varphi_2$ and d_L denoting the diameter of the lumen.

The associated gradient on basis of concentration in cell wall substance is much larger, because the moisture concentration in wood is very high compared to that in air in equilibrium with it. Its value is:

$$\mathrm{grad}_v\, \rho^{\gamma} = \frac{\mathrm{d}mc \cdot \varrho'}{\mathrm{d}_L} \tag{5.25}$$

with ϱ' denoting the density of the moist cell wall substance. ϱ' can be calculated as cell wall density in the oven-dry state divided by moist volume as:

$$\varrho' = \frac{\varrho_0}{1 + \frac{\varrho_0}{\varrho_w} \cdot mc} = \frac{1530}{1 + \frac{1530}{\varrho_w} \cdot mc} \left[\frac{\mathrm{kg}}{\mathrm{m}^3}\right] \tag{5.26}$$

where ϱ_w is the density of water according to (5.11). With the Equations (5.24) and (5.25) the expression for D_v (5.18) can be rewritten as:

$$D_v = D_a \cdot \frac{\mathrm{grad}_a\, \rho^{\gamma}}{\mathrm{grad}_v\, \rho^{\gamma}} = D_a \cdot \frac{M \cdot p_0}{\varrho' \cdot R \cdot T} \cdot \frac{\mathrm{d}\varphi}{\mathrm{d}mc} \tag{5.27}$$

where the inverse slope of the sorption isotherm is expressed as a derivative. Values of D_v calculated from Equation (5.27) are plotted in Figure 5.9.

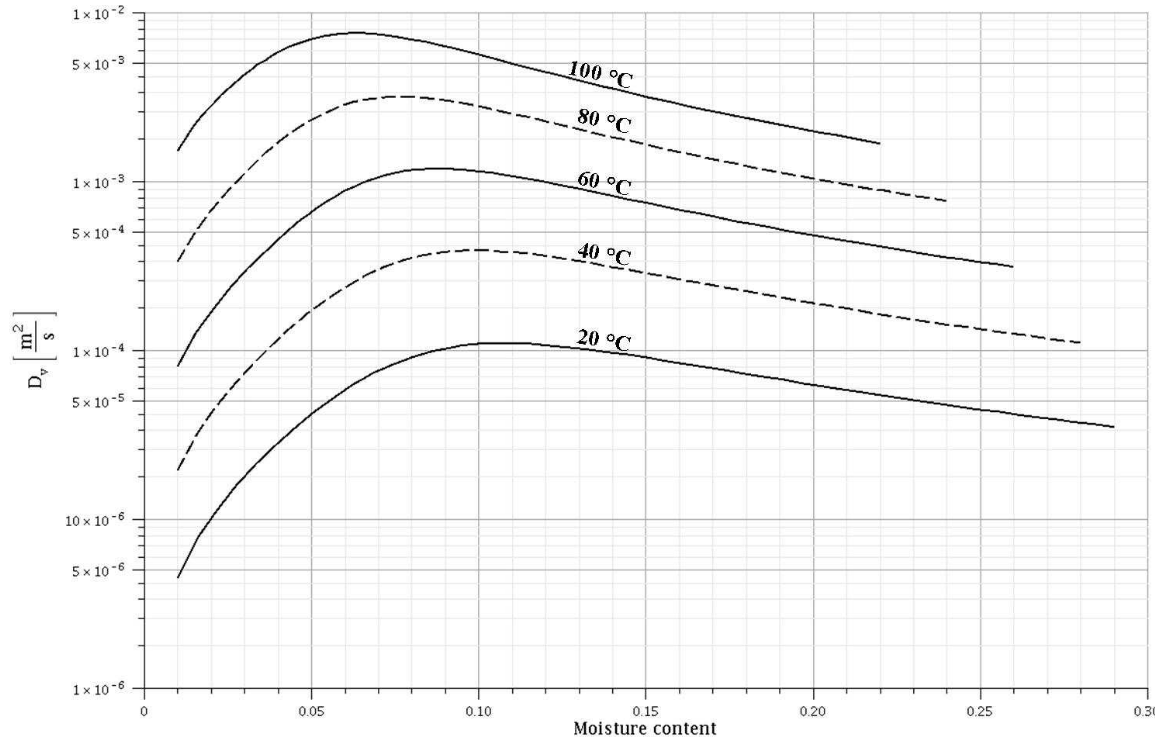

Figure 5.9: Water-vapor diffusion coefficient in the lumens at five temperatures

As can be seen, D_v increases with the moisture content mc at lower moisture content and temperatures and then decreases significantly at higher moisture contents. The reason for this is the inflection point of the sorption isotherm (see Figure 5.2). As stated previously, the calculations in this diploma thesis are based on the sorption data given in the Wood Handbook [34]. When applied to a specific wood specimen, sorption data determined for that specimen should be used in order to improve the fit of the model [31].

5.4.3 Assembly of the diffusion tensor

With the one-dimensional diffusion coefficient of the lumen, D_v, the diffusion tensor of the lumen can be assembled. Since D_v is expressed on the basis of moisture concentration in the cell wall substance in wood, it must be divided by the volume fraction of the cell wall substance in wood, $f_{cellwall}$, in order to relate it to the whole wood substance. The diffusion tensor of the lumen thus is:

$$\mathbb{D}_{lumen} = \begin{bmatrix} \frac{D_v}{f_{cellwall}} & 0 & 0 \\ 0 & \frac{D_v}{f_{cellwall}} & 0 \\ 0 & 0 & \frac{D_v}{f_{cellwall}} \end{bmatrix} \tag{5.28}$$

5.5 The diffusion tensor of the cell wall

Diffusion coefficients in solids normally are several orders of magnitude smaller than those in gases or fluids. Thus the cell walls give rise to the main resistance to water diffusion through wood, especially in the transverse direction.

5.5.1 The Arrhenius equation

The diffusion coefficient in solids is described by the Arrhenius equation [31, 42, 46], which is named after the Swedish chemist Svante Arrhenius:

$$D = D_0 \cdot \exp\left(-\frac{E_a}{R \cdot T}\right) \tag{5.29}$$

where the prefactor D_0 is equal to the diffusion coefficient in the limit of infinitely high temperature T. In (5.29) E_a denotes the activation energy and R the universal gas constant. According to Siau [31], the value for D_0 can be taken as $7 \cdot 10^{-6}\,\mathrm{m^2/s}$ for transverse diffusion and as $17.5 \cdot 10^{-6}\,\mathrm{m^2/s}$ for diffusion in longitudinal direction in first approximation.

Siau [31] also published a formula for the activation energy, which constitutes a linear fit of measured results at a temperature of 26.7 °C:

$$E_a = 38500 - 29000 \cdot mc \left[\frac{\mathrm{J}}{\mathrm{mol}}\right] \tag{5.30}$$

Since this empirical formula partly provides inexact results, the topic "activation energy" was studied more deeply in the framework of this diploma thesis. Because of its complexity, the activation energy became one of the most time-consuming items of the thesis.

5.5.2 Energy relationships, activation energy

In thermodynamics and molecular chemistry, the enthalpy or heat content denotes a part of the thermodynamic potential of a system. Each state of water thus has a specific heat content or enthalpy depending on the actual temperature and pressure. The enthalpy can also be interpreted as energy level.

Because of their importance in chemistry and physics, the thermodynamic properties of water and steam are well-known and expressed in tables [11, 30].

Ordinary water exists in three basic physical conditions: the solid state, the liquid state, and the vapor state. Energy increases during transition from the solid to the vapor phase. Moisture in wood can be found in each of these three state, as well as in a fourth "condition" – the sorbed or bound water in the cell wall. At temperatures above the melting point, only three states may coexist: sorbed water in the cell walls, capillary or free water in the lumens at moisture contents above fiber-saturation, and water vapor in the lumens, present at all moisture contents except in fully-saturated wood. Below the melting point, the capillary water is frozen while the two other phases are still present [33].

Sorbed water in the cell wall of wood is similar to water in the frozen or solid state in terms of its lower enthalpy than liquid water. The enthalpy of sorbed water increases with increasing wood moisture content up to fiber-saturation, above which it is more or less the same as for liquid water [33]. Figure 5.10 shows the energy levels of water vapor, liquid water, and bound water at 40 °C, relative to the energy level of liquid water, that was set equal to zero.

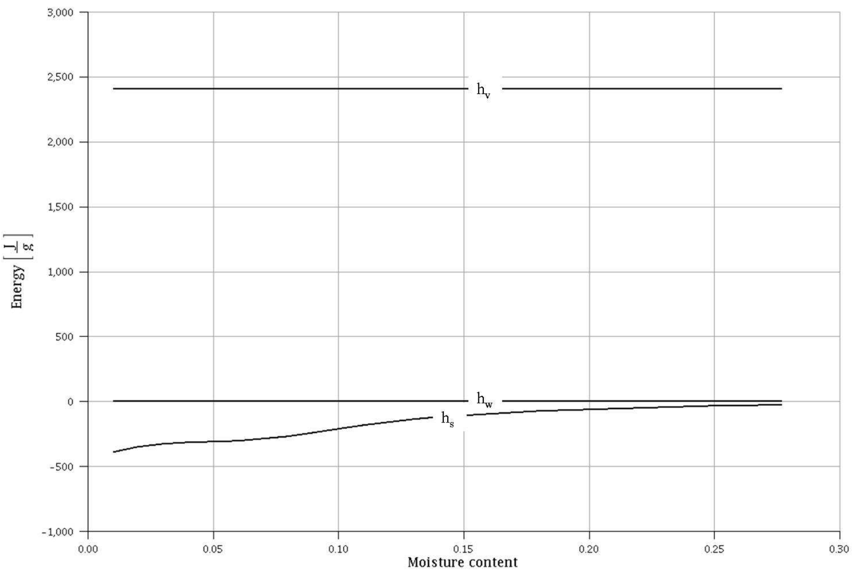

Figure 5.10: Relative energy levels at 40 °C of water vapor, liquid water, and bound water in wood as functions of wood moisture content

As can be seen, the enthalpy of water vapor, h_v, is higher than that of liquid water, h_w, which is in turn higher than that of bound or sorbed water, h_s. The latter increases with increasing moisture content up to fiber-saturation at a moisture content of about 30 %.

The difference between the energy levels of liquid water and water vapor, respectively, is called the differential heat of evaporation, Q_v (see Equation (5.12)), while the difference between the energy levels of bound water and liquid water is denoted by differential heat of sorption Q_w.

There are two different methods of determining the differential heat of sorption. One is the calorimetric method, in which the phase change energy is measured directly. In this diploma thesis the isosteric method is used, based on the Clausius-Clapeyron equation [33, 44]. It requires sorption isotherms at two or more temperatures. Finally, Skaar ends up with the following formula for Q_w:

$$Q_w \simeq R \cdot T^2 \left[\frac{\mathrm{d} \ln \left(\frac{p}{p_0} \right)}{\mathrm{d}T} \right] \tag{5.31}$$

in which the differential can be written as difference quotient in case of constancy of Q_w between temperatures T_1 and T_2,:

$$Q_w \approx R \cdot T_1 \cdot T_2 \left[\frac{\ln \left(\frac{\varphi_2}{\varphi_1} \right)}{T_2 - T_1} \right] \tag{5.32}$$

Therein φ_1 and φ_2 are the relative vapor pressures at temperatures T_1 and T_2, respectively, at a given constant moisture content of the wood. The differential heat of sorption calculated on the basis of sorption data of the U.S. Department of Agriculture [34] (see Equation (5.2)) is displayed in Figure 5.11. It clearly can be seen that the differential heat of sorption strongly depends on temperature as well as on the moisture content.

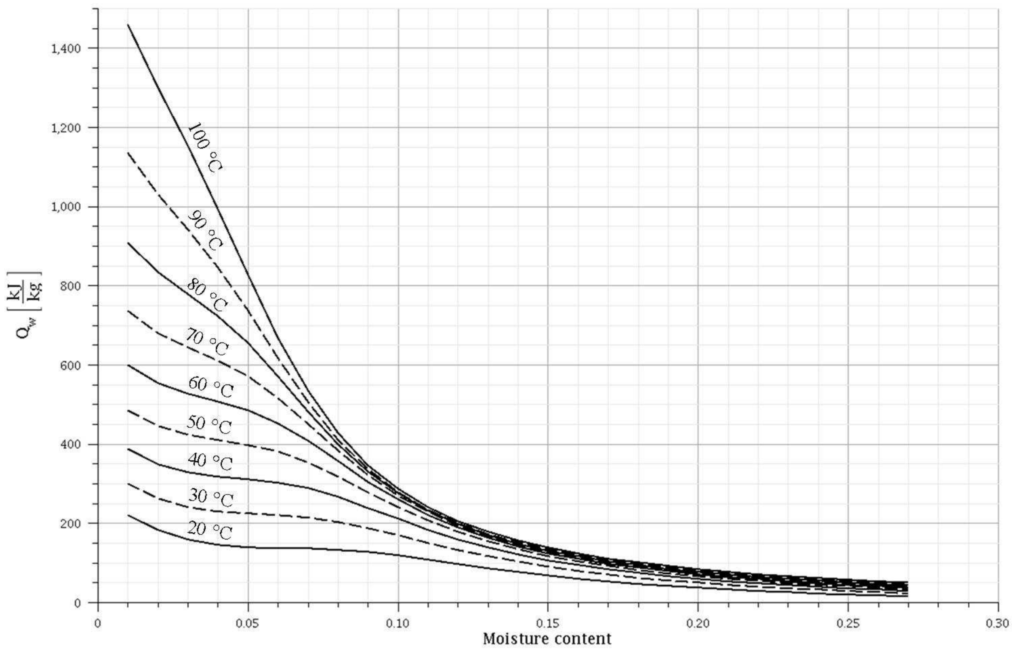

Figure 5.11: Differential heat of sorption at different temperatures

In the state of equilibrium, where no moisture transport occurs, the bound water in the cell wall has enthalpy h_s, and the water vapor in the lumens the higher enthalpy h_v. In case of moisture transport the water molecules in the cell wall must reach an activated state with an energy level that exceeds the enthalpy of bound water by a value E_a – the activation energy. This is because diffusion requires activated jumps, and thus the molecules must possess a certain minimum energy before they can traverse the cell wall. Figure 5.12 illustrates energy changes that water molecules undergo upon passing the cell wall. The red line depicts the mean energy of water passing from the vapor state to the sorbed state and then to the activated state at side 1, or from the activated state to the sorbed state and then to the vapor state at side 2.

Unfortunately the activation energy is not known in detail. Strict theoretical relations only exist for a lower limit, h_r, and an upper limit, h^*, for this energy, which will be specified in the next sections.

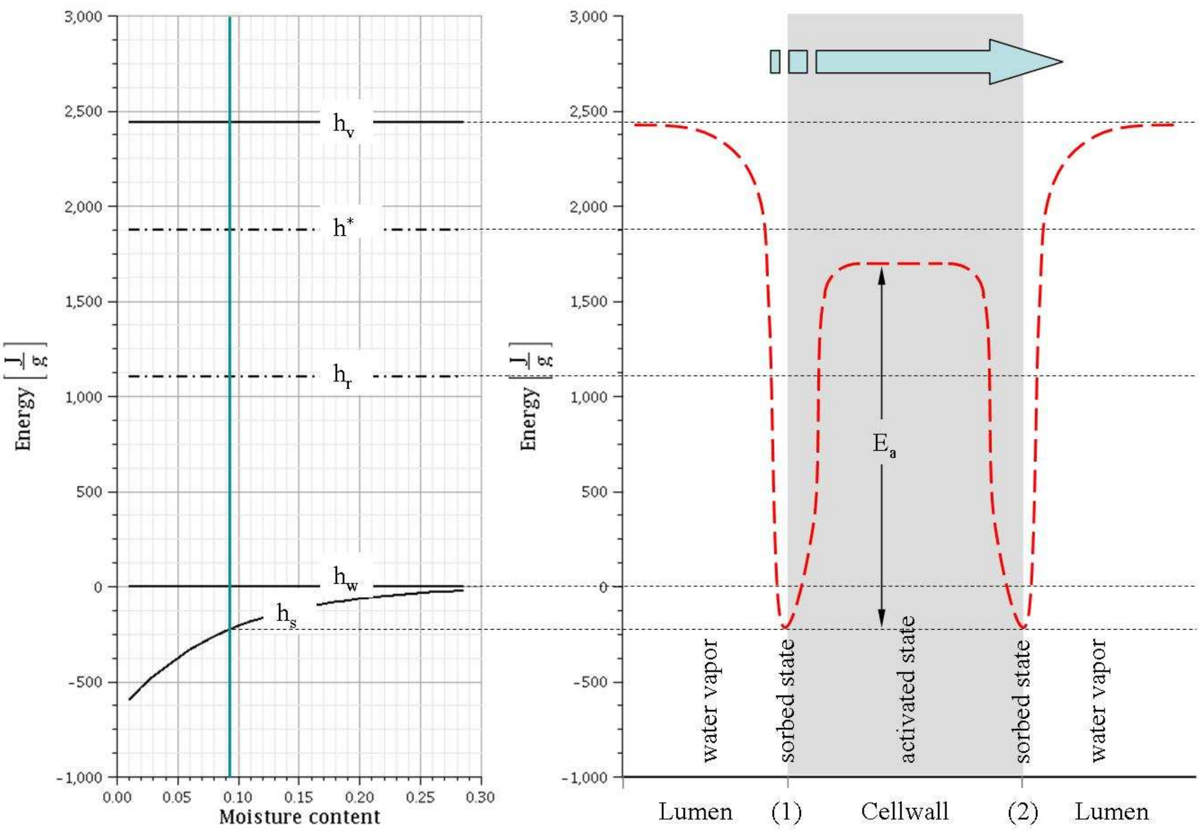

Figure 5.12: Energy relationships for diffusion through cell wall ($mc = 0.09$, $T = 25.5\,°C$)

.

5.5.3 The activation energy, lower limit

A lower limit for the activation energy can be calculated as an energy value h_r, marking the minimum energy the water molecules must possess in order to participate in diffusion.

According to the Einstein diffusion equation [7], the self-diffusion coefficient of liquid water can be calculated as:

$$D_r = \frac{R}{N_A} \frac{T}{6\,\pi\,\eta_w\,r_w} \tag{5.33}$$

with r_w denoting the radius of the diffusing molecule, which is H_2O in this case. Eisenberg [8] specifies a value of $2.272 \cdot 10^{-9}\,\mathrm{m^2/s}$ for D_r at 25 °C. With N_A, R, and η_w as stated in Sections 5.2 and 5.3, the value for the radius r_w results in $1.08137 \cdot 10^{-10}\,\mathrm{m}$. Figure 5.13 shows the self-diffusion coefficient of water over the temperature range from the freezing point up to the boiling point.

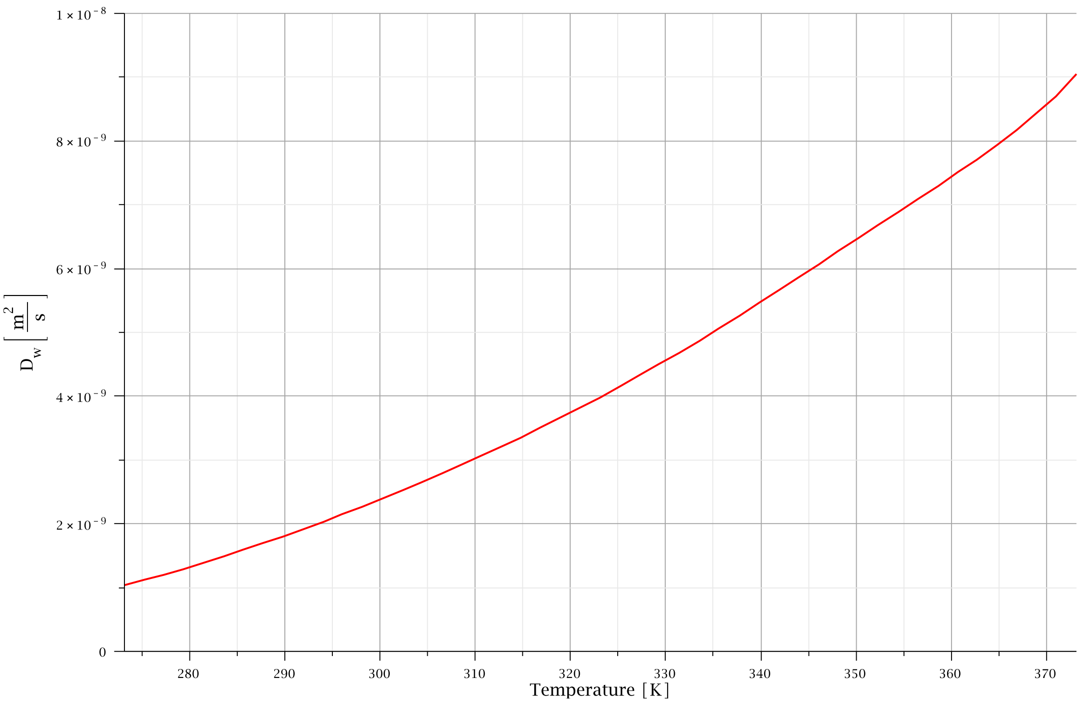

Figure 5.13: Self-diffusion coefficient of water from 273.15 to 373.15 K

.

Further evaluation of the lower limit of the activation energy requires expressions for tortuosity τ and effective area α. The effective path length for diffusion generally exceeds the cell wall thickness since the diffusing molecules must move around stationary polymer molecules. The ratio of the length of the effective path within the cell wall to the cell wall thickness is the tortuosity τ. Furthermore, the diffusive flow of moisture is further affected by the presence of the polymers because the area available for diffusion is smaller than the cell wall cross section. The ratio of total cell wall cross section to available cross section is denoted as the effective area α. The resistance to diffusion is inversely proportional to α, but directly proportional to τ. Nelson [24] proposes a combined factor for tortuosity and effective area in terms of the following empirical equation:

$$\frac{\alpha}{\tau} = \frac{1}{2 - \frac{0.9\,mc}{0.685+0.9\,mc}} \tag{5.34}$$

With the Arrhenius Equation (5.29) the activation energy for self-diffusion therefore is:

$$E_r = -\ln\left(\frac{D_r \cdot \tau}{D_0 \cdot \alpha}\right) \cdot R \cdot T \tag{5.35}$$

Finally the energy level h_r marking the lower limit for the activation energy follows from:

$$h_r = h_w + E_r \tag{5.36}$$

5.5.4 The activation energy, upper limit

When water passes from the vapor state in the lumen into the cell wall, the wall absorbs the heat generated at the condensation of the vapor. After transport through the cell wall, this heat is released again and absorbed by the water upon evaporation. Apparently, water diffusion through the cell wall is coupled with a conduction of heat in an direction opposite to the diffusive moisture transport. Thereon, Nelson [24] derives that the upper limit for the activation energy is the mean energy h^*, defined by:

$$h^* = h_v - c_{p,v} \cdot T \tag{5.37}$$

with h_v denoting the enthalpy of water vapor and $c_{p,v}$ the specific heat of steam at constant pressure.

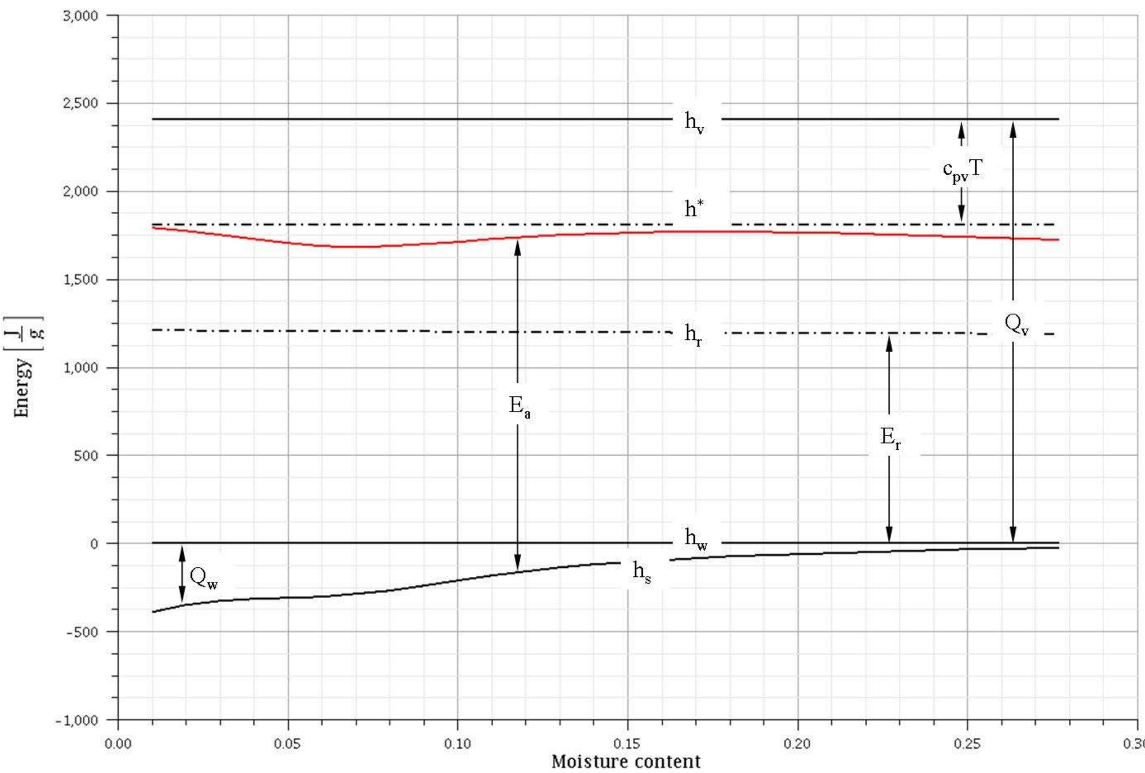

Figure 5.14: Energy relationships of water in wood at 40 °C

With the lower and upper boundary for activation energy bounds for the diffusion coefficients for the cell wall and the whole wood sample can be calculated. The energy relationships with the calculated boundaries are displayed in Figure 5.14 for a temperature of 40 °C. The red line is back-calculated from experimental results for the diffusion coefficients reported by Kollmann [17] for a sample of spruce wood at different moisture contents.

Unfortunately the activation energy has a great influence on the diffusion coefficient because of its appearance in the exponential function in the Arrhenius Equation (5.29). Since no analytical relation or exact experimental result exists for the activation energy, the empirical relation for the activation energy of Siau [32] (see Equation (5.30)) is used in most articles about moisture diffusion in the cell wall. Also in this diploma thesis, Siau's equation is used for the evaluation of the diffusion model, resulting in overestimation of the diffusion coefficients especially at higher temperatures.

5.5.5 Assembly of the diffusion tensor

Assuming that the cell wall is transversal isotropic results in two different diffusion coefficients for the transversal and longitudinal direction. Insertion of Siau's equation for the activation energy (5.30) in (5.29) leads to the following relations:

$$D_{cellwall,trans} = 7 \cdot 10^{-6} \cdot \exp\left(-\frac{38500 - 2900 \cdot mc}{8.314472 \cdot T}\right) \left[\frac{\mathrm{m}^2}{\mathrm{s}}\right] \tag{5.38}$$

$$D_{cellwall,long} = 17.5 \cdot 10^{-6} \cdot \exp\left(-\frac{38500 - 2900 \cdot mc}{8.314472 \cdot T}\right) \left[\frac{\mathrm{m}^2}{\mathrm{s}}\right] \tag{5.39}$$

Since $D_{cellwall,trans}$ and $D_{cellwall,long}$ are expressed on the basis of concentration in the cell wall substance in wood, they both must be divided by the volume fraction of the cell wall substance in wood, $f_{cellwall}$. The diffusion tensor of the cell wall thus is:

$$\mathbb{D}_{cellwall} = \begin{bmatrix} \frac{D_{cellwall,trans}}{f_{cellwall}} & 0 & 0 \\ 0 & \frac{D_{cellwall,trans}}{f_{cellwall}} & 0 \\ 0 & 0 & \frac{D_{cellwall,long}}{f_{cellwall}} \end{bmatrix} \tag{5.40}$$

5.6 The multiscale moisture diffusion model

The calculated diffusion coefficients for the cell wall and the lumen serve as the basis for two homogenization steps for the computation of overall diffusion coefficients of wood as described in Chapter 3. In the first step an overall diffusion coefficient for the cell assembly is calculated. The second, final step refers to the density variation within the annual rings. The results of the diffusion model are compared with values given by Kollmann [17] afterwards.

5.6.1 Homogenization step 1: Diffusion coefficients of the cell assembly

In the first homogenization step the diffusion coefficients of the cell assembly are calculated for a given oven-dry density and a moisture content between zero and the fiber saturation point, based on the model developed in Section 3.2. The Mori-Tanaka scheme is formulated with ellipsoidal inclusions for the lumens for this purpose. Because of the different diffusion tensors of the cell wall material at different moisture contents, the calculation time would be very long due to the time-consuming calculation of the $\mathbb{P}$-tensor with about one minute per step. Therefore the calculation of the $\mathbb{P}$-tensor was split in two steps. First a standardized $\mathbb{P}$-tensor for one specific wood density was calculated. The ratio of $D_{cellwall,trans}$ to $D_{cellwall,long}$ is always the same irrespective of the moisture content and temperature, so that the real $\mathbb{P}$-tensor for each step can easily be gained by dividing the standardized $\mathbb{P}$-tensor by the tensor component $D_{cellwall,trans}$ of the actual diffusion tensor of the cell wall. The standardized $\mathbb{P}$-tensor was calculated as described in Section 3.2 as:

$$\mathbb{D}_{cellwall,standard} = \begin{bmatrix} 1 & 0 & 0 \\ 0 & 1 & 0 \\ 0 & 0 & \frac{D_{cellwall,long}}{D_{cellwall,trans}} \end{bmatrix} \tag{5.41}$$

resulting in:

$$P_{ell,standard,ij} = \frac{1}{4 \cdot \pi} \int_{-1}^{+1} \int_{0}^{2\pi} \xi_i \cdot \xi_j \cdot \left(D_{cellwall,standard,kl} \cdot \xi_k \cdot \xi_l\right)^{-1} \, \mathrm{d}\hat{\varphi} \, \mathrm{d}\hat{\xi}_3 \tag{5.42}$$

The real $\mathbb{P}$-tensor can now be gained as following:

$$\mathbb{P}_{ell} = \frac{\mathbb{P}_{ell,standard}}{D_{cellwall,trans}} \tag{5.43}$$

Now the homogenized diffusion tensor for the cell matrix can be calculated with Equation (3.73).

5.6.2 Homogenization step 2: Diffusion coefficients of a whole sample

Next the second homogenization step as described in Subsection 3.3.3 is executed. The whole diffusion model was programmed with Maple 11.0, the source code is displayed in Appendix B.2.

5.7 Validation of the multiscale diffusion model

The validation of the model is based on experimental moisture diffusion data for wood stated by F. Kollmann in his book [17]. In particular, these data were compared with corresponding model predictions in order to check the behavior of the model at different moisture contents and temperatures.

5.7.1 Radial diffusion coefficient at different moisture contents

By means of the model developed in Section 5.6, the variation of the radial diffusion coefficients for different moisture contents and temperatures was studied. Kollmann [17] published such coefficients for spruce with a density of 404 kg/m^3 at temperatures of 40, 60, 80, and 100 °C which were measured in diffusion tests. For the second homogenization step the densities of earlywood and latewood were set to 280 kg/m^3 and 820 kg/m^3, respectively, which are typical values for Norway spruce [17].

Figure 5.15 shows the results obtained with the developed model (solid lines) in comparison with the data given by Kollmann [17] (crosses denote the measured values, the dash-dotted lines are interpolations of these values). As one can see, the calculated values don't fit very well, especially for higher temperatures. The main reason for the deviation is the application of a linear term for the activation energy, which was derived for a temperature of 26.7 °C without consideration of the density variation within the annual rings.

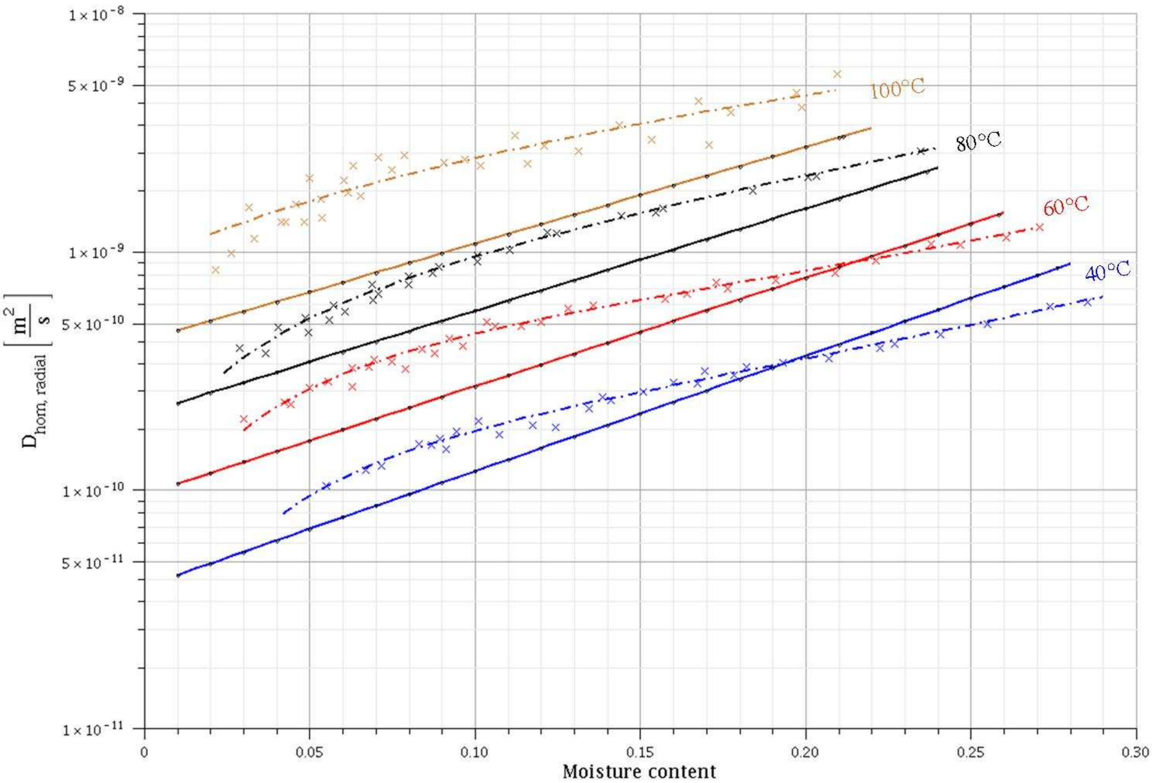

Figure 5.15: Radial diffusion coefficient of spruce wood ($\varrho_{ovendry} = 404\,\mathrm{kg/m^3}$)

5.7.2 Comparison of the activation energies

Because the used term for the activation energy delivered quite inaccurate results, adequate activation energies were back-calculated from the measured values of Kollmann [17] aiming at the identification of any regularities. Figure 5.16 shows the results of the back-calculation in comparison with Siau's term for activation energy (5.30). Several facts can be stated:

- The activation energy seems to be a temperature-dependent quantity.
- A linear approximation of the activation energy over different moisture contents is very rough.
- For 80 °C, the back-calculated curve is quite different in qualitative terms compared to the curves for the other temperatures.
- Although the differences between Siau's equation and the measured values are small (e.g. approximately 7 % for 100 °C at a moisture content of 0.03), they result in huge errors in the values for the diffusion coefficient of the cell wall substance (e.g. 61 % for 100 °C at a moisture content of 0.03).
- The slope of the graph according to Siau's equation doesn't fit very well to the other, back-calculated ones. This is because the activation energy is calculated for a constant density of the whole sample. If the density variations within the annual rings are taken in account, the resistance to diffusion is higher, and therefore the diffusion coefficient and the slope of the activation energy as function of the moisture content are lower.

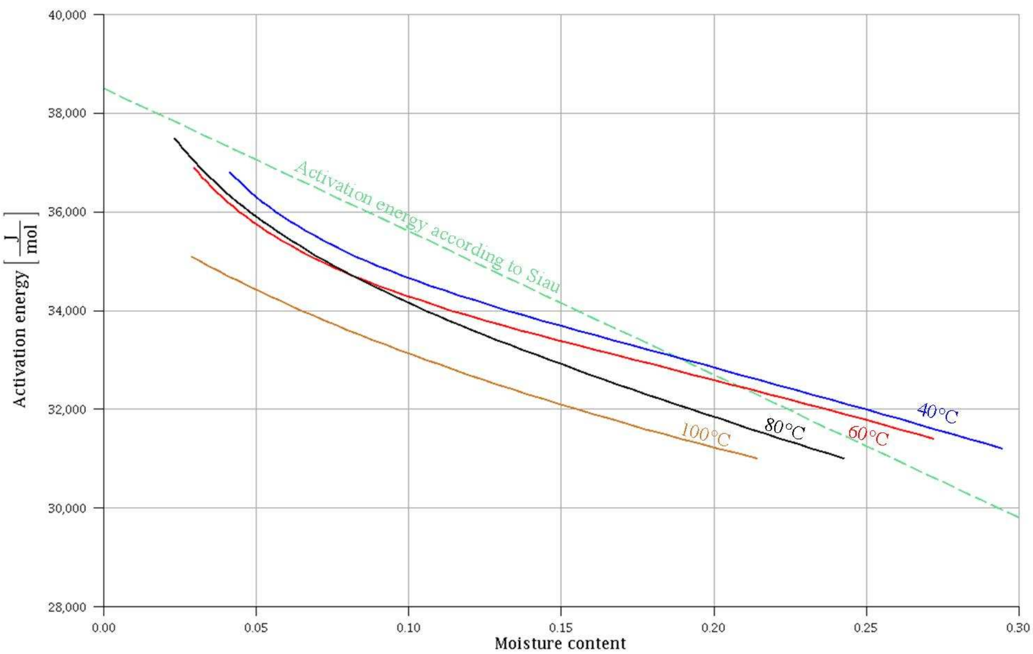

Figure 5.16: Back-calculated activation energies for different temperatures

5.7.3 Discussion

At present the diffusion model provides too inaccurate values for further use. An improvement is possible by replacing Siau's approximated formula for activation energy by a temperature-dependent nonlinear one. The more elegant way would be the completely physics-based calculation as introduced in the Subsections 5.5.3 and 5.5.4. Since the last step from analytical limits to a definite value of the activation energy is still unclear, however, the way of an empirical equation is more practical or, rather, unavoidable. Anyway further research is needed.

Chapter 6

Evaluation of the model for thermal conduction

6.1 Basics

6.1.1 Fourier's law

Thermal conduction is the transfer of thermal energy through matter, from a region of higher temperature to a region of lower temperature, and acts to equalize temperature differences [55]. It is described by the law of heat conduction, also known as Fourier's law, that links the time rate of heat transfer through a material to the negative gradient of temperature:

$$\underline{\phi_q} = -\lambda \cdot \underline{\mathrm{grad}}\, T \tag{6.1}$$

where $\underline{\phi_q}$ is the local heat flux [W/m^2], λ the thermal conductivity [W/m K], and $\underline{\mathrm{grad}}\, T$ the temperature gradient [K/m]. When Equation (6.1) is compared with Equation (3.2b), Fick's law of diffusion, it easily can be seen that the structure of the two equations is the same. Thus the homogenization techniques developed in Chapter 3 for diffusion can also be applied to the prediction of effective thermal conduction properties.

6.1.2 Comparison of thermal conductivities

In Table 6.1 the thermal conductivities of some common materials are specified. As it can be seen, wood is a relatively good insulator, especially perpendicular to the fiber axis. The resistance to flow is high in this direction due to the interruption of the path by the air-filled lumens with only low conductivity [31]. The insulating properties of wood have several advantages in construction engineering, for example with respect to better heat insulation and also to better fire-resistance compared with highly conducting materials such as metals, which soften at high temperatures.

Material	λ [W/m K]	Source
Water (20 °C)	0.598	Eq. (6.2)
Air (20 °C)	0.026	Eq. (6.3)
Cell wall substance transversal	0.439	Siau [31]
Cell wall substance transversal	0.410	Gu [13]
Cell wall substance transversal	0.520	Thunman [35]
Cell wall substance longitudinal	0.876	Siau [31]
Cell wall substance longitudinal	0.730	Thunman[31]
Softwood	0.150	Bautabellen [20]
Hardwood	0.200	Bautabellen [20]
Brick	0.760	Bautabellen [20]
Concrete	1.500	Bautabellen [20]
Limestone	1.700	Bautabellen [20]
Granite	3.500	Bautabellen [20]
Gypsum plasterboard	0.210	Bautabellen [20]
Glass	0.810	Bautabellen [20]
Mineral fibrous insulating material	0.040	Bautabellen [20]
Copper	386.167	Siau [31]
Aluminum	201.729	Siau [31]
Stainless steel	16.282	Siau [31]

Table 6.1: Thermal conductivities of several materials

6.1.3 The thermal conductivity of water

The values for the thermal conductivity of water used in this diploma thesis were again taken from steam tables [11] and fitted (see Section B.1.5) by an empirical correlation:

$$\lambda_w = -0.9449956778\,10^{-2}\,T^2 + 7.298074517\,T - 728.5203013\,[\mathrm{W/m\,K}] \qquad (6.2)$$

Figure 6.1 shows the thermal conductivity of water over the temperature range from the freezing up to the boiling point.

6.1.4 The thermal conductivity of air

The values for the thermal conductivity of air were chosen according to Incropera [16] in this diploma thesis and fitted (see Section B.1.6) by a polynomial in temperature:

$$\lambda_a = -2.917470146\,10^{-8}\,T^2 + 9.49953295\,10^{-5}\,T + 3.102291022\,10^{-4}\,[\mathrm{W/m\,K}] \qquad (6.3)$$

Figure 6.2 shows the thermal conductivity of air over the temperature range from 100 up to 1000 Kelvin.

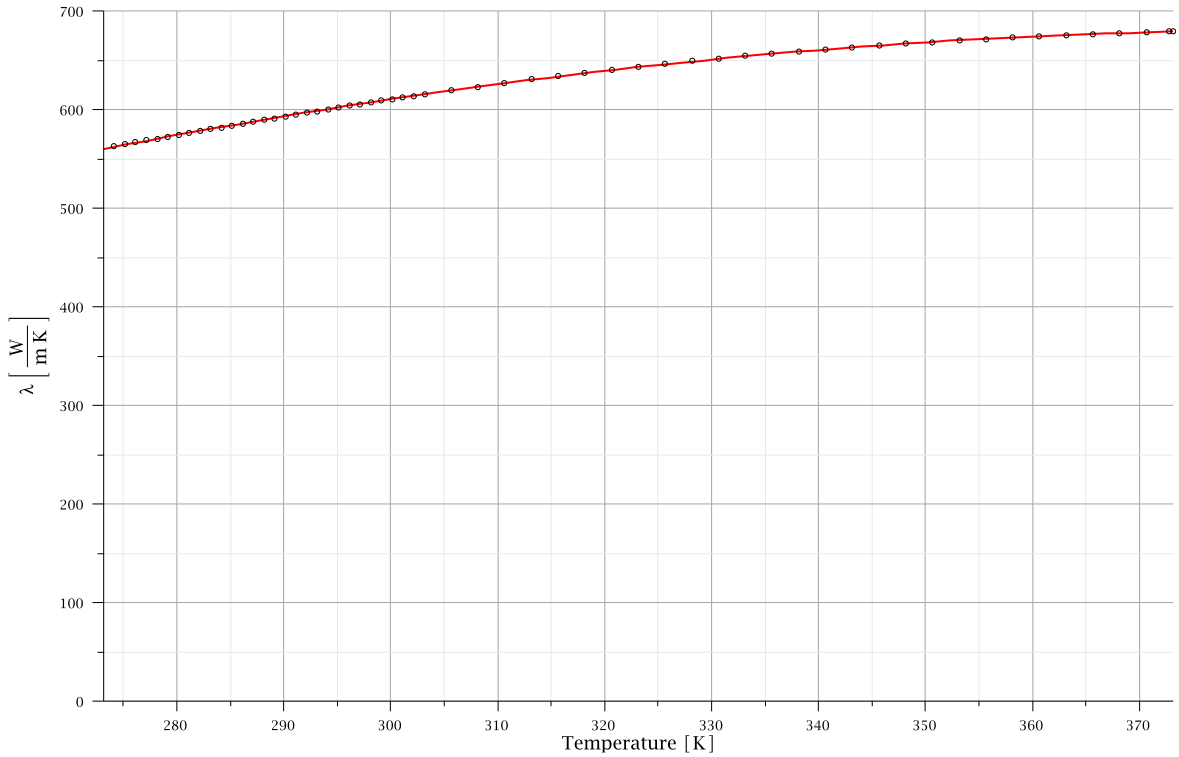

Figure 6.1: Thermal conductivity of water from 273.15 to 373.15 K

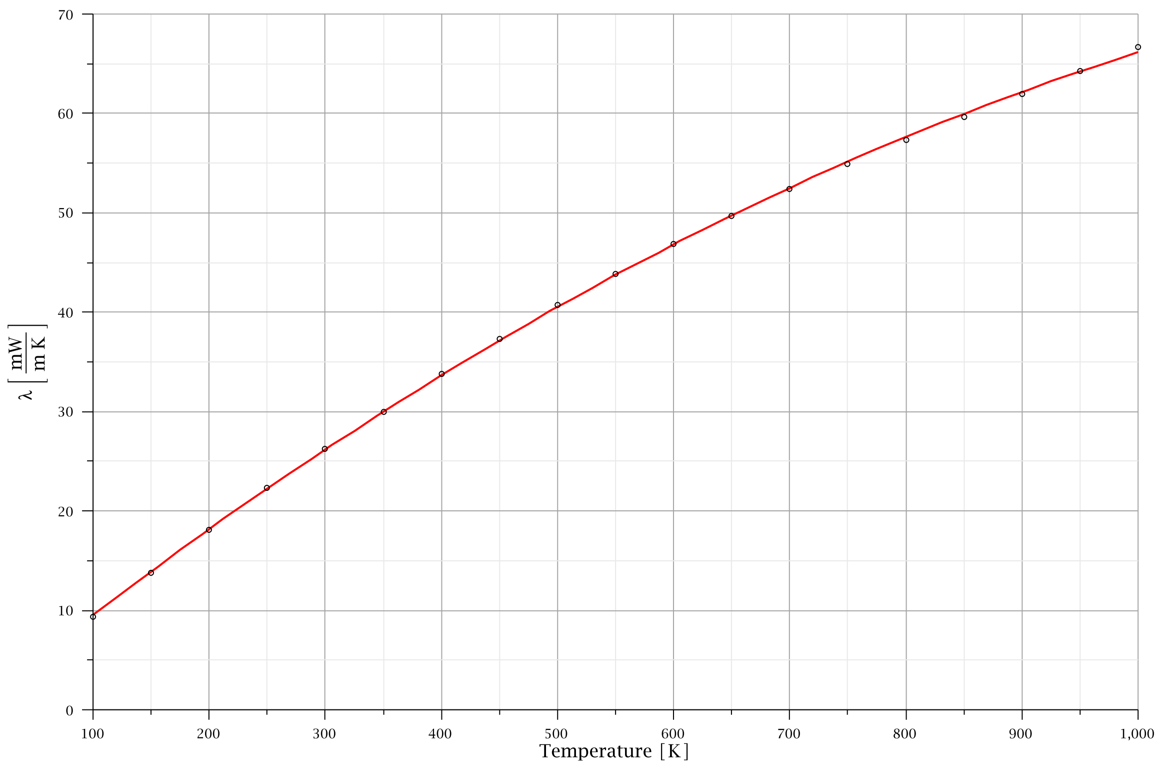

Figure 6.2: Thermal conductivity of air from 100 to 1000 K

6.2 The thermal conductivities of lumen and cell wall

6.2.1 The thermal conductivity of the lumen

Since this diploma thesis discusses only conditions under the fiber saturation point, the lumens never contain water. Therefore the thermal conductivity of the lumen is assumed to be the same like that for air. Using Equation (6.3), the thermal conductivity tensor of the lumen can be written as:

$$\mathbb{K}_{lumen} = \begin{bmatrix} \lambda_a & 0 & 0 \\ 0 & \lambda_a & 0 \\ 0 & 0 & \lambda_a \end{bmatrix} \tag{6.4}$$

6.2.2 The thermal conductivity of the cell wall

Thermal conductivity of the cell wall is calculated by means of mixture rules considering a simple parallel connection of the conductivities of the cell wall substance and the bound water [31]. Hereby it is assumed that the cell wall material is transversal isotropic by means of thermal conductivity, and has therefore two different thermal conductivities for the transversal and longitudinal direction. As can be seen in Table 6.1, the values for the thermal conductivity of the cell wall specified in the literature vary considerably. For this diploma thesis the lowest and newest values were taken with 0.410 [W/m K] according to Gu [13] for the thermal conductivity of the cell wall substance in transversal direction and 0.876 [W/m K] according to Thunman [35] for the thermal conductivity of the cell wall substance in longitudinal direction. Here further refinement of the model is possible by an additional homogenization step for the cell wall material, based on the thermal conductivities of its components hemicellulose, cellulose, and lignin.

The water phase and the cell wall material phase are assumed to be arranged in parallel in the transversal and longitudinal directions of the cell wall [31]. The value for the thermal conductivity of water is calculated according to Equation (6.2). For parallel connection the conductivities of the dry cell wall substance and the bound water are weighted by their volume fractions and added together. Hence, the equations for transversal and longitudinal thermal conductivity of the cell wall are the following:

$$\lambda_{trans} = \lambda_{0,trans} + \lambda_w \cdot mc \tag{6.5}$$

$$\lambda_{long} = \lambda_{0,long} + \lambda_w \cdot mc \tag{6.6}$$

For further use, the thermal conductivities of the cell wall are assembled in the thermal conductivity tensor of the cell wall:

$$\mathbb{K}_{cellwall} = \begin{bmatrix} \lambda_{trans} & 0 & 0 \\ 0 & \lambda_{trans} & 0 \\ 0 & 0 & \lambda_{long} \end{bmatrix} \tag{6.7}$$

6.3 The multiscale thermal conduction model

In most transport processes there is a significant flux through the cell-wall substance and usually, but not always, through the air in the lumens. Frequently, the flow through the pit openings may be neglected because of their small fractional surface area of the cell wall (less than 1 %). The aim of one homogenized thermal conductivity for the whole sample is reached by two homogenization steps.

6.3.1 Homogenization step 1: Thermal conductivities of the cell assembly

In Step 1 the thermal conductivity of the cell assembly for a given oven-dry density is calculated by the model developed in Chapter 3. Again the Mori-Tanaka scheme with ellipsoidal inclusions is used. The standardized $\mathbb{P}$-tensor was calculated as described in Section 3.2 as:

$$P_{ell,ij} = \frac{1}{4 \cdot \pi} \int_{-1}^{+1} \int_{0}^{2\pi} \xi_i \cdot \xi_j \cdot \left(K_{cellwall,kl} \cdot \xi_k \cdot \xi_l\right)^{-1} \,\mathrm{d}\hat{\varphi}\,\mathrm{d}\hat{\xi}_3 \tag{6.8}$$

Now the homogenized thermal conductivity tensor for the cell assembly can be calculated according to Equation (3.73), replacing the diffusion tensors of the cell wall and the lumen by the corresponding thermal conductivity tensors.

6.3.2 Homogenization step 2: Thermal conductivities of a whole sample

Next the second homogenization step as described in Subsection 3.3.3 is executed. The whole thermal conduction model was programmed with Maple 11.0, the source code is displayed in Appendix B.3

6.4 Validation of the multiscale thermal conduction model

The experimental validation of the model developed in this diploma thesis is again based on test results for thermal conductivities of several wood species collected by F. Kollmann in his book [17]. The first comparison of these data with corresponding model estimates was made to check the dependency on density, and the second to test the behavior of the model for different moisture contents.

6.4.1 Thermal conductivity at different densities

By use of the model developed in Section 6.3, the variation of the thermal conductivity across different oven-dry densities was studied. Since the species is not specified for most test results, densities of 280 kg/m^3 for earlywood and of 820 kg/m^3 for latewood were assumed. These values actually apply to Norway spruce [17], but are also roughly valid for other softwoods. For comparability with the data of Kollmann [17], a temperature of 20 °C and a constant moisture content of 12 % were assumed.

Figure 6.3 shows the results of the developed model in comparison with data given by Kollmann [17]. The conductivities in the direction perpendicular to the grain of Kollmann are the arithmetic means of radial and tangential conductivity. The good agreement of test data and model predictions can be clearly seen, also for hardwood.

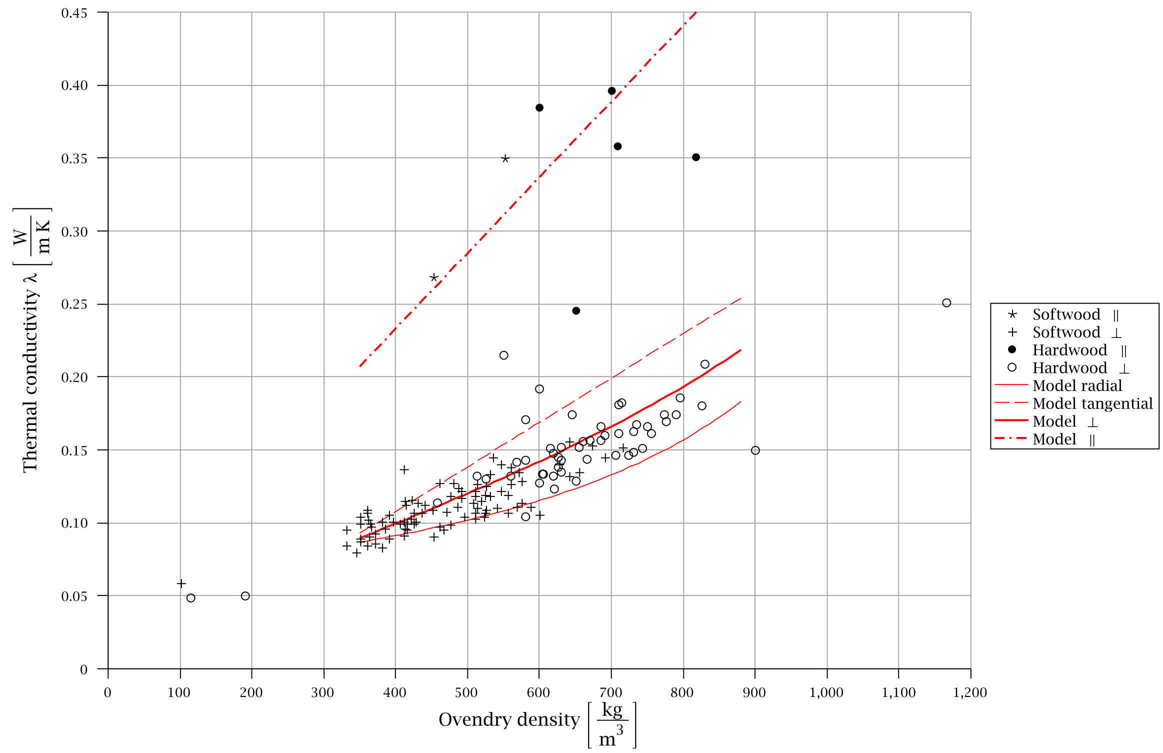

Figure 6.3: Thermal conductivity of wood at 20 °C and 12 % moisture content

6.4.2 Thermal conductivity at different moisture contents

To check the behavior of the model at different moisture contents, test results of three samples given by Kollmann [17] were recalculated. Unfortunately neither the density of the samples nor the temperature during the experiments is reported, so they were fitted for the results at zero moisture content, in order to check at least the slope of the curves of thermal conductivity over moisture content. As can be seen in Figure 6.4, this fits quite well.

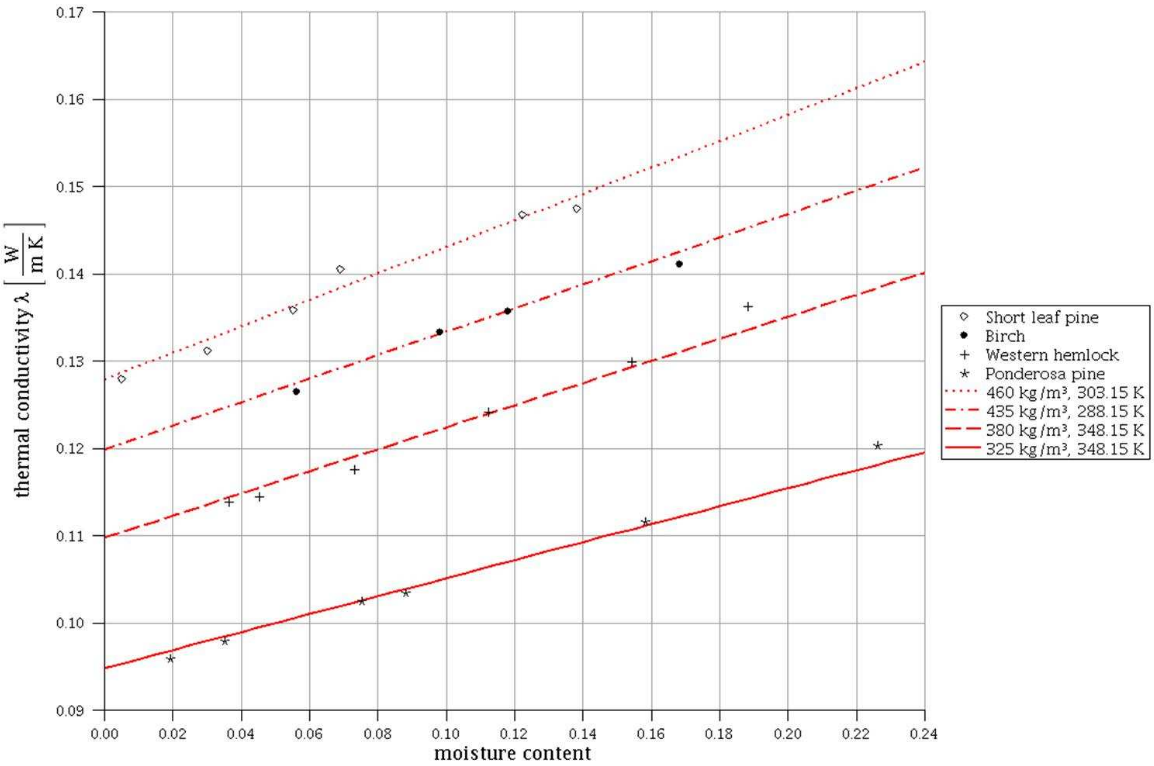

Figure 6.4: Dependence of tangential thermal conductivity of wood on the moisture content

6.4.3 Thermal conductivities for single specimens

At last test results for four single specimens with known values of density, moisture content, and temperature (again according to Kollmann [17]) were recalculated. The results are assembled in Table 6.2. The calculated values for the only softwood specimen in this group, spruce, fit quite well. The too low radial conductivity can be explained by the negligence of the ray cells in the model, which constitute continuous pathways of good thermal conduction in radial direction. The values for hardwood fit not as well as those for softwood because of the more complicated microstructure of hardwood with vessels and distinctive amounts of ray cells. While the vessels act as thermal insulators in longitudinal direction and, thus, result in smaller thermal conductivity, the ray

Wood species	Oven-dry density [kg/m^3]	Moisture content [%]	Temperature [°C]	Measured thermal conductivity λ_{rad} [W/m K]	λ_{tang} [W/m K]	λ_{long} [W/m K]	Calculated thermal conductivity λ_{rad} [W/m K]	λ_{tang} [W/m K]	λ_{long} [W/m K]
Ash	740	15	20	0.3056	0.1758	0.1633	0.4096	0.1518	0.2073
Spruce	410	16	20	0.2219	0.1214	0.1047	0.2399	0.0878	0.1149
Mahogany	700	15	20	0.3098	0.1675	0.1549	0.3888	0.1450	0.1936
Walnut	650	12	20	0.3308	0.1465	0.1382	0.3629	0.1235	0.1840

Table 6.2: Thermal conductivities of single specimens

Chapter 7

Summary, conclusions and future work

The focus of this thesis was the modeling of transport processes in wood (especially softwood) based on microstructural considerations by means of homogenization techniques such as the Mori-Tanaka scheme. Taking the microstructure into account, allows to suitably describe the anisotropic material behavior on the microscale with different properties in the radial, tangential, and longitudinal direction on a physical basis. In theoretical respects, the main task within the model formulation was the derivation of the Hill tensor ($\mathbb{P}$-tensor) for a diffusion process and ellipsoidal inclusion shape.

The successful operation of the model was proved by means of a comparison with a second multiscale model, using the unit cell method as homogenization technique. A good agreement of the results obtained with the two models was observed. The appearing deviations could be explained by the different inclusion shapes, namely ellipsoidal inclusions in the Mori-Tanaka scheme compared with hexagonal inclusions in the unit cell method. The comparison also showed the advantage of the Mori-Tanaka scheme over the unit cell method because of the simple adaptivity to different geometries because of the analytical formulation of this scheme.

First the model was applied to moisture transport in softwood under the fiber saturation point. The main challenge in this context was the determination of the diffusion coefficients for both cell walls and lumens. Especially the diffusion behavior of the cell walls as contributing factor of the diffusion process through wood turned out to be quite complicated to model.

Since the activation energy of the adsorbed water molecules turned out to be decisive, it was investigated in detail. Unfortunately only a lower and an upper bound could be derived for this energy, what is too inaccurate because of the great influence of the activation energy on the resulting diffusion coefficients. Thus, a simplified phenomenological relation describing a linear dependence of the activation energy on the moisture content was used, which is commonly applied in literature to model the moisture transport behavior of the cell wall. Evaluation of the developed multiscale model with this linear equation resulted in partly very inaccurate model predictions for macroscopic diffusion coefficients. It turned out that the reason for these errors was the negligence of the nonlinearity with respect to the moisture content and the temperature dependency of the activation energy. Here further refinement of the model is possible by replacing the approximated formula for this energy by a temperature-dependent nonlinear one. As long as a completely physics-based calculation is not possible, however, the use of an empirical equation is unavoidable.

The application to thermal conduction turned out to be easier because of the better knowledge of the thermal properties of both cell walls and lumens. Nevertheless, also in this area further research is possible. For example an additional homogenization step could be performed in order to calculate the thermal conductivity of the cell wall from the behavior of its constituents. This is expected to result in improved accuracy of the model, since the thermal conductivity of the cell wall is not exactly known but reported differently in the literature. The actual homogenization model for thermal conduction provided estimates for the thermal conductivity of softwood which agree well with corresponding measured results. For hardwood, the agreement is not that good (as supposed) due to the more differentiated microstructure, including large vessels and ray cells. But, again, a further homogenization step would allow to take also these further inhomogeneities into account.

On the whole, the performed calculations and numerical simulations delivered interesting insight into transport processes in wood. With a few refinements, the developed models can be used for a further investigation of moisture dependent procedures in wood. Also an extension to other states is possible. For example, the extension to conditions over the saturation point could be established by taking the liquid water in the cell lumens into account. This would also enable in parts the simulation of wood drying processes starting at green conditions and therefore also provide an interesting simulation tool for both timber engineering and the timber industry.

Bibliography

[1] S. Avramidis. The basics of sorption. In *Mechanical Performance of Wood and Wood Products, Theme: Wood-Water Relations*. International Conference of COST Action E8, 1997.

[2] P. Cruiziat, H. Cochard, and T. Améglio. Hydraulic architecture of trees: main concepts and results. *Annals of Forest Science*, 59:723–752, 2002.

[3] L. Dormieux. *Applied micromechanics of porous materials*. Verlag Springer, Wien, New York, 2005.

[4] L. Dormieux, D. Kondo, and F. Ulm. *Microporomechanics*. John Wiley & Sons, New York, 2006.

[5] L. Dormieux and E. Lemarchand. Modélisation macroscopique du transport diffusif. *Oil & Gas Science and Technology*, 55:15–34, 2000.

[6] L. Dormieux and E. Lemarchand. Homogenization approach of advection and diffusion in cracked porous material. *Journal of Engineering Mechanics*, 127:1267–1274, 2001.

[7] A. Einstein. Über die von der molekularkinetischen Theorie der Wärme geforderte Bewegung von in ruhenden Flüssigkeiten suspendierten Teilchen. *Annalen der Physik*, 17:549–560, 1905.

[8] D. Eisenberg and W. Kauzmann. *The Structure and Properties of Water*. Oxford University Press, 1969.

[9] H. L. Frandsen. Modeling of moisture transport in wood, state of the art and analytic discussion. Technical report, Dept. of Building Technology and Structural Engineering, Aalborg University, March 2005.

[10] H. L. Frandsen and S. Svensson. Implementation of sorption hysteresis in multi-Fickian moisture transport. *Holzforschung*, 61:693–701, 2007.

[11] U. Grigull, J. Straub, and P. Schiebener. *Steam Tables in SI-Units*. Verlag Springer, New York, Berlin, Heidelberg, 3rd edition, 1990.

[12] D. Gross and T. Seelig. *Bruchmechanik, mit einer Einführung in die Mikromechanik*. Verlag Springer, Berlin, Heidelberg, New York, 3rd edition, 2007.

[13] H. Gu and A. Zink-Sharp. Geometric model for softwood transverse thermal conductivity, Part I. *Wood and Fiber Science*, 37:699–711, 2005.

[14] C. Hellmich, J. Barthélémy, and L. Dormieux. Mineral-collagen interactions in elasticity of bone ultrastructure - a continuum micromechanics approach. *European Journal of Mechanics - A/Solids*, 23:783–810, 2004.

[15] K. Hofstetter, C. Hellmich, and J. Eberhardsteiner. Development and experimental validation of a continuum micromechanics model for the elasticity of wood. *European Journal of Mechanics - A/Solids*, 24:1030–1053, 2005.

[16] F. P. Incropera, D. P. Pewitt, T. L. Bergman, and A. S. Lavine. *Fundamentals of Heat and Mass Transfer*. John Wiley & Sons, Hoboken, 6th edition, 2007.

[17] F. Kollmann. *Technologie des Holzes und der Holzwerkstoffe*, volume 1. Verlag Springer, Berlin, Heidelberg, New York, 2nd edition, 1951.

[18] K. Krabbenhoft. *Moisture Transport in Wood, A Study of Physical-Mathematical Models and their Numerical Implementation*. PhD thesis, Technical University of Denmark, 2003.

[19] K. Krabbenhoft and L. Damkilde. A model for non-Fickian moisture transfer in wood. *Materials and Structures*, 37:615–622, 2004.

[20] R. Krapfenbauer. *Bautabellen*. Verlag Jugend & Volk, Wien, 1998.

[21] E. Kreyszig and E. J. Norminton. *Maple Computer Guide*. John Wiley & Sons, New York, 8th edition, 2001.

[22] H. Mang and G. Hofstetter. *Festigkeitslehre*. Verlag Springer, Wien, New York, 2004.

[23] R. M. Nelson. Diffusion of bound water in wood, Part 1: The driving force. *Wood Science and Technology*, 20:125–135, 1986.

[24] R. M. Nelson. Diffusion of bound water in wood, Part 2: A model for isothermal diffusion. *Wood Science and Technology*, 20:235–251, 1986.

[25] R. M. Nelson. Diffusion of bound water in wood, Part 3: A model for nonisothermal diffusion. *Wood Science and Technology*, 20:309–328, 1986.

[26] R. M. Nelson. Heats of transfer and activation energy for bound water diffusion in wood. *Wood Science and Technology*, 25:193–202, 1991.

[27] K. J. Niklas. *Plant Biomechanics*. The University of Chicago Press, Chicago, London, 1992.

[28] P. Perré and I. Turner. Determination of the material property variations across the growth ring of softwood for use in a heterogeneous drying model, Part 1. *Holzforschung*, 55:318–323, 2001.

[29] P. Perré and I. Turner. Determination of the material property variations across the growth ring of softwood for use in a heterogeneous drying model, Part 2. *Holzforschung*, 55:417–425, 2001.

[30] E. Schmidt. *Properties of Water and Steam in SI-Units*. Verlag Springer, New York, Berlin, Heidelberg, 4rd edition, 1989.

[31] J. F. Siau. *Transport Processes in Wood*. Verlag Springer, Berlin, Heidelberg, New York, 1984.

[32] J. F. Siau and Z. Jin. Nonisothermal moisture diffusion experiments analyzed by four alternative equations. *Wood Science and Technology*, 19:151–157, 1985.

[33] C. Skaar. *Transport Processes in Wood*. Verlag Springer, Berlin, Heidelberg, New York, 1988.

[34] Forest Products Society. *Wood Handbook*. U.S. Department of Agriculture, United States of America, 1999.

[35] H. Thunman and B. Leckner. Thermal conductivity of wood - models for different stages of combustion. *Biomass & Bioenergy*, 23:47–54, 2002.

[36] I. Turner. A two-dimensional orthotropic model for simulating wood drying processes. *Applied Mathematical Modeling*, 20:60–81, 1996.

[37] R. Wagenführ. *Holzatlas*. Carl Hanser Verlag, München, 2007.

[38] A. Zaoui. Continuum Micromechanics: Survey. *Journal of Engineering Mechanics*, 128:808–815, 2002.

[39] `http://www.britannica.com/ebc/art-57860`. 28.01.2006.

[40] `http://www.valuecreatedreview.com/softwood.htm`. 28.01.2006.

[41] `http://en.wikipedia.org/wiki/Activation_energy`. 30.03.2008.

[42] `http://en.wikipedia.org/wiki/Arrhenius_equationy`. 24.03.2008.

[43] `http://en.wikipedia.org/wiki/Avogadro's_number`. 01.05.2008.

[44] `http://en.wikipedia.org/wiki/Clausius-Clapeyron_relation`. 22.05.2008.

[45] `http://de.wikipedia.org/wiki/Diffusion`. 15.04.2008.

[46] `http://de.wikipedia.org/wiki/Diffusionskoeffizient`. 17.03.2008.

[47] `http://en.wikipedia.org/wiki/Distribution_%28mathematics%29`. 01.05.2008.

[48] `http://en.wikipedia.org/wiki/Divergence`. 16.05.2008.

[49] `http://en.wikipedia.org/wiki/Divergence_theorem`. 16.05.2008.

[50] http://en.wikipedia.org/wiki/Fick%27s_law_of_diffusion. 08.03.2008.

[51] http://en.wikipedia.org/wiki/Gas_constant. 18.04.2008.

[52] http://en.wikipedia.org/wiki/Ideal_gas_law. 28.04.2008.

[53] http://en.wikipedia.org/wiki/Gibbs_free_energy. 28.03.2008.

[54] http://en.wikipedia.org/wiki/Green%27s_function. 27.04.2008.

[55] http://en.wikipedia.org/wiki/Heat_conduction. 04.05.2008.

[56] http://en.wikipedia.org/wiki/Specific_heat. 01.05.2008.

[57] http://de.wikipedia.org/wiki/T%C3%BCpfel. 01.02.2008.

[58] http://en.wikipedia.org/wiki/Vapor_pressure. 28.04.2008.

[59] http://en.wikipedia.org/wiki/Water_%28molecule%29. 04.05.2008.

[60] http://en.wikipedia.org/wiki/Image:Taxus_wood.jpg. 28.01.2006.

Appendix A

Steam table in SI-Units

In several chapters of this diploma thesis values obtained from steam tables are used. These values were taken from the steam tables given in [11] and [30] are summarized in the Tables A.1, A.2, and A.3

t °C	T K	p_0 MPa	ϱ_w kg/m^3	ϱ_v kg/m^3	h_w kJ/kg	h_v kJ/kg	Q_v kJ/kg	$c_{p,v}$ kJ/kg K	λ_w mW/m K	η_w μPa s
0.0	273.15	0.00061	999.8	0.0049	-0.0416	2500.5	2500.6	1.868	561.0	1793
1.0	274.15	0.00066	999.8	0.0052	4.1832	2502.4	2498.2	1.868	562.9	1732
2.0	275.15	0.00071	999.9	0.0056	8.4010	2504.2	2495.8	1.869	564.8	1674
3.0	276.15	0.00076	999.9	0.0060	12.613	2506.0	2493.4	1.869	566.7	1620
4.0	277.15	0.00081	999.9	0.0064	16.819	2507.9	2491.1	1.870	568.6	1568
5.0	278.15	0.00087	999.9	0.0068	21.021	2509.7	2488.7	1.871	570.5	1519
6.0	279.15	0.00094	999.9	0.0073	25.220	2511.5	2486.3	1.871	572.4	1472
7.0	280.15	0.00100	999.9	0.0078	29.415	2513.4	2484.0	1.872	574.3	1428
8.0	281.15	0.00107	999.8	0.0083	33.608	2515.2	2481.6	1.872	576.2	1385
9.0	282.15	0.00115	999.8	0.0088	37.799	2517.1	2479.3	1.873	578.1	1345
10.0	283.15	0.00123	999.7	0.0094	41.988	2518.9	2476.9	1.874	580.0	1306
11.0	284.15	0.00131	999.6	0.0100	46.175	2520.7	2474.5	1.875	581.9	1270
12.0	285.15	0.00140	999.5	0.0107	50.362	2522.6	2472.2	1.875	583.8	1235
13.0	286.15	0.00150	999.4	0.0114	54.547	2524.4	2469.8	1.876	585.6	1201
14.0	287.15	0.00160	999.2	0.0121	58.732	2526.2	2467.5	1.877	587.5	1169
15.0	288.15	0.00171	999.1	0.0128	62.917	2528.0	2465.1	1.878	589.3	1138
16.0	289.15	0.00182	998.9	0.0136	67.101	2529.9	2462.8	1.879	591.2	1109
17.0	290.15	0.00194	998.8	0.0145	71.285	2531.7	2460.4	1.879	583.0	1080
18.0	291.15	0.00206	998.6	0.0154	75.468	2533.5	2458.1	1.880	594.8	1053
19.0	292.15	0.00220	998.4	0.0163	79.652	2535.3	2455.7	1.881	596.6	1027

Table A.1: Steam table in SI-Units, $0 - 19\,°C$

t °C	T K	p_0 MPa	ϱ_w kg/m^3	ϱ_v kg/m^3	h_w kJ/kg	h_v kJ/kg	Q_v kJ/kg	$c_{p,v}$ kJ/kg K	λ_w mW/m K	η_w μPa s
20.0	293.15	0.00234	998.2	0.0173	83.835	2537.2	2453.3	1.882	598.4	1002
21.0	294.15	0.00249	998.0	0.0183	88.019	2539.0	2451.0	1.883	600.2	978.0
22.0	295.15	0.00264	997.7	0.0194	92.202	2540.8	2448.6	1.884	601.9	954.8
23.0	296.15	0.00281	997.5	0.0206	96.386	2542.6	2446.2	1.885	603.7	932.6
24.0	297.15	0.00299	997.3	0.0218	100.57	2544.5	2443.9	1.886	605.4	911.1
25.0	298.15	0.00317	997.0	0.0231	104.75	2546.3	2441.5	1.887	607.1	890.5
26.0	299.15	0.00336	996.8	0.0244	108.94	2548.1	2439.2	1.888	608.8	870.6
27.0	300.15	0.00357	996.5	0.0258	113.12	2549.9	2436.8	1.889	610.5	851.4
28.0	301.15	0.00378	996.2	0.0273	117.30	2551.7	2434.4	1.890	612.2	832.8
29.0	302.15	0.00401	995.9	0.0288	121.49	2553.5	2432.0	1.891	613.8	815.0
30.0	303.15	0.00425	995.6	0.0304	125.67	2555.3	2429.7	1.892	615.4	797.7
31.0	304.15	0.00451	995.3	0.0322	129.85	2557.1	2427.3	1.893	617.0	781.4
32.0	305.15	0.00476	995.0	0.0339	134.04	2559.0	2424.9	1.894	618.6	765.1
33.0	306.15	0.00504	994.6	0.0358	138.22	2560.8	2422.5	1.896	620.2	749.5
34.0	307.15	0.00533	994.3	0.0377	142.41	2562.6	2420.2	1.897	621.7	734.6
35.0	308.15	0.00563	994.0	0.0397	146.59	2564.4	2417.8	1.898	623.2	719.6
36.0	309.15	0.00596	993.6	0.0419	150.77	2566.2	2415.4	1.899	624.7	705.8
37.0	310.15	0.00629	993.3	0.0440	154.96	2568.0	2413.0	1.900	626.2	692.0
38.0	311.15	0.00664	992.9	0.0463	159.14	2569.8	2410.6	1.902	627.7	678.7
39.0	312.15	0.00701	992.6	0.0488	163.32	2571.6	2408.3	1.903	629.1	666.0
40.0	313.15	0.00738	992.2	0.0512	167.50	2573.4	2405.9	1.904	630.5	653.2
41.0	314.15	0.00780	991.8	0.0539	171.68	2575.2	2403.5	1.906	631.9	641.4
42.0	315.15	0.00821	991.4	0.0566	175.87	2576.9	2401.1	1.907	633.3	629.6
43.0	316.15	0.00865	991.0	0.0595	180.05	2578.7	2398.7	1.909	634.7	618.2
44.0	317.15	0.00912	990.6	0.0625	184.24	2580.5	2396.3	1.910	636.0	607.3
45.0	318.15	0.00959	990.2	0.0655	188.42	2582.3	2393.9	1.912	637.3	596.3
46.0	319.15	0.01011	989.8	0.0689	192.60	2584.1	2391.5	1.913	638.6	586.1
47.0	320.15	0.01063	989.3	0.0722	196.78	2585.9	2389.1	1.914	639.9	575.9
48.0	321.15	0.01118	988.9	0.0757	200.96	2587.7	2386.7	1.916	641.1	566.1
49.0	322.15	0.01176	988.4	0.0794	205.15	2589.4	2384.3	1.917	642.3	556.6
50.0	323.15	0.01234	988.0	0.0831	209.33	2591.2	2381.9	1.919	643.5	547.1
51.0	324.15	0.01299	987.5	0.0872	213.51	2593.0	2379.5	1.921	644.7	538.2
52.0	325.15	0.01364	987.0	0.0913	217.69	2594.7	2377.0	1.923	645.8	529.3
53.0	326.15	0.01432	986.6	0.0955	221.87	2596.5	2374.6	1.925	647.0	520.8
54.0	327.15	0.01503	986.1	0.1000	226.06	2598.2	2372.2	1.926	648.1	512.5
55.0	328.15	0.01575	985.7	0.1045	230.24	2600.0	2369.8	1.928	649.2	504.2
56.0	329.15	0.01655	985.2	0.1094	234.42	2601.8	2367.4	1.930	650.2	496.4
57.0	330.15	0.01734	984.7	0.1143	238.61	2603.5	2364.9	1.931	651.3	488.7
58.0	331.15	0.01818	984.2	0.1195	242.79	2605.3	2362.5	1.933	652.3	481.2
59.0	332.15	0.01905	983.7	0.1249	246.97	2607.0	2360.0	1.935	653.3	473.9
60.0	333.15	0.01993	983.2	0.1303	251.15	2608.8	2357.6	1.937	654.3	466.6
61.0	334.15	0.02090	982.7	0.1362	255.33	2610.5	2355.2	1.939	655.3	459.8
62.0	335.15	0.02187	982.2	0.1421	259.52	2612.2	2352.7	1.941	656.2	452.9
63.0	336.15	0.02288	981.6	0.1483	263.70	2614.0	2350.3	1.943	657.1	446.3
64.0	337.15	0.02395	981.1	0.1548	267.89	2615.7	2347.8	1.945	658.0	439.8

Table A.2: Steam table in SI-Units, $20 - 64\,$°C

t °C	T K	p_0 MPa	ϱ_w kg/m^3	ϱ_v kg/m^3	h_w kJ/kg	h_v kJ/kg	Q_v kJ/kg	$c_{p,v}$ kJ/kg K	λ_w mW/m K	η_w μPa s
65.0	338.15	0.02502	980.5	0.1613	272.08	2617.5	2345.4	1.947	658.9	433.4
66.0	339.15	0.02620	980.0	0.1684	276.26	2619.2	2343.0	1.949	659.8	427.4
67.0	340.15	0.02737	979.5	0.1755	280.45	2620.9	2340.5	1.952	660.7	421.3
68.0	341.15	0.02860	978.9	0.1828	284.63	2622.7	2338.1	1.954	661.5	415.5
69.0	342.15	0.02989	978.3	0.1905	288.82	2624.4	2335.6	1.956	662.3	409.8
70.0	343.15	0.03118	977.7	0.1982	293.01	2626.1	2333.1	1.958	663.1	404.1
71.0	344.15	0.03259	977.1	0.2066	297.20	2627.9	2330.6	1.960	663.9	398.7
72.0	345.15	0.03400	976.6	0.2150	301.39	2629.6	2328.1	1.963	664.6	393.3
73.0	346.15	0.03547	976.0	0.2237	305.58	2631.3	2325.7	1.965	665.4	388.1
74.0	347.15	0.03702	975.4	0.2328	309.77	2633.0	2323.2	1.968	666.1	383.0
75.0	348.15	0.03856	974.8	0.2419	313.96	2634.6	2320.7	1.970	666.8	377.9
76.0	349.15	0.04025	974.2	0.2518	318.15	2636.3	2318.2	1.972	667.4	373.1
77.0	350.15	0.04194	973.6	0.2617	322.34	2638.0	2315.7	1.975	668.1	368.3
78.0	351.15	0.04370	973.0	0.2720	326.54	2639.7	2313.1	1.977	668.7	363.6
79.0	352.15	0.04553	972.4	0.2827	330.73	2641.4	2310.6	1.980	669.4	359.1
80.0	353.15	0.04737	971.8	0.2934	334.93	2643.1	2308.1	1.983	670.0	354.5
81.0	354.15	0.04937	971.2	0.3050	339.13	2644.8	2305.6	1.985	670.6	350.2
82.0	355.15	0.05138	970.5	0.3165	343.32	2646.5	2303.1	1.988	671.2	345.9
83.0	356.15	0.05347	969.9	0.3285	347.52	2648.1	2300.5	1.990	671.8	341.7
84.0	357.15	0.05564	969.2	0.3410	351.72	2649.8	2298.0	1.993	672.3	337.6
85.0	358.15	0.05781	968.6	0.3535	355.92	2651.4	2295.5	1.996	672.8	333.5
86.0	359.15	0.06017	968.0	0.3670	360.12	2653.0	2292.9	1.999	673.3	329.6
87.0	360.15	0.06254	967.3	0.3805	364.32	2654.7	2290.4	2.002	673.8	325.7
88.0	361.15	0.06500	966.7	0.3944	368.52	2656.3	2287.8	2.005	674.3	321.9
89.0	362.15	0.06756	966.0	0.4089	372.73	2658.0	2285.3	2.008	674.8	318.2
90.0	363.15	0.07012	965.3	0.4234	376.93	2659.6	2282.7	2.011	675.3	314.5
91.0	364.15	0.07289	964.6	0.4390	381.14	2661.2	2280.1	2.014	675.7	311.0
92.0	365.15	0.07566	963.9	0.4546	385.35	2662.9	2277.5	2.017	676.2	307.5
93.0	366.15	0.07854	963.3	0.4708	389.56	2664.5	2274.9	2.021	676.6	304.1
94.0	367.15	0.08153	962.6	0.4875	393.77	2666.1	2272.4	2.024	677.0	300.8
95.0	368.15	0.08453	961.9	0.5043	397.98	2667.7	2269.8	2.027	677.4	297.4
96.0	369.15	0.08776	961.2	0.5223	402.20	2669.3	2267.2	2.030	677.8	294.2
97.0	370.15	0.09099	960.5	0.5403	406.41	2671.0	2264.5	2.033	678.1	291.1
98.0	371.15	0.09409	959.9	0.5575	410.32	2672.5	2262.1	2.037	678.4	288.2
99.0	372.15	0.09704	959.3	0.5738	413.91	2673.8	2259.8	2.040	678.7	285.6
99.63	372.78	0.10000	958.7	0.5902	417.51	2675.1	2257.6	2.043	679.0	283.0
100.0	373.15	0.10130	958.4	0.5975	419.06	2675.7	2256.7	2.044	679.1	281.9

Table A.3: Steam table in SI-Units, $65 - 100\,°\mathrm{C}$

Appendix B

Program code

This chapter contains the source codes of the programs developed and used in the framework of this diploma thesis. The used mathematics software package was Maple 11.

B.1 Fitting of tabulated values

This section includes programs for the fitting of tabulated values for water and steam. Each of these programs calculates a polynomial equation with temperature as independent parameter based on given single values and displays the graph of this equation.

B.1.1 The density of water

```
restart:
points := [273.15, 999.8], [274.15, 999.8], [275.15, 999.9], [276.15, 999.9], [277.15, 999.9],
          [278.15, 999.9], [279.15, 999.9], [280.15, 999.9], [281.15, 999.8], [282.15, 999.8],
          [283.15, 999.7], [284.15, 999.6], [285.15, 999.5], [286.15, 999.4], [287.15, 999.2],
          [288.15, 999.1], [289.15, 998.9], [290.15, 998.8], [291.15, 998.6], [292.15, 998.4],
          [293.15, 998.2], [294.15, 998.0], [295.15, 997.7], [296.15, 997.5], [297.15, 997.3],
          [298.15, 997.0], [299.15, 996.8], [300.15, 996.5], [301.15, 996.2], [302.15, 995.9],
          [303.15, 995.6], [305.65, 994.8], [308.15, 994.0], [310.65, 993.1], [313.15, 992.2],
          [315.65, 991.2], [318.15, 990.2], [320.65, 989.1], [323.15, 988.0], [325.65, 986.8],
          [328.15, 985.7], [330.65, 984.4], [333.15, 983.2], [335.65, 981.9], [338.15, 980.5],
          [340.65, 979.2], [343.15, 977.7], [345.65, 976.3], [348.15, 974.8], [350.65, 973.3],
          [353.15, 971.8], [355.65, 970.2], [358.15, 968.6], [360.65, 967.0], [363.15, 965.3],
          [365.65, 963.6], [368.15, 961.9], [370.65, 960.2], [372.78, 958.7], [373.15, 958.4]:

with(plots):
with(CurveFitting):

plot1 := pointplot([points], symbol = circle, symbolsize = 5):
Approx := LeastSquares([points], T, curve = a*T^4+b*T^3+c*T^2+d*T+e);
plot2 := plot(Approx, T = 273.15 .. 373.15, thickness = 2):

display(plot2, plot1, view = [273.15 .. 373.15, 950 .. 1010], gridlines = true,
        labels = [Temperature*[K], varrho[w]*[mu Pa*s]],
        labeldirections = [horizontal, vertical], labelfont = [TIMES, ROMAN, 14]);
```

B.1.2 The heat of evaporation

```
restart:
points := [273.15, 2500.5416], [274.15, 2498.2168], [275.15, 2495.7990], [276.15, 2493.3870],
          [277.15, 2491.0810], [278.15, 2488.6790], [279.15, 2486.2800], [280.15, 2483.9850],
          [281.15, 2481.5920], [282.15, 2479.3010], [283.15, 2476.9120], [284.15, 2474.5250],
          [285.15, 2472.2380], [286.15, 2469.8530], [287.15, 2467.4680], [288.15, 2465.0830],
          [289.15, 2462.7990], [290.15, 2460.4150], [291.15, 2458.0320], [292.15, 2455.6480],
          [293.15, 2453.3650], [294.15, 2450.9810], [295.15, 2448.5980], [296.15, 2446.2140],
          [297.15, 2443.9300], [298.15, 2441.5500], [299.15, 2439.1600], [300.15, 2436.7800],
          [301.15, 2434.4000], [302.15, 2432.0100], [303.15, 2429.6300], [305.65, 2423.7700],
          [308.15, 2417.8100], [310.65, 2411.8500], [313.15, 2405.9000], [315.65, 2399.8400],
          [318.15, 2393.8800], [320.65, 2387.9300], [323.15, 2381.8700], [325.65, 2375.8200],
          [328.15, 2369.7600], [330.65, 2363.7000], [333.15, 2357.6500], [335.65, 2351.4900],
          [338.15, 2345.4200], [340.65, 2339.2600], [343.15, 2333.0900], [345.65, 2326.9200],
          [348.15, 2320.6400], [350.65, 2314.4600], [353.15, 2308.1700], [355.65, 2301.8800],
          [358.15, 2295.4800], [360.65, 2289.0800], [363.15, 2282.6700], [365.65, 2276.2500],
          [368.15, 2269.7200], [370.65, 2263.2800], [372.78, 2257.5900], [373.15, 2256.6400]:

with(plots):
with(CurveFitting):

plot1 := pointplot([points], symbol = circle, symbolsize = 5):
Approx := LeastSquares([points], T, curve = a*T^2+b*T+c);
plot2 := plot(Approx, T = 273.15 .. 373.15, thickness = 2):

display(plot2, plot1, view = [273.15 .. 373.15, 2000 .. 2600], gridlines = true,
        labels = [Temperature*[K], h[wv]*[kJ/kg]], labeldirections = [horizontal, vertical],
        labelfont = [TIMES, ROMAN, 14]);
```

B.1.3 The viscosity of water

```
restart:
points := [273.15, 1793], [274.15, 1732], [275.15, 1674], [276.15, 1620], [277.15, 1568],
          [278.15, 1519], [279.15, 1472], [280.15, 1428], [281.15, 1385], [282.15, 1345],
          [283.15, 1306], [284.15, 1270], [285.15, 1235], [286.15, 1201], [287.15, 1169],
          [288.15, 1138], [289.15, 1109], [290.15, 1080], [291.15, 1053], [292.15, 1027],
          [293.15, 1002], [294.15, 978.0], [295.15, 954.8], [296.15, 932.6], [297.15, 911.1],
          [298.15, 890.5], [299.15, 870.6], [300.15, 851.4], [301.15, 832.8], [302.15, 815.0],
          [303.15, 797.7], [305.65, 757.0], [308.15, 719.6], [310.65, 685.1], [313.15, 653.2],
          [315.65, 623.7], [318.15, 596.3], [320.65, 570.8], [323.15, 547.1], [325.65, 524.9],
          [328.15, 504.2], [330.65, 484.8], [333.15, 466.6], [335.65, 449.5], [338.15, 433.4],
          [340.65, 418.3], [343.15, 404.1], [345.65, 390.6], [348.15, 377.9], [350.65, 365.9],
          [353.15, 354.5], [355.65, 343.7], [358.15, 333.5], [360.65, 323.8], [363.15, 314.5],
          [365.65, 305.8], [368.15, 297.4], [370.65, 289.5], [372.78, 283.0], [373.15, 281.9]:

with(plots):
with(CurveFitting):

plot1 := pointplot([points], symbol = circle, symbolsize = 5):
Approx := LeastSquares([points], T, curve = a*T^5+b*T^4+c*T^3+d*T^2+e*T+f);
plot2 := plot(Approx, T = 273.15 .. 373.15, thickness = 2):

display(plot2, plot1, view = [273.15 .. 373.15, 0 .. 2000], gridlines = true,
        labels = [Temperature*[K], eta[w]*[mu Pa*s]], labeldirections = [horizontal, vertical],
        labelfont = [TIMES, ROMAN, 14]);
```

B.1.4 The specific heat of steam

```
restart:
points := [273.15, 1.868], [274.15, 1.868], [275.15, 1.869], [276.15, 1.869], [277.15, 1.870],
          [278.15, 1.871], [279.15, 1.871], [280.15, 1.872], [281.15, 1.872], [282.15, 1.873],
          [283.15, 1.874], [284.15, 1.875], [285.15, 1.875], [286.15, 1.876], [287.15, 1.877],
          [288.15, 1.878], [289.15, 1.879], [290.15, 1.879], [291.15, 1.880], [292.15, 1.881],
          [293.15, 1.882], [294.15, 1.883], [295.15, 1.884], [296.15, 1.885], [297.15, 1.886],
          [298.15, 1.887], [299.15, 1.888], [300.15, 1.889], [301.15, 1.890], [302.15, 1.891],
```

```
          [303.15, 1.892], [305.65, 1.895], [308.15, 1.898], [310.65, 1.901], [313.15, 1.904],
          [315.65, 1.908], [318.15, 1.912], [320.65, 1.915], [323.15, 1.919], [325.65, 1.924],
          [328.15, 1.928], [330.65, 1.932], [333.15, 1.937], [335.65, 1.942], [338.15, 1.947],
          [340.65, 1.953], [343.15, 1.958], [345.65, 1.964], [348.15, 1.970], [350.65, 1.976],
          [353.15, 1.983], [355.65, 1.989], [358.15, 1.996], [360.65, 2.004], [363.15, 2.011],
          [365.65, 2.019], [368.15, 2.027], [370.65, 2.035], [372.78, 2.043], [373.15, 2.044]:

with(plots):
with(CurveFitting):

plot1 := pointplot([points], symbol = circle, symbolsize = 5):
Approx := LeastSquares([points], T, curve = a*T^3+b*T^2+c*T+d);
plot2 := plot(Approx, T = 273.15 .. 373.15, thickness = 2):

display(plot2, plot1, view = [273.15 .. 373.15, 1.8 .. 2.1], gridlines = true,
        labels = [Temperature*[K], c[p, v]*[kJ/(kg*K)]], labeldirections = [horizontal, vertical],
        labelfont = [TIMES, ROMAN, 14]);
```

B.1.5 The thermal conductivity of water

```
restart:
points := [273.15, 561.0], [274.15, 562.9], [275.15, 564.8], [276.15, 566.7], [277.15, 568.6],
          [278.15, 570.5], [279.15, 572.4], [280.15, 574.3], [281.15, 576.2], [282.15, 578.1],
          [283.15, 580.0], [284.15, 581.9], [285.15, 583.8], [286.15, 585.6], [287.15, 587.5],
          [288.15, 589.3], [289.15, 591.2], [290.15, 593.0], [291.15, 594.8], [292.15, 596.6],
          [293.15, 598.4], [294.15, 600.2], [295.15, 601.9], [296.15, 603.7], [297.15, 605.4],
          [298.15, 607.1], [299.15, 608.8], [300.15, 610.5], [301.15, 612.2], [302.15, 613.8],
          [303.15, 615.4], [305.65, 619.4], [308.15, 623.2], [310.65, 627.0], [313.15, 630.5],
          [315.65, 634.0], [318.15, 637.3], [320.65, 640.5], [323.15, 643.5], [325.65, 646.4],
          [328.15, 649.2], [330.65, 651.8], [333.15, 654.3], [335.65, 656.7], [338.15, 658.9],
          [340.65, 661.1], [343.15, 663.1], [345.65, 665.0], [348.15, 666.8], [350.65, 668.4],
          [353.15, 670.0], [355.65, 671.5], [358.15, 672.8], [360.65, 674.1], [363.15, 675.3],
          [365.65, 676.4], [368.15, 677.4], [370.65, 678.3], [372.78, 679.0], [373.15, 679.1]:

with(plots):
with(CurveFitting):

plot1 := pointplot([points], symbol = circle, symbolsize = 5):
Approx := LeastSquares([points], T, curve = a*T^2+b*T+c);
plot2 := plot(Approx, T = 273.15 .. 373.15, thickness = 2):

display(plot2, plot1, view = [273.16 .. 373.16, 0 .. 700], gridlines = true,
        labels = [Temperature*[K], lambda*[W/(m*K)]], labeldirections = [horizontal, vertical],
        labelfont = [TIMES, ROMAN, 14]);
```

B.1.6 The thermal conductivity of air

```
restart:
points := [100, 9.34], [150, 13.8], [200, 18.1], [250, 22.3], [300, 26.3], [350, 30.0], [400, 33.8],
          [450, 37.3], [500, 40.7], [550, 43.9], [600, 46.9], [650, 49.7], [700, 52.4], [750, 54.9],
          [800, 57.3], [850, 59.6], [900, 62.0], [950, 64.3], [1000, 66.7]:

with(plots):
with(CurveFitting):

plot1 := pointplot([points], symbol = circle, symbolsize = 5):
Approx := LeastSquares([points], T, curve = a*T^2+b*T+c);
plot2 := plot(Approx, T = 100 .. 1000, thickness = 2):

display(plot2, plot1, view = [100 .. 1000, 0 .. 70], gridlines = true,
        labels = [Temperature*[K], lambda*[mW/(m*K)]], labeldirections = [horizontal, vertical],
        labelfont = [TIMES, ROMAN, 14]);
```

B.2 The multiscale moisture diffusion model

This section contains the source code of the program for the homogenization model for water diffusion. This program has the following structure:

B.2.1 Program structure

- Input of variables
  - Oven-dry density of the wood sample
  - Earlywood density
  - Latewood density
- Input of constants
- Procedures for computation of different properties:
  - Diffusion tensor of the cell wall
  - Activation energy
  - Heat of evaporation of water
  - Heat of sorption
  - Specific heat of steam
  - Diffusion tensor of the lumen
  - Relative humidity
  - Slope $\mathrm{d}\varphi/\mathrm{d}mc$
  - Specific gravity of the cell wall
  - Density of water
  - Vapor pressure
  - Volume fraction of the cell wall
  - Volume fraction of the lumen
  - Radial cell size
  - Cell wall thickness
  - Diameter ratio
  - Aspect ratio
  - P-tensor
  - Fiber saturation point
- Calculation of the homogenized diffusion tensor for 40, 60, 80 and 100 °C
- Plotting of the results compared to values reported by Kollmann [17]

B.2.2 Source code

```
#-----------------------------------------------------------------------------------------------------
# Calculation of the homogenized diffusion tensor
#-----------------------------------------------------------------------------------------------------

# Start settings
#---------------

restart:
with(linalg):
with(Units[Standard]):

# Input
#------

# Variables
densitywood := 404*Unit('kg'/'m'^3):
densityearlywood := 280*Unit('kg'/'m'^3):
densitylatewood := 820*Unit('kg'/'m'^3):


# Constants

densitycellwall := 1530*Unit('kg'/'m'^3):
cellsizelongitudinal := 1.8*10^(-3)*Unit('m'):
cellsizetangential := 50*10^(-6)*Unit('m'):
cellsizeradial200 := 50*10^(-6)*Unit('m'):
cellsizeradial1000 := 20*10^(-6)*Unit('m'):
R := 8.314472*Unit('J'/('mol'*'K')):
molmasswater := 18.01528*Unit('g'/'mol'):
D0transversal := 7*10^(-6)*Unit('m'^2/'s'):
D0longitudinal := 17.5*10^(-6)*Unit('m'^2/'s'):


# Procedures
------------

# Diffusion tensor of the cell wall

DIFFUSIONTENSORCELLWALL := proc ()
   local DBT, DBL, a:
   description "calculates the actual diffusion tensor for the cell wall":
      a := simplify(temperaturekelvin*Unit(1/'K'));
      DBT := D0transversal*exp(-ACTIVATIONENERGY()/(R*temperaturekelvin))/VOLUMEFRACTIONCELLWALL();
      DBL := DBT*D0longitudinal/D0transversal;
      matrix([[DBT, 0, 0],
              [0, DBT, 0],
              [0, 0, DBL]])
   end proc:


# Activation energy

ACTIVATIONENERGY := proc ()
   description "calculates the activation energy for bound water in the cell wall";
      (38500-29000*moisturecontent)*Unit('J'/'mol')
      #(HEATOFEVAPORATION()+HEATOFSORPTION()-temperaturekelvin*SPECIFICHEAT())*molmasswater
   end proc:


# Heat of evaporation of water

HEATOFEVAPORATION := proc ()
   local T;
   description "calculates the heat of vaporization for the actual temperature";
      T := temperaturekelvin/Unit('K');
      simplify((3033.019010-1.601883570*T-0.1278794562e-2*T^2)*Unit('kJ'/'kg'))
   end proc:
```

```
# Heat of sorption

HEATOFSORPTION := proc ()
   local W, K, K1, K2, M, T, T1, T2, h, h1, h2, h11, h22;
   description "calculates the heat of sorption by integration of the sorption isotherms";
      T1 := temperaturekelvin+(-1)*.1*Unit('K');
      T := T1/Unit('K')-273.16;
      M := 4000.*h*(-5.840216510*10^24*h*T^6-1.268201413*10^36*h^2*T-2.840236168*10^34*h *T^2
                  -7.707429775*10^21*h*T^7-1.490348416*10^16*h^2*T^9+1.190989816*10^19*h*T^8
                  +3.023094436*10^36*h*T+5.267115000*10^37-1.753245859*10^27*h^2*T^5
                  -1.887848874*10^32*h*T^3-1.980162000*10^34*T+2.792561411*10^27*h*T^5
                  +1.625701098*10^13*T^10*h^2+9.056451018*10^31*h^2*T^3+2.701186854*10^24*h^2*T^6
                  +1.009642716*10^30*h*T^4+1.051012861*10^34*h^2*T^2+9.063286487*10^21*h^2*T^7
                  -1.776605400*10^30*T^3-5.622520638*10^37*h^2-2.435992020*10^33*T^2
                  +1.396899538*10^38*h+7.444710000*10^27*T^4-3.756775783*10^29*h^2*T^4
                  -9.929295389*10^18*h^2*T^8)/((6.98000*10^5+2580.*T+27.*T^2)*(1*10^8
                  -8.0500000*10^7*h-73600.*h*T+273.*h*T^2)*(1*10^28+5.047350000*10^28*h
                  -2.93618*10^25*h*T-2.679357800*10^24*h*T^2-1.974006000*10^21*h*T^3
                  +8.2719*10^18*h*T^4+1.679496909*10^27*h^2*T+1.551423006*10^18*h^2*T^5
                  -3.244564727*10^15*h^2*T^6+7.760552992*10^28*h^2+5.609126200*10^20*h^2*T^4
                  -4.281905431*10^12*h^2*T^7+6.616610091*10^9*h^2*T^8-1.048804930*10^23*h^2*T^3
                  -1.577908982*10^25*h^2*T^2));
      h1 := fsolve(M=moisturecontent,h=0..1);
      T2 := temperaturekelvin+.1*Unit('K');
      T := T2/Unit('K')-273.16;
      M := 4000.*h*(-5.840216510*10^24*h*T^6-1.268201413*10^36*h^2*T-2.840236168*10^34*h *T^2
                  -7.707429775*10^21*h*T^7-1.490348416*10^16*h^2*T^9+1.190989816*10^19*h*T^8
                  +3.023094436*10^36*h*T+5.267115000*10^37-1.753245859*10^27*h^2*T^5
                  -1.887848874*10^32*h*T^3-1.980162000*10^34*T+2.792561411*10^27*h*T^5
                  +1.625701098*10^13*T^10*h^2+9.056451018*10^31*h^2*T^3+2.701186854*10^24*h^2*T^6
                  +1.009642716*10^30*h*T^4+1.051012861*10^34*h^2*T^2+9.063286487*10^21*h^2*T^7
                  -1.776605400*10^30*T^3-5.622520638*10^37*h^2-2.435992020*10^33*T^2
                  +1.396899538*10^38*h+7.444710000*10^27*T^4-3.756775783*10^29*h^2*T^4
                  -9.929295389*10^18*h^2*T^8)/((6.98000*10^5+2580.*T+27.*T^2)*(1*10^8
                  -8.0500000*10^7*h-73600.*h*T+273.*h*T^2)*(1*10^28+5.047350000*10^28*h
                  -2.93618*10^25*h*T-2.679357800*10^24*h*T^2-1.974006000*10^21*h*T^3
                  +8.2719*10^18*h*T^4+1.679496909*10^27*h^2*T+1.551423006*10^18*h^2*T^5
                  -3.244564727*10^15*h^2*T^6+7.760552992*10^28*h^2+5.609126200*10^20*h^2*T^4
                  -4.281905431*10^12*h^2*T^7+6.616610091*10^9*h^2*T^8-1.048804930*10^23*h^2*T^3
                  -1.577908982*10^25*h^2*T^2));
      h2 := fsolve(M = moisturecontent, h = 0 .. 1);
      simplify(R*T1*T2*ln(h2/h1)/(molmasswater*(T2-T1)))
   end proc:


# Specific heat of steam

SPECIFICHEAT := proc ()
   local T;
   description "calculates the specific heat of steam for the actual temperature";
      T := temperaturekelvin/Unit('K');
      simplify((1.09012526+0.914954871e-2*T-0.378467624e-4*T^2+5.40714299e-7*T^3)*Unit('kJ'/('kg'*'K')))
      #simplify((1.31980370+0.164464028e-2*T-0.102698084e-4*T^2+1.96778034e-8*T^3)*Unit('kJ'/('kg'*'K')))
   end proc:


# Diffusion tensor of the lumen

DIFFUSIONTENSORLUMEN := proc ()
   local Da, Dv;
   description "calculates the actual diffusion tensor of air in the lumen";
      Da := 2.31e-5*RELATIVEHUMIDITY()*(temperaturekelvin/(273.16*Unit('K')))^1.81*Unit('m'^2/'s');
      Dv := simplify((molmasswater*Da*VAPORPRESSURE()*SLOPEDHDM())/
                   (SPECIFICGRAVITYCELLWALL()*R*temperaturekelvin*VOLUMEFRACTIONCELLWALL()));
      matrix([[Dv, 0, 0],
              [0, Dv, 0],
              [0, 0, Dv]])
```

```
   end proc:


# Relative humidity

RELATIVEHUMIDITY := proc ()
   description "calculates the actual relative humidity for a given moisture content";
   local T, b, h;
      T := temperaturekelvin/Unit('K')-273.16;
      h := ((18*((.805+0.736e-3*T-0.273e-5*T^2)*b/(1-(.805+0.736e-3*T-0.273e-5*T^2)*b)+((6.27-0.938e
             -2*T-0.303e-3*T^2)*(.805+0.736e-3*T-0.273e-5*T^2)*b+(2*(6.27-0.938e-2*T-0.303e-3*T^2))
             *(1.91+0.407e-1*T-0.293e-3*T^2)*(.805+0.736e-3*T-0.273e-5*T^2)^2*b^2)/(1+(6.27-0.938e
             -2*T-0.303e-3*T^2)*(.805+0.736e-3*T-0.273e-5*T^2)*b+(6.27-0.938e-2*T-0.303e-3*T^2)
             *(1.91+0.407e-1*T-0.293e-3*T^2)*(.805+0.736e-3*T-0.273e-5*T^2)^2*b^2)))
             /(349+1.29*T+0.135e-1*T^2) = moisturecontent, b)[1]
   end proc:


# Slope dh/dM

SLOPEDHDM := proc ()
   description "calculates the actual slope of the sorption isotherm dH/dM";
   local T, b, h;
      T := temperaturekelvin/Unit('K')-273.16;
      h := ((18*((.805+0.736e-3*T-0.273e-5*T^2)*b/(1-(.805+0.736e-3*T-0.273e-5*T^2)*b)+((6.27-0.938e
             -2*T-0.303e-3*T^2)*(.805+0.736e-3*T-0.273e-5*T^2)*b+(2*(6.27-0.938e-2*T-0.303e-3*T^2))
             *(1.91+0.407e-1*T-0.293e-3*T^2)*(.805+0.736e-3*T-0.273e-5*T^2)^2*b^2)/(1+(6.27-0.938e
             -2*T-0.303e-3*T^2)*(.805+0.736e-3*T-0.273e-5*T^2)*b+(6.27-0.938e-2*T-0.303e-3*T^2)
             *(1.91+0.407e-1*T-0.293e-3*T^2)*(.805+0.736e-3*T-0.273e-5*T^2)^2*b^2)))
             /(349+1.29*T+0.135e-1*T^2) = moisturecontent, b)[1];
      -(10^8*(2.063641731*10^55*h^02*T^07-3.675749638*10^52*h^02*T^08+1.078329103*10^12*T^20*h^05
             -8.077141728*10^61*h^01*T^04+5.412110003*10^57*h^02*T^06-1.027829935*10^60*h^02*T^05
             -2.106846000*10^69*h^00*T^00+4.520901016*10^65*h^04*T^02-3.096164295*10^59*h^03*T^05
             +7.149378516*10^29*h^05*T^14+5.887059432*10^39*h^05*T^10+3.055465902*10^56*h^03*T^06
             +2.301720675*10^65*h^04*T^03+8.424221918*10^42*h^03*T^11-1.068853722*10^61*h^05*T^00
             -1.391476219*10^51*h^03*T^08+7.063379834*10^35*h^04*T^15+9.743968080*10^64*T^02*T^00
             -1.499611817*10^29*h^03*T^14+3.464587822*10^32*h^05*T^13+7.106421600*10^61*T^03*T^00
             +6.032899276*10^56*h^04*T^07+1.409333952*10^22*h^03*T^16+7.192210464*10^57*h^05*T^02
             -1.238463654*10^24*h^05*T^16-9.126357169*10^34*h^05*T^12+1.228920340*10^66*h^03*T^02
             +4.672173208*10^56*h^01*T^06+1.267828976*10^47*T^10*h^02+3.057046019*10^20*h^05*T^17
             -6.835811784*10^26*h^05*T^15-3.941737740*10^53*h^05*T^04-5.744289226*10^57*h^04*T^06
             -4.431187872*10^48*h^04*T^10-7.649605429*10^14*h^05*T^19-6.375915268*10^37*h^05*T^11
             -7.241806605*10^69*h^03*T^00+6.165943820*10^53*h^01*T^07-9.167593471*10^69*h^02*T^00
             +3.227982985*10^17*h^05*T^18-7.047680916*10^48*h^03*T^09-1.774447257*10^61*h^04*T^05
             -4.231321955*10^61*h^03*T^04-1.534476018*10^56*h^05*T^03+1.345633201*10^64*h^03*T^03
             +2.395342334*10^43*h^04*T^12+2.155772896*10^66*h^02*T^02-1.699654213*10^68*h^03*T^01
             +7.086243882*10^42*h^05*T^09+3.727535815*10^49*h^05*T^06-4.727748888*10^44*h^05*T^08
             +3.111981319*10^26*h^03*T^15-9.527918528*10^50*h^01*T^08-2.234049128*10^59*h^01*T^05
             -2.405335416*10^47*h^05*T^07+4.675993515*10^45*h^03*T^10-1.067847737*10^50*h^02*T^09
             -9.805509457*10^68*h^04*T^01-6.728861094*10^29*h^04*T^17+2.251261084*10^54*h^03*T^07
             +7.491197318*10^46*h^04*T^11-7.101117937*10^39*h^03*T^12-1.659453149*10^57*h^05*T^01
             -1.970349732*10^41*T^12*h^02+1.745305975*10^44*h^02*T^11+1.510279099*10^64*h^01*T^03
             -9.861258080*10^36*h^04*T^14-1.920172449*10^62*h^02*T^04-9.668314996*10^51*h^04*T^09
             -2.977884000*10^59*h^00*T^04-1.117519630*10^70*h^01*T^00-2.659153086*10^70*h^04*T^00
             +7.920648000*10^65*h^00*T^01+4.302652124*10^26*h^04*T^18+9.562256318*10^61*h^04*T^04
             -2.418475548*10^68*h^01*T^01-2.199880451*10^32*h^04*T^16+1.337561493*10^64*h^02*T^03
             +2.272188934*10^66*h^01*T^02+7.770551426*10^66*h^02*T^01+2.084514389*10^53*h^04*T^08
               -3.144165774*10^41*h^04*T^13+3.826766107*10^32*h^03*T^13+7.069296861*10^51*h^05*T^05)
      /((6.98000*10^5+2580.*T+27.*T^2)*(1.00000000*10^8-8.0500000*10^7*h-73600.*h*T+273.*h*T^2)^2
            *(1.000000000*10^28*h^00*T^00+5.047350000*10^28*h^01*T^00-2.936180000*10^25*h^01*T^01
             -2.679357800*10^24*h^01*T^02-1.974006000*10^21*h^01*T^03+8.271900000*10^18*h^01*T^04
             +1.679496909*10^27*h^02*T^01+5.609126200*10^20*h^02*T^04-3.244564727*10^15*h^02*T^06
             -4.281905431*10^12*h^02*T^07+1.551423006*10^18*h^02*T^05-1.048804930*10^23*h^02*T^03
             +6.616610091*10^09*h^02*T^08-1.577908982*10^25*h^02*T^02+7.760552992*10^28*h^02)^2))^(-1)
end proc:


# Specific gravity of the cell wall
```

```
SPECIFICGRAVITYCELLWALL := proc ()
   description "calculates the specific gravity of the cell wall for the actual moisture content";
      densitycellwall/(1+(densitycellwall/DENSITYWATER())*moisturecontent)
   end proc:


# Density of water

DENSITYWATER := proc ()
   description "calculates the density of water for the actual temperature";
   local T;
      T := temperaturekelvin/Unit('K');
      simplify((-1.390021658*10^(-7)*T^4+0.1956853951*10^(-3)*T^3-0.1058224883*T^2
                +25.39735328*T-1256.217406)*Unit('kg'/('m'^3)))
   end proc:

# Vapor pressure

VAPORPRESSURE := proc ()
   description "calculates the actual relative vapor pressure";
   local T, tau;
      T := temperaturekelvin/Unit('K');
      tau := 1+(-1)*T/647.14;
      220.64*10^5*Unit('bar')*exp(647.14*(-7.85823*tau+1.83991*tau^1.5-11.7811*tau^3+22.6705*tau^3.5
                                    -15.9393*tau^4+1.77516*tau^7.5)/T)
   end proc:


# Volume fraction of the cell wall

VOLUMEFRACTIONCELLWALL := proc ()
   description "calculates the volume fraction of the cell wall";
      evalf(specificdensitywood/densitycellwall)
   end proc:


# Volume fraction of the lumen

VOLUMEFRACTIONLUMEN := proc ()
   description "calculates the volume fraction of the lumen";
      evalf(1-VOLUMEFRACTIONCELLWALL())
   end proc:


# Radial Cell Size

CELLSIZERADIAL := proc ()
   local c1, c2;
   description "calculates the radial cell size for the given specific wood density";
      c2 := (1/800)*(cellsizeradial1000-cellsizeradial200)/Unit('kg'/'m'^3);
      c1 := cellsizeradial200-200*Unit('kg'/'m'^3)*c2;
      evalf(c1+c2*specificdensitywood)
   end proc:


# Cellwall thickness

CELLWALLTHICKNESS := proc ()
   local cellsizeradial, x;
   description "calculates the cell wall thickness for the given specific wood density";
      cellsizeradial := CELLSIZERADIAL();
      solve(VOLUMEFRACTIONCELLWALL()=1-(cellsizeradial-2*x*Unit('m'))*(cellsizetangential-2*x*Unit('m'))/
            (cellsizeradial*cellsizetangential), x)*Unit('m')
   end proc:


# Diameter ratio

DIAMETERRATIO := proc ()
```

```
   local cellwallthickness;
   description "calculates the diameter ratio for the given specific wood density";
      cellwallthickness := CELLWALLTHICKNESS();
      (CELLSIZERADIAL()-2*cellwallthickness)/(cellsizetangential-2*cellwallthickness)
   end proc:


# Aspect ratio

ASPECTRATIO := proc ()
   local cellwallthickness;
   description "calculates the aspect ratio for the given specific wood density";
      cellwallthickness := CELLWALLTHICKNESS();
      (cellsizelongitudinal-2*cellwallthickness)/(cellsizetangential-2*cellwallthickness)
   end proc:


# P-Tensor

PTENSOR := proc ()
   local a1, a2, a3, diffusiontensorcellwall, z3, xi, i, j, g, gdach, P, phi;
   description "calculates the P-Tensor";
      a2 := 1;
      a1 := a2*DIAMETERRATIO();
      a3 := a2*ASPECTRATIO();
      diffusiontensorcellwall := array(1..3,1..3,[[1,0,0],[0,1,0],[0,0,D0longitudinal/D0transversal]])
      xi[1] := cos(phi)*sqrt(1-z3^2)/a1;
      xi[2] := sin(phi)*sqrt(1-z3^2)/a2;
      xi[3] := z3/a3;
      i := 'i';
      j := 'j';
      g := sum(sum(diffusiontensorcellwall()[i,j]*xi[i]*xi[j],i=1..3),j=1..3);
      gdach := 1/g;
      P := array(1 .. 3, 1 .. 3);
      i := 'i';
      j := 'j';
      for i to 3 do
         for j to 3 do
            P[i,j] := simplify(evalf((1/4*pi)*(int(int(gdach*xi[i]*xi[j],phi=0..2*pi),z3=-1..1))))
         end do
      end do;
      P
   end proc:


# Fiber saturation point

FIBERSATURATIONPOINT := proc ()
   local h, T, W, K, K1, K2;
   description "calculates the fiber saturation point for the actual temperature";
      T := evalf(temperaturekelvin/Unit('K')-273.16);
      h := 1.00;
      W := 349+1.29*T+0.135e-1*T^2;
      K := 0.805+0.736e-3*T-0.273e-5*T^2;
      K1 := 6.270-0.938e-2*T-0.303e-3*T^2;
      K2 := 1.91+0.407e-1*T-0.293e-3*T^2;
      18*(K*h/(1-K*h)+(K1*K*h+2*K1*K2*K^2*h^2)/(1+K1*K*h+K1*K2*K^2*h^2))/W
   end proc


# Assembly and Results
#---------------------

# Calculation of the properties of the example given by F. Kollmann for 20-100 C

specificdensitywood := densityearlywood:
PTensorearlywood := PTENSOR():

specificdensitywood := densitylatewood:
```

```
PTensorlatewood := PTENSOR():

fearlywood := (densitywood-densitylatewood)/(densityearlywood-densitylatewood):
flatewood := 1-fearlywood:


temperaturekelvin := (273.16+20)*Unit('K'):

amin := 1;
amax := trunc(100*FIBERSATURATIONPOINT())+1:
amax20 := amax:

results20 := array(1..amax-amin+2,1..8):
results20[1,1] := Moisture Content:
results20[1,2] := D[v]:
results20[1,3] := Activation Energy:
results20[1,4] := D[cellwall,transversal]:
results20[1,5] := D[cellwall,longitudinal]:
results20[1,6] := D[hom,radial]:
results20[1,7] := D[hom,tangential]:
results20[1,8] := D[hom,longitudinal]:

for a from amin to amax do
   if a < amax
      then moisturecontent := 0.01*a
      else moisturecontent := FIBERSATURATIONPOINT()-0.001
   end if

   specificdensitywood := densityearlywood

   f0 := VOLUMEFRACTIONCELLWALL():
   f1 := VOLUMEFRACTIONLUMEN():
   D0 := DIFFUSIONTENSORCELLWALL():
   D1 := DIFFUSIONTENSORLUMEN():
   P := evalm(PTensorearlywood/D0[1,1]):
   U := matrix([[1,0,0],[0,1,0],[0,0,1]]):

   numerator := simplify(evalm(f0*D0+f1*D1/(U+P*(D1-D0)))):
   denumerator := simplify(evalm(f0*U+f1/(U+P*(D1-D0)))):
   Dhomearlywood := simplify(evalm(numerator/denumerator)):

   specificdensitywood := densitylatewood:

   f0 := VOLUMEFRACTIONCELLWALL():
   f1 := VOLUMEFRACTIONLUMEN():
   D0 := DIFFUSIONTENSORCELLWALL():
   D1 := DIFFUSIONTENSORLUMEN():
   P := evalm(PTensorlatewood/D0[1,1]):
   U := matrix([[1,0,0],[0,1,0],[0,0,1]]):

   numerator := simplify(evalm(f0*D0+f1*D1/(U+P*(D1-D0)))):
   denumerator := simplify(evalm(f0*U+f1/(U+P*(D1-D0)))):
   Dhomlatewood := simplify(evalm(numerator/denumerator)):

   results20[a-amin+2,1] := moisturecontent:
   results20[a-amin+2,2] := 0:
   results20[a-amin+2,3] := 0:
   results20[a-amin+2,4] := 0:
   results20[a-amin+2,5] := 0:
   results20[a-amin+2,6] := 1/(fearlywood/Re(Dhomearlywood[1,1])+flatewood/Re(Dhomlatewood[1,1])):
   results20[a-amin+2,7] := Re(Dhomearlywood[2,2])*fearlywood+Re(Dhomlatewood[2,2])*flatewood:
   results20[a-amin+2,8] := Re(Dhomearlywood[3,3])*fearlywood+Re(Dhomlatewood[3,3])*flatewood:
end do:


temperaturekelvin := (273.16+40)*Unit('K'):

amin := 1;
amax := trunc(100*FIBERSATURATIONPOINT())+1:
```

```
amax40 := amax:

results40 := array(1..amax-amin+2,1..8):
results40[1,1] := Moisture Content:
results40[1,2] := D[v]:
results40[1,3] := Activation Energy:
results40[1,4] := D[cellwall,transversal]:
results40[1,5] := D[cellwall,longitudinal]:
results40[1,6] := D[hom,radial]:
results40[1,7] := D[hom,tangential]:
results40[1,8] := D[hom,longitudinal]:

for a from amin to amax do
   if a < amax
      then moisturecontent := 0.01*a
      else moisturecontent := FIBERSATURATIONPOINT()-0.001
   end if

   specificdensitywood := densityearlywood

   f0 := VOLUMEFRACTIONCELLWALL():
   f1 := VOLUMEFRACTIONLUMEN():
   D0 := DIFFUSIONTENSORCELLWALL():
   D1 := DIFFUSIONTENSORLUMEN():
   P := evalm(PTensorearlywood/D0[1,1]):
   U := matrix([[1,0,0],[0,1,0],[0,0,1]]):

   numerator := simplify(evalm(f0*D0+f1*D1/(U+P*(D1-D0)))):
   denumerator := simplify(evalm(f0*U+f1/(U+P*(D1-D0)))):
   Dhomearlywood := simplify(evalm(numerator/denumerator)):

   specificdensitywood := densitylatewood:

   f0 := VOLUMEFRACTIONCELLWALL():
   f1 := VOLUMEFRACTIONLUMEN():
   D0 := DIFFUSIONTENSORCELLWALL():
   D1 := DIFFUSIONTENSORLUMEN():
   P := evalm(PTensorlatewood/D0[1,1]):
   U := matrix([[1,0,0],[0,1,0],[0,0,1]]):

   numerator := simplify(evalm(f0*D0+f1*D1/(U+P*(D1-D0)))):
   denumerator := simplify(evalm(f0*U+f1/(U+P*(D1-D0)))):
   Dhomlatewood := simplify(evalm(numerator/denumerator)):

   results40[a-amin+2,1] := moisturecontent:
   results40[a-amin+2,2] := 0:
   results40[a-amin+2,3] := 0:
   results40[a-amin+2,4] := 0:
   results40[a-amin+2,5] := 0:
   results40[a-amin+2,6] := 1/(fearlywood/Re(Dhomearlywood[1,1])+flatewood/Re(Dhomlatewood[1,1])):
   results40[a-amin+2,7] := Re(Dhomearlywood[2,2])*fearlywood+Re(Dhomlatewood[2,2])*flatewood:
   results40[a-amin+2,8] := Re(Dhomearlywood[3,3])*fearlywood+Re(Dhomlatewood[3,3])*flatewood:
end do:


temperaturekelvin := (273.16+60)*Unit('K'):

amin := 1;
amax := trunc(100*FIBERSATURATIONPOINT())+1:
amax60 := amax:

results60 := array(1..amax-amin+2,1..8):
results60[1,1] := Moisture Content:
results60[1,2] := D[v]:
results60[1,3] := Activation Energy:
results60[1,4] := D[cellwall,transversal]:
results60[1,5] := D[cellwall,longitudinal]:
results60[1,6] := D[hom,radial]:
results60[1,7] := D[hom,tangential]:
```

```
results60[1,8] := D[hom,longitudinal]:

for a from amin to amax do
   if a < amax
      then moisturecontent := 0.01*a
      else moisturecontent := FIBERSATURATIONPOINT()-0.001
   end if

   specificdensitywood := densityearlywood

   f0 := VOLUMEFRACTIONCELLWALL():
   f1 := VOLUMEFRACTIONLUMEN():
   D0 := DIFFUSIONTENSORCELLWALL():
   D1 := DIFFUSIONTENSORLUMEN():
   P := evalm(PTensorearlywood/D0[1,1]):
   U := matrix([[1,0,0],[0,1,0],[0,0,1]]):

   numerator := simplify(evalm(f0*D0+f1*D1/(U+P*(D1-D0)))):
   denumerator := simplify(evalm(f0*U+f1/(U+P*(D1-D0)))):
   Dhomearlywood := simplify(evalm(numerator/denumerator)):

   specificdensitywood := densitylatewood:

   f0 := VOLUMEFRACTIONCELLWALL():
   f1 := VOLUMEFRACTIONLUMEN():
   D0 := DIFFUSIONTENSORCELLWALL():
   D1 := DIFFUSIONTENSORLUMEN():
   P := evalm(PTensorlatewood/D0[1,1]):
   U := matrix([[1,0,0],[0,1,0],[0,0,1]]):

   numerator := simplify(evalm(f0*D0+f1*D1/(U+P*(D1-D0)))):
   denumerator := simplify(evalm(f0*U+f1/(U+P*(D1-D0)))):
   Dhomlatewood := simplify(evalm(numerator/denumerator)):

   results60[a-amin+2,1] := moisturecontent:
   results60[a-amin+2,2] := 0:
   results60[a-amin+2,3] := 0:
   results60[a-amin+2,4] := 0:
   results60[a-amin+2,5] := 0:
   results60[a-amin+2,6] := 1/(fearlywood/Re(Dhomearlywood[1,1])+flatewood/Re(Dhomlatewood[1,1])):
   results60[a-amin+2,7] := Re(Dhomearlywood[2,2])*fearlywood+Re(Dhomlatewood[2,2])*flatewood:
   results60[a-amin+2,8] := Re(Dhomearlywood[3,3])*fearlywood+Re(Dhomlatewood[3,3])*flatewood:
end do:


temperaturekelvin := (273.16+80)*Unit('K'):

amin := 1;
amax := trunc(100*FIBERSATURATIONPOINT())+1:
amax80 := amax:

results80 := array(1..amax-amin+2,1..8):
results80[1,1] := Moisture Content:
results80[1,2] := D[v]:
results80[1,3] := Activation Energy:
results80[1,4] := D[cellwall,transversal]:
results80[1,5] := D[cellwall,longitudinal]:
results80[1,6] := D[hom,radial]:
results80[1,7] := D[hom,tangential]:
results80[1,8] := D[hom,longitudinal]:

for a from amin to amax do
   if a < amax
      then moisturecontent := 0.01*a
      else moisturecontent := FIBERSATURATIONPOINT()-0.001
   end if

   specificdensitywood := densityearlywood
```

```
   f0 := VOLUMEFRACTIONCELLWALL():
   f1 := VOLUMEFRACTIONLUMEN():
   D0 := DIFFUSIONTENSORCELLWALL():
   D1 := DIFFUSIONTENSORLUMEN():
   P := evalm(PTensorearlywood/D0[1,1]):
   U := matrix([[1,0,0],[0,1,0],[0,0,1]]):

   numerator := simplify(evalm(f0*D0+f1*D1/(U+P*(D1-D0)))):
   denumerator := simplify(evalm(f0*U+f1/(U+P*(D1-D0)))):
   Dhomearlywood := simplify(evalm(numerator/denumerator)):

   specificdensitywood := densitylatewood:

   f0 := VOLUMEFRACTIONCELLWALL():
   f1 := VOLUMEFRACTIONLUMEN():
   D0 := DIFFUSIONTENSORCELLWALL():
   D1 := DIFFUSIONTENSORLUMEN():
   P := evalm(PTensorlatewood/D0[1,1]):
   U := matrix([[1,0,0],[0,1,0],[0,0,1]]):

   numerator := simplify(evalm(f0*D0+f1*D1/(U+P*(D1-D0)))):
   denumerator := simplify(evalm(f0*U+f1/(U+P*(D1-D0)))):
   Dhomlatewood := simplify(evalm(numerator/denumerator)):

   results80[a-amin+2,1] := moisturecontent:
   results80[a-amin+2,2] := 0:
   results80[a-amin+2,3] := 0:
   results80[a-amin+2,4] := 0:
   results80[a-amin+2,5] := 0:
   results80[a-amin+2,6] := 1/(fearlywood/Re(Dhomearlywood[1,1])+flatewood/Re(Dhomlatewood[1,1])):
   results80[a-amin+2,7] := Re(Dhomearlywood[2,2])*fearlywood+Re(Dhomlatewood[2,2])*flatewood:
   results80[a-amin+2,8] := Re(Dhomearlywood[3,3])*fearlywood+Re(Dhomlatewood[3,3])*flatewood:
end do:


temperaturekelvin := (273.16+100)*Unit('K'):

amin := 1;
amax := trunc(100*FIBERSATURATIONPOINT())+1:
amax100 := amax:

results100 := array(1..amax-amin+2,1..8):
results100[1,1] := Moisture Content:
results100[1,2] := D[v]:
results100[1,3] := Activation Energy:
results100[1,4] := D[cellwall,transversal]:
results100[1,5] := D[cellwall,longitudinal]:
results100[1,6] := D[hom,radial]:
results100[1,7] := D[hom,tangential]:
results100[1,8] := D[hom,longitudinal]:

for a from amin to amax do
   if a < amax
      then moisturecontent := 0.01*a
      else moisturecontent := FIBERSATURATIONPOINT()-0.001
   end if

   specificdensitywood := densityearlywood

   f0 := VOLUMEFRACTIONCELLWALL():
   f1 := VOLUMEFRACTIONLUMEN():
   D0 := DIFFUSIONTENSORCELLWALL():
   D1 := DIFFUSIONTENSORLUMEN():
   P := evalm(PTensorearlywood/D0[1,1]):
   U := matrix([[1,0,0],[0,1,0],[0,0,1]]):

   numerator := simplify(evalm(f0*D0+f1*D1/(U+P*(D1-D0)))):
   denumerator := simplify(evalm(f0*U+f1/(U+P*(D1-D0)))):
   Dhomearlywood := simplify(evalm(numerator/denumerator)):
```

```
   specificdensitywood := densitylatewood:

   f0 := VOLUMEFRACTIONCELLWALL():
   f1 := VOLUMEFRACTIONLUMEN():
   D0 := DIFFUSIONTENSORCELLWALL():
   D1 := DIFFUSIONTENSORLUMEN():
   P := evalm(PTensorlatewood/D0[1,1]):
   U := matrix([[1,0,0],[0,1,0],[0,0,1]]):

   numerator := simplify(evalm(f0*D0+f1*D1/(U+P*(D1-D0)))):
   denumerator := simplify(evalm(f0*U+f1/(U+P*(D1-D0)))):
   Dhomlatewood := simplify(evalm(numerator/denumerator)):

   results100[a-amin+2,1] := moisturecontent:
   results100[a-amin+2,2] := 0:
   results100[a-amin+2,3] := 0:
   results100[a-amin+2,4] := 0:
   results100[a-amin+2,5] := 0:
   results100[a-amin+2,6] := 1/(fearlywood/Re(Dhomearlywood[1,1])+flatewood/Re(Dhomlatewood[1,1])):
   results100[a-amin+2,7] := Re(Dhomearlywood[2,2])*fearlywood+Re(Dhomlatewood[2,2])*flatewood:
   results100[a-amin+2,8] := Re(Dhomearlywood[3,3])*fearlywood+Re(Dhomlatewood[3,3])*flatewood:
end do:

# Plot for the results of the calculation and the data of Kollmann
#------------------------------------------------------------------

column := 6

with(plots)
with(CurveFitting)

if column = 1
then
   b := 1:
   mode2 := 1:
else
   if column = 3
   then
      b := Unit('mol'/'J'):
      mode2 := 1:
   else
      b := Unit('s'/'m'^2):
      mode2 := 2
   end if:
end if:

pointsY20  := array(1..amax20 -amin+1):
pointsY40  := array(1..amax40 -amin+1):
pointsY60  := array(1..amax60 -amin+1):
pointsY80  := array(1..amax80 -amin+1):
pointsY100 := array(1..amax100-amin+1):

a := 'a':
for a from amin to amax20 do pointsY20[a-amin+1]   := simplify(results20 [a-amin+2,column]*b) end do:
for a from amin to amax40 do pointsY40[a-amin+1]   := simplify(results40 [a-amin+2,column]*b) end do:
for a from amin to amax60 do pointsY60[a-amin+1]   := simplify(results60 [a-amin+2,column]*b) end do:
for a from amin to amax80 do pointsY80[a-amin+1]   := simplify(results80 [a-amin+2,column]*b) end do:
for a from amin to amax100 do pointsY100[a-amin+1] := simplify(results100[a-amin+2,column]*b) end do:

a := 'a':
points20  := seq([results20 [a-amin+2,1],pointsY20 [a-amin+1]],a=amin..amax20 ):
points40  := seq([results40 [a-amin+2,1],pointsY40 [a-amin+1]],a=amin..amax40 ):
points60  := seq([results60 [a-amin+2,1],pointsY60 [a-amin+1]],a=amin..amax60 ):
points80  := seq([results80 [a-amin+2,1],pointsY80 [a-amin+1]],a=amin..amax80 ):
points100 := seq([results100[a-amin+2,1],pointsY100[a-amin+1]],a=amin..amax100):

plot20  := pointplot({points20 },colour=black,symbol=circle,symbolsize=4):
plot40  := pointplot({points40 },colour=black,symbol=circle,symbolsize=4):
```

```
plot60  := pointplot({points60 },colour=black,symbol=circle,symbolsize=4):
plot80  := pointplot({points80 },colour=black,symbol=circle,symbolsize=4):
plot100 := pointplot({points100},colour=black,symbol=circle,symbolsize=4):

splineplot20  := plot(Spline([points20 ],m),m=(1/100)*amin..(1/100)*amax20 ,colour=green, thickness=1):
splineplot40  := plot(Spline([points40 ],m),m=(1/100)*amin..(1/100)*amax40 ,colour=blue,  thickness=1):
splineplot60  := plot(Spline([points60 ],m),m=(1/100)*amin..(1/100)*amax60 ,colour=red,   thickness=1):
splineplot80  := plot(Spline([points80 ],m),m=(1/100)*amin..(1/100)*amax80 ,colour=black, thickness=1):
splineplot100 := plot(Spline([points100],m),m=(1/100)*amin..(1/100)*amax100,colour=gold,  thickness=1):


kollmann40  := [0.0545,1.0556*10^(-10)],[0.0665,1.2222*10^(-10)],[0.0712,1.2778*10^(-10)],
               [0.0825,1.5833*10^(-10)],[0.0865,1.5556*10^(-10)],[0.0890,1.6667*10^(-10)],
               [0.0908,1.5000*10^(-10)],[0.0940,1.7778*10^(-10)],[0.1005,1.9722*10^(-10)],
               [0.1068,1.7222*10^(-10)],[0.1170,1.8889*10^(-10)],[0.1240,1.8611*10^(-10)],
               [0.1340,2.2222*10^(-10)],[0.1382,2.4722*10^(-10)],[0.1407,2.4167*10^(-10)],
               [0.1505,2.6111*10^(-10)],[0.1595,2.8611*10^(-10)],[0.1670,2.8333*10^(-10)],
               [0.1690,3.1944*10^(-10)],[0.1778,3.0556*10^(-10)],[0.1817,3.3333*10^(-10)],
               [0.1927,3.4722*10^(-10)],[0.2065,3.6111*10^(-10)],[0.2222,4.0000*10^(-10)],
               [0.2266,4.1667*10^(-10)],[0.2403,4.5278*10^(-10)],[0.2545,5.0278*10^(-10)],
               [0.2735,5.9722*10^(-10)],[0.2850,6.2222*10^(-10)]:
kollmann60  := [0.0295,2.0000*10^(-10)],[0.0418,2.3611*10^(-10)],[0.0440,2.3056*10^(-10)],
               [0.0494,2.7222*10^(-10)],[0.0553,2.8889*10^(-10)],[0.0624,3.2778*10^(-10)],
               [0.0625,2.7500*10^(-10)],[0.0676,3.3333*10^(-10)],[0.0692,3.5833*10^(-10)],
               [0.0744,3.5000*10^(-10)],[0.0786,3.2500*10^(-10)],[0.0836,3.9444*10^(-10)],
               [0.0873,3.8056*10^(-10)],[0.0918,4.3611*10^(-10)],[0.0959,4.0556*10^(-10)],
               [0.1031,5.1111*10^(-10)],[0.1058,4.9444*10^(-10)],[0.1137,4.9444*10^(-10)],
               [0.1197,5.1111*10^(-10)],[0.1279,5.8611*10^(-10)],[0.1352,6.0000*10^(-10)],
               [0.1570,6.3889*10^(-10)],[0.1636,6.7222*10^(-10)],[0.1727,7.5556*10^(-10)],
               [0.1760,7.1111*10^(-10)],[0.1906,7.6667*10^(-10)],[0.2086,8.1944*10^(-10)],
               [0.2208,9.3333*10^(-10)],[0.2374,1.0917*10^(-09)],[0.2465,1.0778*10^(-09)],
               [0.2601,1.1556*10^(-09)],[0.2704,1.2833*10^(-09)]:
kollmann80  := [0.0284,3.9722*10^(-10)],[0.0364,3.7778*10^(-10)],[0.0401,4.8611*10^(-10)],
               [0.0484,5.3333*10^(-10)],[0.0492,4.6389*10^(-10)],[0.0554,5.2222*10^(-10)],
               [0.0568,6.0000*10^(-10)],[0.0604,5.6944*10^(-10)],[0.0684,7.3889*10^(-10)],
               [0.0689,6.3611*10^(-10)],[0.0702,6.7222*10^(-10)],[0.0794,8.0000*10^(-10)],
               [0.0795,7.3333*10^(-10)],[0.0868,8.1944*10^(-10)],[0.0888,8.7500*10^(-10)],
               [0.1002,9.7222*10^(-10)],[0.1003,9.2222*10^(-10)],[0.1101,1.0222*10^(-09)],
               [0.1213,1.2194*10^(-09)],[0.1244,1.2056*10^(-09)],[0.1438,1.4333*10^(-09)],
               [0.1543,1.4778*10^(-09)],[0.1566,1.5361*10^(-09)],[0.1837,1.8278*10^(-09)],
               [0.2004,2.0750*10^(-09)],[0.2029,2.1000*10^(-09)],[0.2345,2.6694*10^(-09)]:
kollmann100 := [0.0211,8.4444*10^(-10)],[0.0259,9.9722*10^(-10)],[0.0311,1.5583*10^(-09)],
               [0.0329,1.1444*10^(-09)],[0.0410,1.3472*10^(-09)],[0.0423,1.3500*10^(-09)],
               [0.0453,1.5972*10^(-09)],[0.0481,1.3444*10^(-09)],[0.0496,2.0583*10^(-09)],
               [0.0531,1.6889*10^(-09)],[0.0532,1.4056*10^(-09)],[0.0598,2.0083*10^(-09)],
               [0.0612,1.7917*10^(-09)],[0.0629,2.3222*10^(-09)],[0.0649,1.7389*10^(-09)],
               [0.0704,2.5167*10^(-09)],[0.0744,2.2361*10^(-09)],[0.0782,2.5667*10^(-09)],
               [0.0902,2.3833*10^(-09)],[0.0966,2.4583*10^(-09)],[0.1012,2.3222*10^(-09)],
               [0.1116,3.1167*10^(-09)],[0.1154,2.3583*10^(-09)],[0.1205,2.8083*10^(-09)],
               [0.1310,2.6639*10^(-09)],[0.1432,3.4278*10^(-09)],[0.1529,2.9778*10^(-09)],
               [0.1672,4.3417*10^(-09)],[0.1704,2.8306*10^(-09)],[0.1771,3.8667*10^(-09)],
               [0.1968,4.7056*10^(-09)],[0.1983,4.0972*10^(-09)],[0.2093,5.6528*10^(-09)]:

kollmann40plot1  := pointplot([kollmann40], symbol=diagonalcross,symbolsize=5,colour=blue):
kollmann60plot1  := pointplot([kollmann60], symbol=diagonalcross,symbolsize=5,colour=red):
kollmann80plot1  := pointplot([kollmann80], symbol=diagonalcross,symbolsize=5,colour=black):
kollmann100plot1 := pointplot([kollmann100],symbol=diagonalcross,symbolsize=5,colour=gold):

kollmann40plot2  := plot(2.842666470*10^(-8)*x^3-9.128236704*10^(-9)*x^2+2.534640867*10^(-9)*x
                         -1.323359679*10^(-11),x=0.042..0.29,linestyle=dashdot,colour=blue, thickness=2):
kollmann60plot2  := plot(5.920661911*10^(-8)*x^3+5.711533729*10^(-9)*x-2.018730940*10^(-8)*x^2
                         +2.327765984*10^(-11),x=0.030..0.27,linestyle=dashdot,colour=red,  thickness=2):
kollmann80plot2  := plot(-9.092464889*10^(-9)*x^2+8.509373191*10^(-9)*x+7.986240847*10^(-8)*x^3
                         +1.112713233*10^(-10),x=0.024..0.24,linestyle=dashdot,colour=black,thickness=2):
kollmann100plot2  := plot(9.198470913*10^(-10)+1.282704261*10^(-8)*x+2.675278982*10^(-8)*x^2,
                                             x=0.020..0.21,linestyle=dashdot,colour=gold, thickness=2):

if column = 3
then
```

```
   ylabel := convert(combine(results40[1, column]/b, 'units'), 'units', J/mol):
else
   ylabel := results40[1, column]/b:
end if:

unwith(Units[Standard]):

if column = 2
then
   display(splineplot20, splineplot40, splineplot60, splineplot80, splineplot100, plot20, plot40,
           plot60, plot80, plot100, axes=normal, gridlines=true,
           axis[1]=[tickmarks=[7,subticks=4]],axis[2]=[tickmarks=[10,subticks=4],mode=log],
           labels=[moisture*content,ylabel],labeldirections=[horizontal,vertical],
           view=[0..0.30,1*10^(-6)..1*10^(-2)],labelfont = [TIMES, ROMAN, 14])
end if;
if column = 3
then
   display(splineplot20, splineplot40, splineplot60, splineplot80, splineplot100, plot20, plot40,
           plot60, plot80, plot100, axes=normal, gridlines=true,
           axis[1]=[tickmarks=[7,subticks=4]],axis[2]=[tickmarks=[10,subticks=4]],
           labels=[moisture*content,ylabel],labeldirections=[horizontal,vertical],
           view=[0..0.30,0..55000],labelfont = [TIMES, ROMAN, 14])
end if;
if column = 4
then
   display(splineplot40, splineplot60, splineplot80, splineplot100, plot40, plot60, plot80, plot100,
           axes=normal, gridlines=true,
           axis[1]=[tickmarks=[7,subticks=4]],axis[2]=[tickmarks=[10,subticks=3],mode=log],
           labels=[moisture*content,ylabel],labeldirections=[horizontal,vertical],
           view=[0..0.30,5*10^(-13)..10^(-9)],labelfont = [TIMES, ROMAN, 14])
end if;
if column = 5
then
   display(splineplot40, splineplot60, splineplot80, splineplot100, plot40, plot60, plot80, plot100,
           axes=normal,gridlines=true,
           axis[1]=[tickmarks=[7,subticks=4]],axis[2]=[tickmarks=[10,subticks=3],mode=log],
           labels=[moisture*content,ylabel],labeldirections=[horizontal,vertical],
           view=[0..0.30,5*10^(-13)..5*10^(-9)],labelfont = [TIMES, ROMAN, 14])
end if;
if column = 6
then
   display(splineplot40, splineplot60, splineplot80, splineplot100, plot40, plot60, plot80, plot100,
           kollmann40plot1, kollmann40plot2, kollmann60plot1, kollmann60plot2, kollmann80plot1,
           kollmann80plot2, kollmann100plot1, kollmann100plot2, axes=normal, gridlines=true,
           axis[1]=[tickmarks=[7,subticks=4]],axis[2]=[tickmarks=[10,subticks=4],mode=log],
           labels=[moisture*content,ylabel],labeldirections=[horizontal,vertical],
           view=[0..0.30,9*10^(-12)..3*10^(-8)],labelfont = [TIMES, ROMAN, 14])
end if;
if column = 7
then
   display(splineplot40, splineplot60, splineplot80, splineplot100, plot40, plot60, plot80, plot100,
           axes=normal,gridlines=true,
           axis[1]=[tickmarks=[7,subticks=4]],axis[2]=[tickmarks=[10,subticks=3],mode=log],
           labels=[moisture*content,ylabel],labeldirections=[horizontal,vertical],
           view=[0..0.30,9*10^(-12)..3*10^(-8)],labelfont = [TIMES, ROMAN, 14])
end if;
if column = 8
then
   display(splineplot20, splineplot40, splineplot60, splineplot80, splineplot100, plot20, plot40, plot60,
           plot80, plot100, axes=normal, gridlines=true,
           axis[1]=[tickmarks=[7,subticks=4]],axis[2]=[tickmarks=[10,subticks=3],mode=log],
           labels=[moisture*content,ylabel],labeldirections=[horizontal,vertical],
           view=[0..0.30,9*10^(-10)..3*10^(-7)],labelfont = [TIMES, ROMAN, 14])
end if;

with(Units[Standard]):
```

B.3 The multiscale thermal conduction model

This section contains the source code of the program for the homogenization model for thermal conduction. This program has the following structure:

B.3.1 Program structure

- Input of variables
  - Earlywood density
  - Latewood density
- Input of constants
- Procedures for computation of different properties:
  - Thermal conductivity tensor of the cell wall
  - Thermal conductivity of water
  - Thermal conductivity tensor of the lumen
  - Thermal conductivity of air
  - Volume fraction of the cell wall
  - Volume fraction of the lumen
  - Radial cell size
  - Cell wall thickness
  - Diameter ratio
  - Aspect ratio
  - P-tensor
- Calculation of the thermal conductivity tensor for a given temperature and moisture-content
- Plotting of the results compared to values reported by Kollmann [17]

B.3.2 Source code

```
#-----------------------------------------------------------------------------------------------------
# Calculation of the homogenized thermal conductivity tensor
#-----------------------------------------------------------------------------------------------------

# Start settings
#---------------

restart:
with(linalg):
with(Units[Standard]):

# Input
#------
```

```
# Variables

densityearlywood := 280*Unit('kg'/'m'^3):
densitylatewood := 820*Unit('kg'/'m'^3):


# Constants

densitycellwall := 1530*Unit('kg'/'m'^3):
cellsizelongitudinal := 2.8*10^(-3)*Unit('m'):
cellsizetangential := 50*10^(-6)*Unit('m'):
cellsizeradial200 := 50*10^(-6)*Unit('m'):
cellsizeradial1000 := 20*10^(-6)*Unit('m'):
lambda0transversal := 0.410*Unit('W'/('m'*'K')):
lambda0longitudinal := .730*Unit('W'/('m'*'K')):

# Procedures
#-----------

# Thermal conductivity tensor of the cell wall

CONDUCTIVITYTENSORCELLWALL := proc ()
   local lambdatransversal, lambdalongitudinal;
   description "calculates the actual thermal conductivity tensor for the cell wall";
      lambdatransversal := lambda0transversal+LAMBDABOUNDWATER()*moisturecontent;
      lambdalongitudinal := lambda0longitudinal+LAMBDABOUNDWATER()*moisturecontent;
      matrix([[lambdatransversal,      0        ,        0        ],
              [      0         ,lambdatransversal,        0        ],
              [      0         ,      0        , lambdalongitudinal]])
   end proc:


# Thermal conductivity of water

LAMBDABOUNDWATER := proc ()
   local T;
   description "calculates the bound water thermal conductivity for the actual temperature";
      T := simplify(temperaturekelvin*Unit(1/'K'));
      (-728.198686+7.298716648*T-0.9453916040e-2*T^2)*Unit('mW'/('m'*'K'))
   end proc:


# Thermal conductivity tensor of the lumen

CONDUCTIVITYTENSORLUMEN := proc ()
   local lambdaa;
   description "calculates the actual thermal conductivity tensor for the lumen";
      lambdaa := LAMBDAAIR();
      matrix([[lambdaa,   0   ,   0   ],
              [   0   ,lambdaa,   0   ],
              [   0   ,   0   ,lambdaa]])
   end proc:


# Thermal conductivity of air

LAMBDAAIR := proc ()
   local T;
   description "calculates the actual thermal conductivity of air";
      T := simplify(temperaturekelvin*Unit(1/'K'));
      (.3102291022+0.9499532950e-1*T-0.2917470146e-4*T^2)*Unit('mW'/('m'*'K'))
   end proc:


# Volume fraction of the cell wall

VOLUMEFRACTIONCELLWALL := proc ()
   description "calculates the volume fraction of the cell wall";
      evalf(specificdensitywood / densitycellwall)
```

```
   end proc:


# Volume fraction of the lumen

VOLUMEFRACTIONLUMEN := proc ()
   description "calculates the volume fraction of the lumen";
      evalf(1-VOLUMEFRACTIONCELLWALL())
   end proc:


# Radial Cell Size

CELLSIZERADIAL := proc ()
   local c1, c2;
   description "calculates the radial cell size for the given specific wood density";
      c2 := (1/800)*(cellsizeradial1000-cellsizeradial200)/Unit('kg'/'m'^3);
      c1 := cellsizeradial200-200*Unit('kg'/'m'^3)*c2;
      evalf(c1+c2*specificdensitywood)
   end proc:


# Cellwallthickness

CELLWALLTHICKNESS := proc ()
   local cellsizeradial, x;
   description "calculates the cell wall thickness for the given specific wood density";
      cellsizeradial := CELLSIZERADIAL();
      solve(VOLUMEFRACTIONCELLWALL()=1-(cellsizeradial-2*x*Unit('m'))*(cellsizetangential-2*x*Unit('m'))/
            (cellsizeradial*cellsizetangential), x)*Unit('m')
   end proc:


# Diameter ratio

DIAMETERRATIO := proc ()
   local cellwallthickness;
   description "calculates the diameter ratio for the given specific wood density";
      cellwallthickness := CELLWALLTHICKNESS();
      (CELLSIZERADIAL()-2*cellwallthickness)/(cellsizetangential-2*cellwallthickness)
   end proc:


# Aspect ratio

ASPECTRATIO := proc ()
   local cellwallthickness;
   description "calculates the aspect ratio for the given specific wood density";
      cellwallthickness := CELLWALLTHICKNESS();
      (cellsizelongitudinal-2*cellwallthickness)/(cellsizetangential-2*cellwallthickness)
   end proc:


# P-Tensor

PTENSOR := proc ()
   local a1, a2, a3, z3, xi, i, j, g, gdach, P, phi;
   description "calculates the P-Tensor";
      a2 := 1;
      a1 := a2*DIAMETERRATIO();
      a3 := a2*ASPECTRATIO();
      xi[1] := cos(phi)*sqrt(1-z3^2)/a1;
      xi[2] := sin(phi)*sqrt(1-z3^2)/a2;
      xi[3] := z3/a3;
      i := 'i';
      j := 'j';
      g := sum(sum(CONDUCTIVITYTENSORCELLWALL()[i,j]*xi[i]*xi[j],i=1..3),j=1..3);
      gdach := 1/g;
      P := array(1 .. 3, 1 .. 3);
```

```
      i := 'i';
      j := 'j';
      for i to 3 do
         for j to 3 do
            P[i,j] := simplify(evalf((1/4*pi)*(int(int(gdach*xi[i]*xi[j],phi=0..2*pi),z3=-1..1))))
         end do
      end do;
      P
   end proc:


# Assembly and Results
#---------------------

# Calculation of the Thermal Conductivity Tensor for a given temperature and moisturecontent

temperaturekelvin := (273.16+20)*Unit('K'):
moisturecontent := 0.16:

specificdensitywood := densityearlywood:
P := PTENSOR():
f0 := VOLUMEFRACTIONCELLWALL():
f1 := VOLUMEFRACTIONLUMEN():
K0 := CONDUCTIVITYTENSORCELLWALL():
K1 := CONDUCTIVITYTENSORLUMEN():
U := matrix([[1,0,0],[0,1,0],[0,0,1]]):
numerator := simplify(evalm(f0*K0+f1*K1/(U+P*(K1-K0)))):
denumerator := simplify(evalm(f0*U+f1/(U+P*(K1-K0))))
Khomearlywood := simplify(evalm(numerator/denumerator)):

specificdensitywood := densitylatewood:
P := PTENSOR():
f0 := VOLUMEFRACTIONCELLWALL():
f1 := VOLUMEFRACTIONLUMEN():
K0 := CONDUCTIVITYTENSORCELLWALL():
K1 := CONDUCTIVITYTENSORLUMEN():
U := matrix([[1,0,0],[0,1,0],[0,0,1]]):
numerator := simplify(evalm(f0*K0+f1*K1/(U+P*(K1-K0)))):
denumerator := simplify(evalm(f0*U+f1/(U+P*(K1-K0)))):
Khomlatewood := simplify(evalm(numerator/denumerator)):

amin := round(densityearlywood/10*Unit('m'^3/'kg')):
amax := round(densitylatewood/10*Unit('m'^3/'kg')):

results := array(1..amax-amin+2,1..7):
results[1,1] := Specific wood density:
results[1,2] := K[lumen]:
results[1,3] := K[cellwall,transversal]:
results[1,4] := K[cellwall,longitudinal]:
results[1,5] := K[hom,radial]:
results[1,6] := K[hom,tangential]:
results[1,7] := K[hom,longitudinal]:

for a from amin to amax do
   specificdensitywood := a*10*Unit('kg'/'m'^3):
   fearlywood := (specificdensitywood-densitylatewood)/(densityearlywood-densitylatewood):
   flatewood := 1-fearlywood:
   Khom := matrix([[1,0,0],[0,1,0],[0,0,1]]):
   Khom[1,1] := 1/simplify(fearlywood/Khomearlywood[1, 1]+flatewood/Khomlatewood[1, 1]):
   Khom[2,2] := Khomearlywood[2,2]*fearlywood+Khomlatewood[2,2]*flatewood:
   Khom[3,3] := Khomearlywood[3,3]*fearlywood+Khomlatewood[3,3]*flatewood:
   results[a-amin+2,1] := specificdensitywood:
   results[a-amin+2,2] := K1[1,1]:
   results[a-amin+2,3] := K0[1,1]:
   results[a-amin+2,4] := K0[3,3]:
   results[a-amin+2,5] := Re(Khom[1,1]):
   results[a-amin+2,6] := Re(Khom[2,2]):
   results[a-amin+2,7] := Re(Khom[3,3]):
end do:
```

```
print(results);


# Plot for the results of the calculation and the data of Kollmann
#-----------------------------------------------------------------

with(plots):
with(CurveFitting):

b := Unit('m'^3/'kg'):
c := Unit('s'^3*'K'/('m'*'kg')):

a := 'a':
pointsX := array(1..amax-amin+1):
pointsY := array(1..amax-amin+1):
for a from amin to amax do
   pointsX[a-amin+1] := simplify(results[a-amin+2,1]*b):
   pointsY[a-amin+1] := simplify((results[a-amin+2,5]*c+results[a-amin+2, 6]*c)*1/2):
end do:
a := 'a':
pointsradial := seq([pointsX[a-amin+1],pointsY[a-amin+1]],a=amin..amax):
radialplot := pointplot({pointsradial},colour=black,symbol=circle,symbolsize=4):
radialsplineplot := plot(Spline([pointsradial],x),x=10*amin..10*amax,colour=red,thickness=2):

a := 'a':
pointsX := array(1..amax-amin+1):
pointsY := array(1..amax-amin+1):
for a from amin to amax do
   pointsX[a-amin+1] := simplify(results[a-amin+2,1]*b):
   pointsY[a-amin+1] := simplify(results[a-amin+2,7]*c):
end do:
a := 'a':
pointslongitudinal := seq([pointsX[a-amin+1],pointsY[a-amin+1]],a=amin..amax):
longitudinalplot := pointplot({pointslongitudinal},colour=black,symbol=circle,symbolsize=4):
longitudinalsplineplot := plot(Spline([pointslongitudinal],x),x=10*amin..10*amax,colour=red,thickness=2):

readings1 := matrix([[452, 0.23100], [551, 0.30100]]):
kollmannsoftwoodparallel := seq([readings1[x,1],1.163*readings1[x,2]],x=1..2):

readings2 := matrix([[100, 0.51e-1], [330, 0.73e-1], [330, 0.82e-1], [345, 0.69e-1], [350, 0.86e-1],
                     [350, 0.90e-1], [350, 0.75e-1], [350, 0.77e-1], [360, 0.73e-1], [362, 0.78e-1],
                     [370, 0.74e-1], [380, 0.72e-1], [390, 0.77e-1], [370, 0.80e-1], [385, 0.83e-1],
                     [365, 0.84e-1], [364, 0.86e-1], [361, 0.88e-1], [360, 0.92e-1], [360, 0.94e-1],
                     [380, 0.87e-1], [390, 0.91e-1], [395, 0.87e-1], [410, 0.79e-1], [452, 0.78e-1],
                     [412, 0.83e-1], [415, 0.82e-1], [460, 0.84e-1], [465, 0.82e-1], [475, 0.85e-1],
                     [405, 0.86e-1], [410, 0.87e-1], [415, 0.86e-1], [425, 0.86e-1], [420, 0.89e-1],
                     [427, 0.87e-1], [424, 0.92e-1], [435, 0.92e-1], [450, 0.94e-1], [470, 0.93e-1],
                     [485, 0.96e-1], [412, 0.99e-1], [414, 0.97e-1], [422, 0.10000], [430, 0.98e-1],
                     [440, 0.97e-1], [460, 0.11000], [495, 0.90e-1], [510, 0.89e-1], [522, 0.90e-1],
                     [510, 0.92e-1], [512, 0.95e-1], [524, 0.92e-1], [525, 0.94e-1], [540, 0.95e-1],
                     [555, 0.92e-1], [568, 0.96e-1], [575, 0.98e-1], [587, 0.96e-1], [600, 0.91e-1],
                     [475, 0.10200], [480, 0.11000], [486, 0.10700], [490, 0.10500], [510, 0.10500],
                     [490, 0.10100], [510, 0.10200], [507, 0.98e-1], [518, 0.99e-1], [523, 0.10300],
                     [530, 0.10200], [545, 0.10500], [555, 0.10300], [560, 0.10900], [575, 0.11100],
                     [513, 0.10900], [525, 0.10800], [530, 0.11500], [570, 0.11600], [545, 0.12100],
                     [560, 0.11900], [410, 0.11800], [535, 0.12500], [627, 0.12100], [640, 0.11400],
                     [655, 0.11600], [640, 0.13400], [673, 0.13200], [690, 0.12500], [715, 0.13100]]):
kollmannsoftwoodperpendicular := seq([readings2[x,1],1.163*readings2[x,2]],x=1..90):

readings3 := matrix([[650, 0.21100], [600, 0.33100], [700, 0.34100], [708, 0.30800], [817, 0.30200]]):
kollmannhardwoodparallel := seq([readings3[x,1],1.163*readings3[x,2]],x=1..5):

readings4 := matrix([[115, 0.42e-1], [190, 0.43e-1], [458, 0.98e-1], [580, 0.90e-1], [512, 0.11400],
                     [525, 0.11200], [560, 0.11400], [568, 0.12200], [580, 0.12300], [580, 0.14700],
                     [550, 0.18500], [600, 0.16500], [600, 0.11000], [603, 0.11500], [620, 0.10600],
                     [650, 0.11100], [605, 0.11500], [618, 0.11400], [625, 0.11900], [630, 0.11600],
                     [665, 0.12400], [665, 0.12400], [630, 0.12300], [625, 0.12500], [618, 0.12700],
                     [615, 0.13000], [630, 0.13100], [705, 0.12600], [723, 0.12600], [730, 0.12800],
```

```
                    [743, 0.13000], [655, 0.13100], [660, 0.13400], [670, 0.13500], [685, 0.13500],
                    [690, 0.13800], [645, 0.15000], [710, 0.13900], [685, 0.14300], [710, 0.15600],
                    [713, 0.15700], [730, 0.14000], [735, 0.14400], [750, 0.14300], [755, 0.13900],
                    [773, 0.15000], [776, 0.14600], [790, 0.15000], [795, 0.16000], [825, 0.15500],
                    [830, 0.18000], [900, 0.12900], [1165, 0.2160]]):
kollmannhardwoodperpendicular := seq([readings4[x,1],1.163*readings4[x,2]],x=1..53):

kollmannsoftwoodparallelplot := pointplot({kollmannsoftwoodparallel},colour=black,symbol=asterisk,
                                symbolsize=7,legend="Softwood parallel"):
kollmannsoftwoodperpendicularplot := pointplot({kollmannsoftwoodperpendicular},colour=black,symbol=cross,
                                     symbolsize=7,legend="Softwood normal"):
kollmannhardwoodparallelplot := pointplot({kollmannhardwoodparallel},colour=black,symbol=solidcircle,
                                symbolsize=7,legend="Hardwood parallel"):
kollmannhardwoodperpendicularplot := pointplot({kollmannhardwoodperpendicular},colour=black,symbol=circle,
                                     symbolsize=7,legend="Hardwood normal"):

display(radialsplineplot,longitudinalsplineplot,kollmannsoftwoodparallelplot,
        kollmannsoftwoodperpendicularplot,kollmannhardwoodparallelplot,kollmannhardwoodperpendicularplot,
        view=[0..1200,0..0.45],gridlines=true,
        axis[1]=[tickmarks=[12,subticks=4]],axis[2]=[tickmarks=[10,subticks=4]],
        labels=[ovendry density [kg/m^3],thermal conductivity lambda [W/(m*K)]],
        labeldirections=[horizontal,vertical],labelfont=[TIMES,ROMAN,14],
        legendstyle=[location=right,font=[TIMES,ROMAN,12]]);
```

List of Figures

1.1 Shrinking of wood because of variations in moisture content 1

2.1 Hierarchical organization of wood 6
2.2 Cross section of a taxus tree [60] 7
2.3 Structure of softwood (red pine) [39] 8
2.4 Earlywood and latewood tracheid cells [32] 9
2.5 Unaspirated bordered pit in a sapwood tracheid [32] 9
2.6 Cross section of a bordered pit in the unaspirated state (left) and the aspirated state (right) [18] 10
2.7 Structure of diffusive porous hardwood (aspen) [39] 11
2.8 Structure of ring porous hardwood (red oak) [39] 11
2.9 Cross section of a basic building block (a), and the layered structure of the cell wall (b) [18] 12

3.1 Multistep homogenization 14
3.2 Spherical coordinate system 20

4.1 Periodic material microstructure with unit cell 29
4.2 Geometry of the transversal unit cell for earlywood 30
4.3 Geometry of the longitudinal unit cell for earlywood 31
4.4 Geometry of the transversal unit cell for latewood 32
4.5 Geometry of the longitudinal unit cell for latewood 32
4.6 Temperature distribution in earlywood resulting from a radial temperature gradient 34
4.7 Heat flux distribution in earlywood resulting from a radial temperature gradient 34
4.8 Concentration distribution in latewood resulting from a tangential concentration gradient 35
4.9 Distribution of fluxes in latewood resulting from a tangential concentration gradient 35

5.1 Schematic diagram showing the different moisture distributions in the cell wall and the lumen in a wood cell cross-section 37
5.2 Mean sorption isotherms of wood at five temperatures calculated from (5.2) 39
5.3 Saturation vapor pressure from 273.15 to 373.15 K 41
5.4 Density of water from 273.15 to 373.15 K 42
5.5 Heat of evaporation of water from 273.15 to 373.15 K 43
5.6 Viscosity of water from 273.15 to 373.15 K 44
5.7 Specific heat at constant pressure of steam from 273.15 to 373.15 K 45
5.8 Illustration of the corresponding moisture concentration gradients in the cell wall and in the lumen 47
5.9 Water-vapor diffusion coefficient in the lumens at five temperatures 48
5.10 Relative energy levels at 40 °C of water vapor, liquid water, and bound water in wood as functions of wood moisture content 50
5.11 Differential heat of sorption at different temperatures 51
5.12 Energy relationships for diffusion through cell wall ($mc = 0.09$, $T = 25.5\,°C$) 52
5.13 Self-diffusion coefficient of water from 273.15 to 373.15 K 53
5.14 Energy relationships of water in wood at 40 °C 54
5.15 Radial diffusion coefficient of spruce wood ($\varrho_{ovendry} = 404\,kg/m^3$) 57
5.16 Back-calculated activation energies for different temperatures 58

6.1 Thermal conductivity of water from 273.15 to 373.15 K 62
6.2 Thermal conductivity of air from 100 to 1000 K 62
6.3 Thermal conductivity of wood at 20 °C and 12 % moisture content 65
6.4 Dependence of tangential thermal conductivity of wood on the moisture content 66

List of Tables

1.1 Quantities and units used in this thesis 4
1.2 Indices used in this thesis 4

4.1 Diffusion coefficient ratios used in the comparison of the homogenization models 29
4.2 Comparison of unit cell method to Mori-Tanaka scheme, $\varrho_{ovendry} = 200\,\mathrm{kg/m^3}$ 31
4.3 Comparison of unit cell method to Mori-Tanaka scheme, $\rho_{ovendry} = 1000\,\mathrm{kg/m^3}$ 33

6.1 Thermal conductivities of several materials 61
6.2 Thermal conductivities of single specimens 66

A.1 Steam table in SI-Units, $0 - 19\,°\mathrm{C}$ 73
A.2 Steam table in SI-Units, $20 - 64\,°\mathrm{C}$ 74
A.3 Steam table in SI-Units, $65 - 100\,°\mathrm{C}$ 75